Author:
Simons, Melanie F

Title:
Wearable smart haptic interfaces towards embodied assistive devices

Wearable smart haptic interfaces towards embodied assistive devices

By

MELANIE SIMONS

Department of Engineering Mathematics
UNIVERSITY OF BRISTOL

A dissertation submitted to the University of Bristol in accordance with the requirements for award of the degree of Doctor of Philosophy in the Faculty of Engineering.

JUNE 2022

Word count: Thirty thousand and ten

Abstract

The advancement of smart materials and structures has made wearable technology more attainable and versatile. The exploration of these materials and structures is of importance in order to develop wearable technology further and find new applications. The World Health Organization (WHO) estimates that the prevalence of physical disabilities across the globe is 0.5%, some 32 million people based on a global population of 6.4 billion in 2004. This includes people requiring a prosthesis, orthosis or some form of rehabilitation service. The uses and development of mobility aids for those with a physical disability are rapidly increasing. Although success rates of these devices are high in small, targeted groups, many problems still exist in addressing the range of conditions and needs in the wider population. The research presented in this thesis focuses on exploring the characteristics of various smart materials and structures for potential use in addressing the problems which originate from the interface between hard assistive devices and soft tissue of the human body, with a particular interest in prosthetic limbs. We aim to develop innovative technologies through the use of smart materials and structures to address these issues, targeting two key potential applications: to increase comfort and fit; and to use the body-device interface as a communication channel.

Fit and comfort of the prosthetic socket is addressed by exploring the use of auxetic structures as a means to accommodate residual limb volume changes that amputees experience throughout the day. Tiled auxetic cylinders (TACs) were designed, fabricated and characterised. These TACs can be tuned through design and geometric parameters, and we demonstrate their ability to react to the environment, highlighting their potential to improve the fit of prosthetic sockets.

The diversity of mechanoreceptors which are distributed through the skin, in addition to the great surface area of the skin, makes it ideal for its potential use as a communication channel. We developed wearable tactile devices that can communicate with the skin to convey a range of information. These devices succeeded in conveying natural and pleasant tactile sensations that could enable non-intrusive notifications to the user. Furthermore, we developed a sensory feedback device for potential use with upper limb prostheses which could increase the sense of embodiment. This device contains simple computation, and we demonstrate its potential use in everyday tasks.

All the devices created are wearable and we explored how these devices could be incorporated into fabrics with the hope of making them comfortable and discreet without interfering with the environment. This thesis highlights the potential of smart materials and structures to address the issues identified at the body-device interface of medical assistive devices.

Dedication and acknowledgements

First and foremost, a huge thank you to my supervisor Jonathan Rossiter for his immense support over the years. No idea was ever too wacky, or deadline too soon, and always reminding me to go for 'minimal effort, maximal return'. Not only has he guided me academically, but he also always looked out for my well-being. I could not have asked for a better supervisor and cannot thank him enough.

A warm thanks to all my colleagues at the Bristol Robotics Lab, especially the SoftLab research team, BRL technicians and those with whom I worked closely with on projects, for always taking the time to help me and answer my never-ending questions and for making my time here so very enjoyable and unforgettable.

I would also like to acknowledge the Engineering and Physical Sciences Research Council for funding me through my degree program.

These past five years have surely had its ups and downs and I must thank all my family and friends for their continued support, always believing in me and for helping me complete my PhD.

Author's declaration

I declare that the work in this dissertation was carried out in accordance with the requirements of the University's Regulations and Code of Practice for Research Degree Programmes and that it has not been submitted for any other academic award. Except where indicated by specific reference in the text, the work is the candidate's own work. Work done in collaboration with, or with the assistance of, others, is indicated as such. Any views expressed in the dissertation are those of the author.

SIGNED: ..... DATE: .....

Table of Contents

List of Tables

Table **Page**

List of Figures

Figure **Page**

CHAPTER 1

INTRODUCTION

With the advancement of smart materials and structures, wearable technology has become increasingly attainable and versatile. From uses in the medical field to the gaming community, smart wearable devices can be used for a range of applications. This area of Human Computer Interaction (HCI) is rapidly developing as more smart materials and structures are engineered. Design criteria for specific applications can limit the use of some of these materials and structures, so further research into new materials and structures and their applications is necessary.

The research presented in this thesis focuses on materials and structures for wearable technologies within healthcare. More specifically, a focus is given on the problems which originate from the interface between hard assistive devices and soft tissue of the human body. The innovative technologies developed are designed to highlight their potential in increasing the embodiment of assistive devices. A specific focus is given to those with a limb difference who require a prosthetic limb. However, the technology presented here could be adapted and tailored to the specific needs for any of these physically impaired groups and potentially target countless number of people. A special consideration is also given to the suitability of this technology in low-income countries.

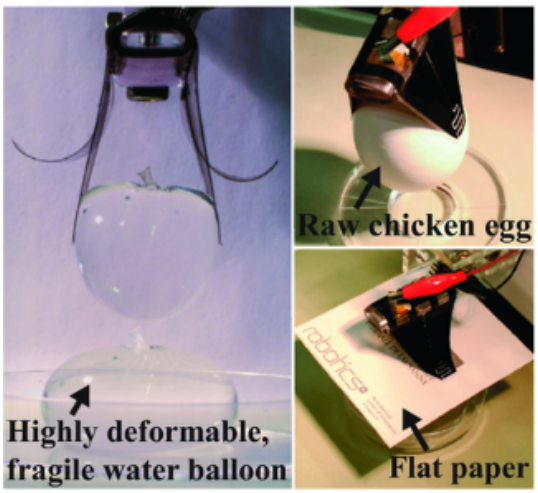

FIGURE 1.1. Image demonstrating the ability of a soft gripper to form around the object, reducing the complexity of control. Figure reproduced from [1].

1.1 Soft Robotics

Conventional robots are hard, rigid-bodied structures that require careful programming to complete certain tasks. Soft robotics is a relatively new field, but it is growing rapidly. It is an area of research that focuses on robotic systems that are compliant and versatile. This gives them an advantage over conventional robots as they require less programming for specific tasks and are able to adapt according to their surroundings. Consider a robotic arm with the 'simple' task of picking up an object. Using conventional, rigid, robotics, this arm will need to be programmed with the exact grip pattern to match the shape of the object and have sufficient grip strength so as not to drop or crush it. When using a soft robotic gripper however, such as one that uses electroadhesion and electrostatic actuation with self-sensing capabilities [1], the gripper will form around the object reducing the need for programming grip pattern or grip strength (fig. 1.1). When designing technology for wearable applications, it is desirable to turn to soft robotics to create biologically compatible technology which is, just as biological systems are, compliant and versatile.

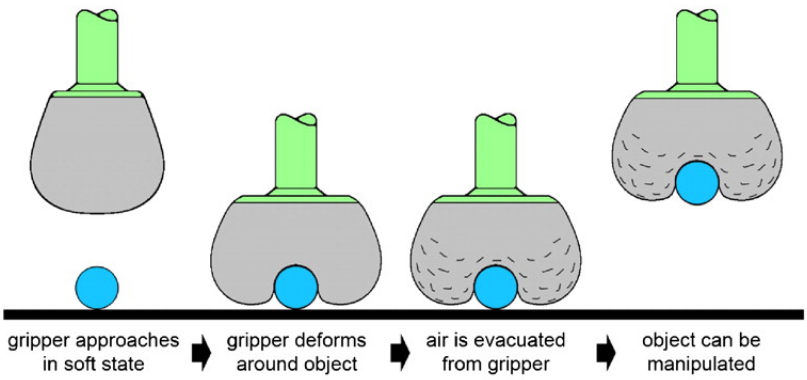

FIGURE 1.2. Image demonstrating particle jamming technology. In the inflated state, the material is flexible and can wrap around various shaped objects. As the air is removed the material stiffens. Figure reproduced from [4].

1.1.1 Smart Materials and Structures

The term 'smart materials' covers a wide range of technologies that could differ on a number of factors, including the material used, the fabrication method and the sensing/actuation principle. Here we overview the most applicable technologies for wearable human-computer interfaces [2].

Elastomers, such as silicone, are advantageous for use in soft robots due to their tunable softness and large strain to failure, meaning they can easily deform and stretch [3]. One drawback of using silicones for wearable applications is their lack of breathability when in contact with the skin.

Variable stiffness materials are ones which can alter their stiffness. This can be achieved by a variety of different methods. One such method is by particle jamming. This is where the material contains particles, such as ground coffee or saw dust, which when inflated is flexible. However, as the air is removed from the material the structure hardens as the particles pack together. This principle is also used in various robotic grippers (fig. 1.2) [4].

Other smart materials exploit the principle of thermal shape memory. A simple polymer fibre used for fishing lines and sewing thread, for example, can be coiled to create an artificial muscle.

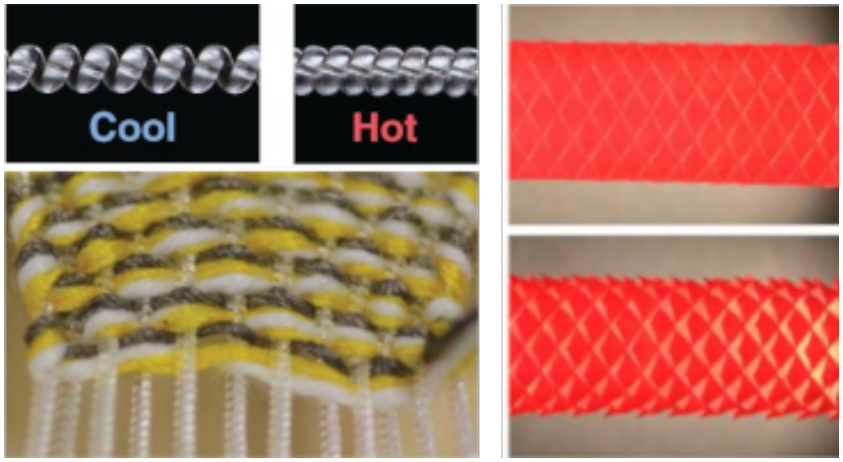

FIGURE 1.3. (Left) Artificial muscle generated by the coiling of polymer fibres that contracts when heated (top). This technology can easily be incorporated into wearable fabrics (bottom). Figures reproduced from [5]. (Right) Kirigami structure to mimic the movement of a snake. The air bellow inside the structure is inflated to push parts of the structure out and create directional friction. Figures reproduced from [7].

As the material is heated, the structure contracts. This structure can be braided and woven into various structures and, in addition to being lightweight, would therefore be suitable for use in wearable devices (fig. 1.3, left) [5]. Coiled shape memory alloys (SMAs) work in a very similar way, but are significantly more expensive [6].

Origami (the Japanese art of paper folding) and Kirigami (which includes cutting the paper) can also be used to create smart structures. This has been demonstrated in a snake-bot [7], which consists of a cylindrical kirigami structure with an air bellow inside, that when inflated pushes parts of the kirigami structure out to create directional friction favouring movement in one direction (fig. 1.3, right).

Electroactive polymers (EAPs) are materials that can expand and contract when stimulated by a voltage. They are very compliant and can undergo large deformations. Two main EAPs used in the field of soft robotics are dielectric elastomer actuators (DEAs) and ionic polymer-metal composites (IPMCs). DEAs consist of an elastomer sandwiched between two compliant electrodes.

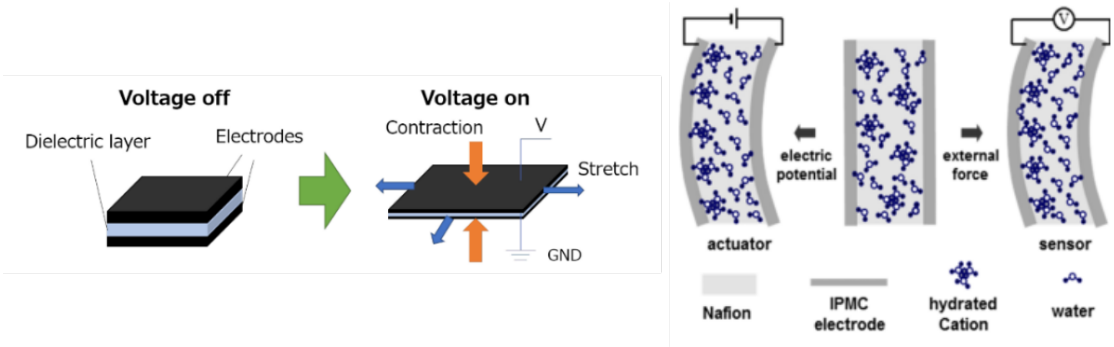

FIGURE 1.4. Mechanism of actuation of two electroactive polymers: dielectric elastomer actuators (left) and ionic polymer-metal composites (right). Figures reproduced from [9] and [10] respectively.

When exposed to a voltage, these electrodes attract each other, squeezing the elastomer and resulting in the structure expanding (fig. 1.4, left). IPMCs differ in that they contain an ionic layer between the two electrodes. As a voltage is applied across the electrodes, the ions migrate (fig. 1.4, right) [8]. Ionic EAPs are suitable for wearable and biomedical applications due to only requiring low voltages, but electrostatic actuators such as DEAs require higher voltages in the order of kilo volts.

Auxetic structures have become increasingly more popular. They expand perpendicular to the direction in which they are stretched, as opposed to conventional materials which become narrower. Fig. 1.5 illustrates the behaviour of auxetic structures compared to conventional ones when exposed to a planar force [11]. They have been used in energy absorbing foams [12], cardiovascular stents [13] and deployable structures [14]. Recently, an auxetic structure has been created that allows for tunable shape-changing and can be used for different applications such as encoded displays, easy packing and transformation into a helmet [15]. Auxetic structures possess characteristics that make them favourable for wearable applications and therefore could potentially improve comfort and fit for prosthesis wearers. These characteristics are explored in more detail in chapter 2 (section 2.6).

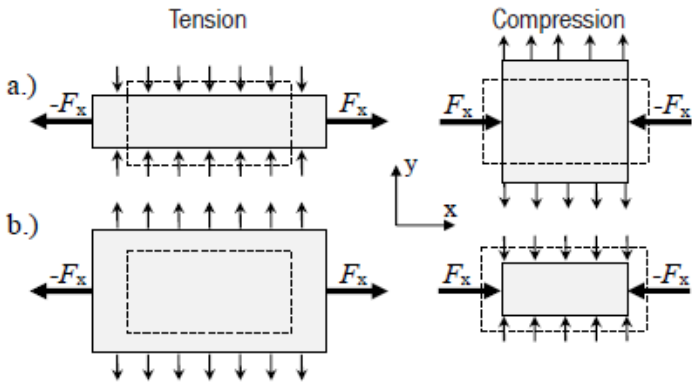

FIGURE 1.5. Behavioural characteristics of (a) a conventional (i.e. non-auxetic) structure and (b) an auxetic structure under tension and compression. The auxetic structure increases in width when stretched longitudinally which is depicted by a negative Poisson's ratio. Figure reproduced from [11].

1.1.2 Wearable Technology

As more smart materials and structures are discovered and explored, there is a greater scope for incorporating these into wearable technology. Especially in the field of health and fitness, smart watches that can measure your heart rate and sleep cycles amongst other parameters have become increasingly popular. Electronics have become smaller and with the advancement of softer and more pliable smart materials, technology can be developed that can comfortably sit against the skin for more wearable applications [16].

Wearable technology can be particularly beneficial in healthcare. Various head-mounted displays have been developed for use in surgery and imaging. Other wearable devices in the form of body-sensors can be used to measure patients' vital signs and to improve posture [17]. One smart fabric that can aid in rehabilitation is the Frozen Suit (fig. 1.6) [18]. It uses particle jamming to restrict particular joint movement to aid control.

Another wearable sleeve that can be used in healthcare is a prosthetic socket liner with integrated EAP pads which can actively expand or contract [19]. This ensures a dynamic fit

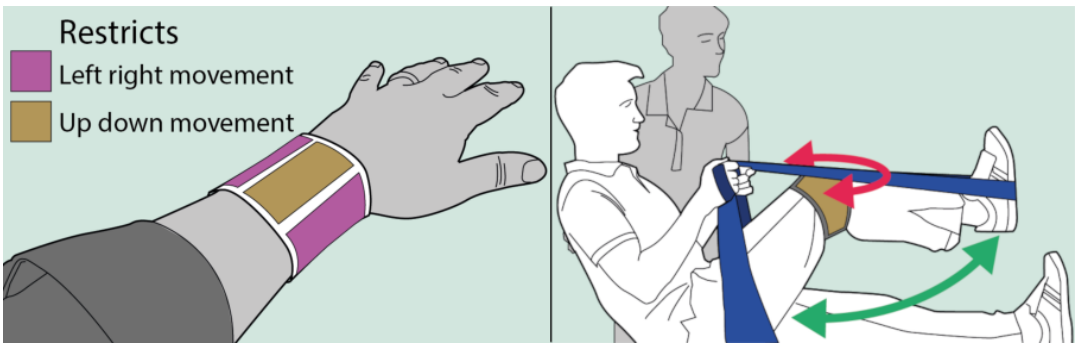

FIGURE 1.6. Image demonstrating a wearable exoskeleton with force feedback, named Frozen Suit. (Left) The method of operation of the exoskeleton which can restrict movement in specific directions and can be used to aid in rehabilitation (right). Figures reproduced from [18].

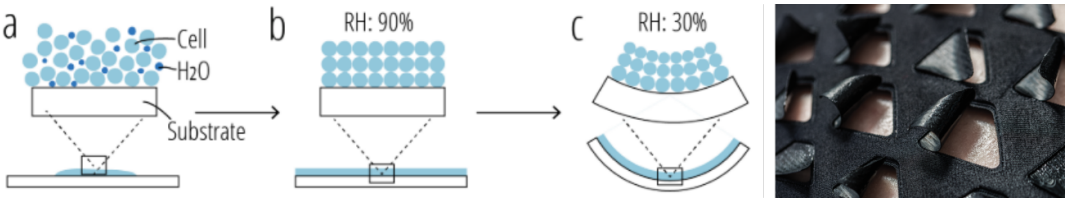

FIGURE 1.7. Heat activated material developed by MIT. The biological cells expand and contract with changing relative humidity (RH), causing movement of the underlying substrate. Figures reproduced from [21].

between the socket and the residual limb throughout the day despite limb volume changes (discussed in section 2.5.3).

MIT developed a smart wearable fabric that can react to heat using bacteria, called bioLogic. These bacteria expand and contract relative to the surrounding moisture levels. When the wearer gets too hot, the bacteria react to the change in humidity resulting in the fabric opening up pores to allow increased breathability of the skin for cooling (fig. 1.7) [20].

As there are many different smart materials and structures that can potentially be used to create wearable technologies, the design criteria of the final device with a specific application needs to be considered.

1.2 Physical Disabilities

Physical disabilities, physical impairments or differently abled bodies, as sometimes is preferred [22], are receiving more attention, particularly in developed countries. There is a movement to create equity for this group of people, where it is widely accepted that disability is not solely a medical condition but also, or maybe even more so, a social problem, giving rise to the medical and social models of disability [23]. The medical model of disability relates to the physical impairments, whereas the social model refers to society not being suitable to include all those with a physical impairment leading to them feeling disabled, isolated or discriminated against. It is nearly impossible to get an estimate of the prevalence of disabilities across the globe, as there are many different definitions of disability in terms of what level is included or excluded. Even for a single country it has proven difficult to get accurate representations, such as that shown in Ireland, where two different surveys conducted in the same year came up with a significant different outcome [24].

The World Health Organization (WHO) estimates that the prevalence of physical disabilities across the globe is 0.5%, some 32 million people based on a global population of 6.4 billion in 2004 [25]. This includes people requiring a prosthesis, orthosis or some form of rehabilitation service. Noticeably, 80% of these people live in low-income countries [26] and only 5% are thought to have access to prosthetic services and devices that are affordable [27].

The uses and development of mobility aids for those with a physical disability are rapidly increasing. These devices are tailored to their particular condition and needs in order to assist in every-day activities, aid in rehabilitation, or increase abilities. These include prostheses for replacing a limb for amputees, orthoses for supporting a part of the body for example for children with cerebral palsy, wheelchairs for spinal cord injury patients, rehabilitation devices such as

crutches, and mobility aids for elderly people such as walker frames. Although success rates are high in achieving these goals in small, targeted groups [28], many problems still exist in addressing the range of conditions and needs in the wider population.

1.2.1 Limb Differences

Limb difference is a term used to describe someone with a partial or complete absence or malformation of a limb or limbs [29]. Limb differences can occur either as a result of a congenital (birth) defect, or as a result of surgical amputation. In developed countries, the latter is most commonly due to peripheral vascular diseases such as diabetes. In more developing countries however, trauma as a result of accidents tend to play a bigger role, also resulting in a younger demographic of patients [30]. Amputees are generally categorised into upper and lower limb, corresponding to the arms and legs respectively. The different levels of amputation are shown in fig. 1.8 where the most common upper limb amputations are transhumeral (above elbow) and transradial (below elbow), and the most common lower limb amputations are transfemoral (above knee) and transtibial (below knee) [31]. People may experience more than one limb difference. When the limb difference affects both sides of the body, it is said to be bilateral, as opposed to unilateral.

1.2.2 Prosthetic Devices

Prosthetic devices are made up of an end terminal (such as a hand or foot), shank, and socket into which the residual limb fits (see fig. 1.9 and 1.11). The socket is where the residual limb fits into the prosthetic and is therefore the component which is in contact with the body. As it is a solid structure, a silicone liner is sometimes worn for comfort.

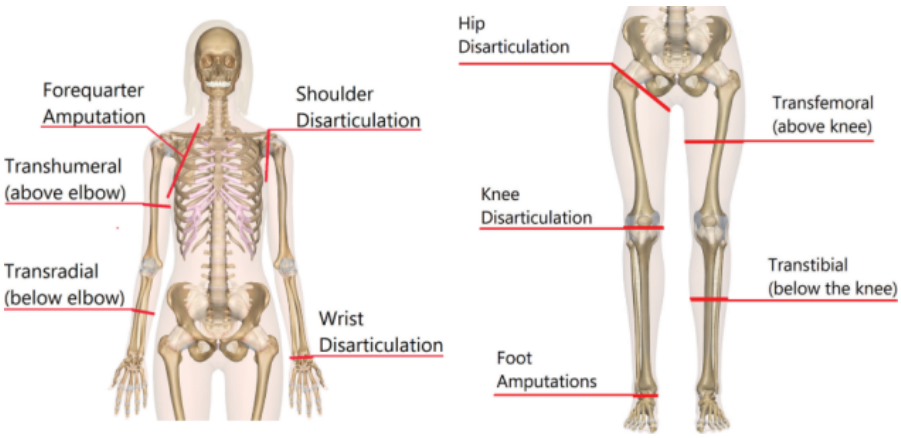

FIGURE 1.8. The different levels of amputation of both the upper (left) and lower (right) extremities. Figures reproduced from [32].

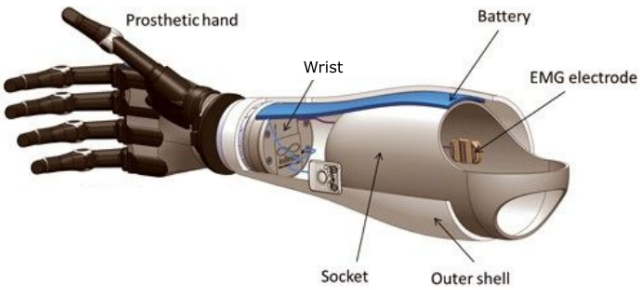

FIGURE 1.9. The different components that make up a typical transradial prosthetic device. Image shows myo-electric prosthetic arm. Figure adapted from [33].

1.2.2.1 Upper Limb Prostheses

There are three main categories of upper limb prostheses depending on the mechanism of activation; passive, body-powered, and electric. Passive prosthetic arms, as the name suggests, do not have a mechanism of action and is worn mainly for aesthetic purposes. Body-powered prosthetic arms are worn with a harness that straps around the contra-lateral shoulder which acts as an anchor point. A cable runs from here to the end of the prosthetic arm to a prosthetic hand or hook. On flexion of the shoulder of the residual limb, the cable tensions, resulting in

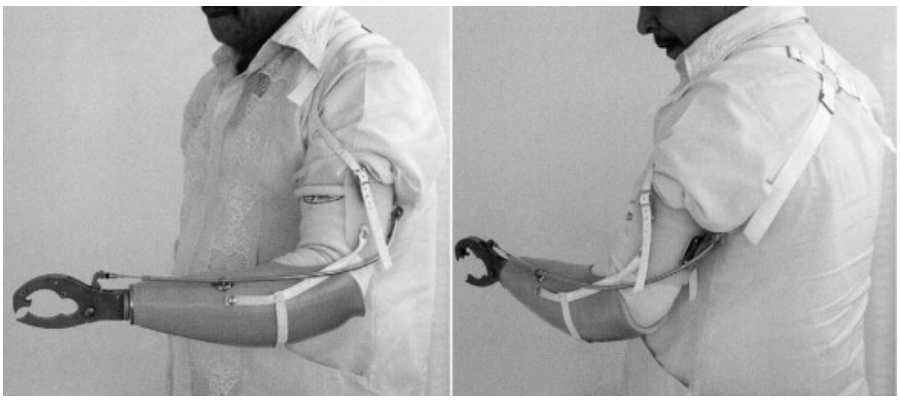

FIGURE 1.10. Body-powered prosthetic arm that actuates with the use of a cable. Figure reproduced from [34].

Type of Actuation	Advantages	Disadvantages
Passive	Aesthetic & lightweight	Lack of function
Body-powered	Durable & short training time	Bulky & lack of control
Electric	Function	Heavy

TABLE 1.1. Comparison of the main categories of upper limb prosthetic devices [35, 36].

opening and closing of the end terminal (see fig. 1.10) [34]. Although these prostheses tend to be durable and easy to use and provide some more functionality compared with passive prostheses, they can be bulky and difficult to control.

Electric prostheses are powered by motors. Most common are myo-electric prostheses, which are controlled by the muscles in the residual limb with the use of electromyography (EMG) electrodes (fig. 1.9). These electrodes are in contact with the skin and pick up muscle activity of the underlying muscle. Although function can be improved with these types of prostheses, the need for a battery pack to power the motors can greatly increase the weight of these devices.

An overview of the comparison between these three categories is shown in table 1.1.

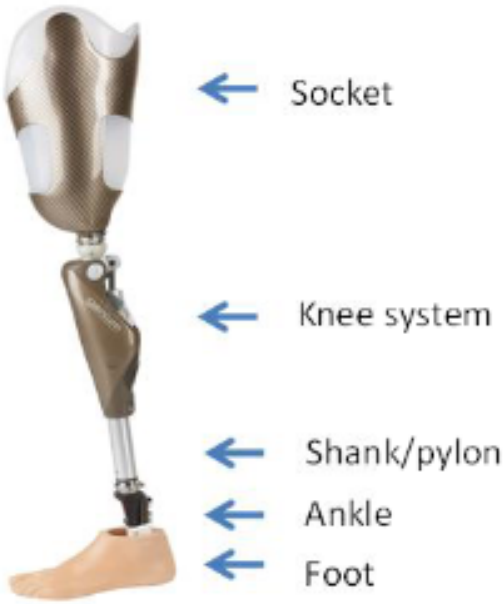

FIGURE 1.11. Components of a trans-humeral prosthesis. Figure reproduced from [37].

Type of Knee	Advantages	Disadvantages
Single axis constant friction	Simple & lightweight	Limited stability
Weight-activated friction	Simple to use	Level-ground walking only
Polycentric	Improved control & increased toe clearance	Heavy
Hydraulic	Suitable for uneven ground	Requires training

TABLE 1.2. Comparison of the types of prosthetic knee joints available for above-knee prostheses [37].

1.2.2.2 Lower Limb Prostheses

A typical lower limb prosthesis is shown in fig. 1.11. This image shows a trans-humeral or above knee prosthesis. There are a number of different knee-joint types that offer different levels of control of the leg. More control typically requires more physically able users [37]. A summary is shown in table 1.2, listed from least to most amount of control.

1.2.2.3 Suspension Systems

One major aspect of prostheses is the suspension system, i.e. how the devices are attached to the body to ensure they stay attached with use. There are a number of different mechanisms:

1. Straps
2. Suction
3. Self-suspending
4. Lock and pin
5. Osseointegration

Straps are one of the most basic suspension systems and hold the prosthesis up with straps that fasten around other parts of the body, such as the shoulder joint for upper limbs (fig. 1.10) or the hips for lower limbs. They are easy to use and do not rely on a perfect fit of the socket to work. Suction systems create a vacuum in the socket, between the residual limb and the socket or liner (fig. 1.12a). This can be done with the use of one-way valves, where air is forced out of the socket as the residual limb is pushed into it, or with the use of a pump which sucks the air out between the residual limb and the socket or liner. Self-suspending sockets are created with the mould of the socket by extending over a joint and narrowing just past the joint. For example, the elbow joint can be used for trans-radial prostheses, or the knee joint for trans-tibial prostheses. This suspension system is simple to use, however requires expert knowledge to fabricate and is unsuitable for all levels of amputation. Lock and pin mechanisms work with a liner that is rolled over the residual limb onto which a pin is attached (fig. 1.12b). This pin can then be inserted into the bottom of the socket and locked into place. This system is especially beneficial for those with reduced mobility as it can be donned in a seated position (especially in the case of lower limb prostheses). Lastly, osseointegration is the newest form of prostheses suspension. It requires surgery to insert an implant into the end of the bone of the residual limb. The prosthetic device

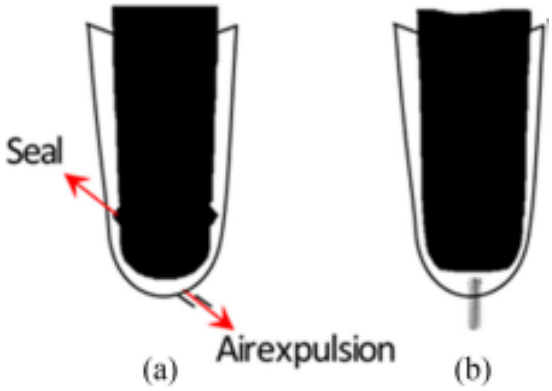

FIGURE 1.12. Two types of suspension systems for prosthetic devices: suction (a) and lock and pin (b). Figure reproduced from [37].

Type of Suspension	Advantages	Disadvantages
Straps	Inexpensive & simple & stays on with fluctuating residual limb	Bulky
Suction	Even pressure distribution	Requires mobility
Self-suspending	Simple	Requires expertise
Lock and pin	Easy to don	Requires some strength
Osseointegration	No socket & better control	Infection risk

TABLE 1.3. Comparison of the types of suspension systems [37, 38].

can then be directly attached to this implant, so there is no need for a socket. Although this method overcomes all the problems associated with the body-device interface seen with the socket (discussed in more detail in section 1.4) there is a much bigger risk of infection at the site of implant. Osseointegration is discussed in more detail in chapter 2.

An overview of the different types of suspension systems is shown in table 1.3.

1.3 Considerations for Low-Income Countries

The United Nations (UN) identifies low-income countries as those with a gross national income (GNI) per capita of $1,018 or below (as of 2021 [39]). Currently, 47 countries are in this category,

the vast majority of which lie in Africa (32 countries).

As mentioned before, it is estimated that 80% of those in need of some form of mobility or rehabilitation device/services live in low-income countries, equalling to some 25.5 million people. In these low-income countries it is estimated that no more than 3% of those in need have access to professional help, and therefore many are not recorded in the health system [40]. This can be due to a number of factors, including the inability to access health clinics, which are normally only situated in big cities and can be miles away from their homes. They may be dependent on public transport to get them to the clinics, which is expensive and can be unreliable. In addition, amputees may be dependent on others physically (to get to the clinic) but also financially as they may find it hard to get a job which are predominantly manual labour-intense in rural areas [41] [42].

Prevalence of disabilities increases with age, regardless of the income status of the country, mainly due to the global ageing population [24]. Amputees in low-income countries, on average, tend to be younger, with the cause of amputation mainly being due to trauma, such as a road traffic accident, and diseases that have long been eradicated in higher-income countries, such as polio [42] [30].

One of the big problems of delivering prosthetic/rehabilitation services is the lack of resources. Materials for making new prostheses or maintaining/repairing devices are scarce, where governments may not be supporting these services [42]. Providing inadequate information to patients, especially in terms of educating them in the benefits of attending physiotherapy after being fitted with a prosthetic device, results in patients not accessing the necessary rehabilitation services and consequently rejecting their device [41]. In addition, there is an overall lack of trained professionals who can provide prosthetic, orthotic and rehabilitation services. 75% of developing countries do not provide training programmes and of those that do, a mere 400 professionals a

year graduate, with differing standard levels [26].

In addition to low-income countries needing generally more resources, materials, trained personnel and rural clinics, there may also be country-specific requirements. Cultural, political, social, religious and even weather aspects may need to be taken into account to ensure the necessary aid is provided. These should be tailored specifically to that country in order to result in the highest device acceptance rates and give users the best opportunity to integrate back into society [30].

1.4 The Challenge

Despite efforts, prosthetic devices have progressed slowly since they were first developed, especially when looking at the interface with the body. It is estimated that up to 50% of the power supplied to move an exoskeleton is absorbed by compression of the soft tissue [43]. This can be the cause of the common deep sheer tissue injury which can lead to ulcerations [44]. Other common issues at this site include excess heat leading to perspiration and improper fit. The majority of prosthetic sockets are generated with the use of Plaster-of-Paris which requires skilled prosthetists to ensure the correct fit that minimises rubbing and pressure points. However, as they are all custom made systems, the fit will depend on the clinician's knowledge and experience. In addition, residual limbs have a compromised lymphatic system and therefore an amputee's residual limb can fluctuate in volume dramatically with fluid build up over the course of even a few hours. As the socket is solid it does not accommodate for these changes during the day, leading to the socket becoming too tight or loose.

In addition to these issues surrounding comfort, device weight plays a big role in prosthetic user satisfaction, along with functionality. Especially for upper limb prostheses, it is harder to

replicate the functionality of the many degrees of freedom of the fingers. Lack of sensory feedback also limits the use of these assistive devices and therefore their success rates [45].

Lower limb prosthetic devices tend to provide a greater level of independence, giving amputees the ability to move around freely without the need for crutches or a wheelchair. The benefits of using these therefore tend to outweigh the many problems that still exist with them. In contrast, many upper limb amputees learn to function without their hand - especially in congenital cases. The problems associated with upper limb prostheses are therefore more likely to outweigh the benefits.

In summary, the main issues with prosthetic devices are as follows:

- pressure points leading to skin degradation
- excessive heat and perspiration
- improper fit with fluctuating residual limb volume
- weight of device
- lack of functionality (including lack of sensory feedback)

1.5 Aims and Objectives

The research outlined in this thesis focuses on this body-device interface and will target two key potential applications: 1. to increase comfort and fit; and 2. as a communication channel. Discomfort leads to the reluctance of using these assistive devices, causing patients to become highly dependent on others, unable to move around freely. Additional problems such as fluctuations in residual stump volume and oedema often require the patient to attend multiple follow-up appointments in order to alter the fit of the prosthetic socket or wearable device [46].

The lack of sensory feedback, particularly in upper limb prosthesis users, is also one of the main contributors for the high device rejection rates recorded [47]. This research will focus on the exploration of smart materials and structures suitable for being developed into intelligent interfaces between human tissue and machine materials, with the potential of being able to adapt to the patients' ever fluctuating conditions and alleviate deep sheer tissue injury. In addition, the innovative interface could be used as a communication channel for sensory feedback. Lastly, an attempt has been made to develop totally soft prosthetic sockets and assist devices in the form of smart clothing for elderly people, which would eliminate the hard-device-to-soft-tissue interface altogether.

The ultimate aim of this research is to develop new technologies with the use of smart materials and structures to highlight their potential in eradicating the problems associated with the body-device interface as detailed above. To address this aim we define the following objectives:

1. To explore the use and characteristics of different auxetic structures in a cylindrical shape as a potential metamaterial to improve the fit of prosthetic sockets

2. To develop wearable tactile devices able to convey non-intrusive information to the skin with the use of shape memory alloys (SMAs)

3. To develop a sensory feedback device for the potential use with upper limb prostheses

4. To explore the fabrication of smart textiles as a step towards making more discreet and comfortable smart wearable interfaces

Fig. 1.13 illustrates the areas of the body-device interface defined by the objectives where improvements can be made, along with the chapters of this thesis that will explore these areas further.

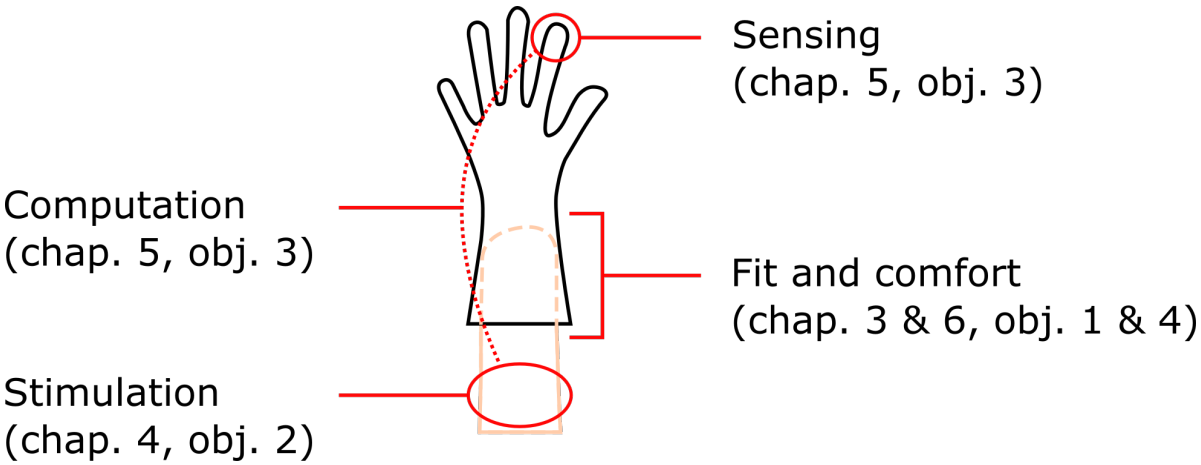

FIGURE 1.13. Areas for innovation to improve body-device interfaces and corresponding chapters.

1.6 Publications

Journals

- **Simons, M. F.**, Digumarti, K. M., Le, N. H., Chen, H. Y., Carreira, S. C., Zaghloul, N. S. S., Diteesawat, R. S., Garrad, M., Conn, A. T., Kent, C., Rossiter, J. (2021). B:Ionic Glove: A Soft Smart Wearable Sensory Feedback Device for Upper Limb Robotic Prostheses. *IEEE Robotics and Automation Letters*, vol. 6. no. 2, pp. 3311-3316.

- Haynes, A., **Simons, M. F.**, Helps, T., Nakamura, Y., Rossiter, J. (2019). A Wearable Skin-Stretching Tactile Interface for Human–Robot and Human–Human Communication. *IEEE Robotics and Automation Letters*, vol. 4, no. 2, pp. 1641-1646.

- Chen, H. Y., Diteesawat, R. S., Haynes, A., Partridge, A. J., **Simons, M. F.**, Werner, E., Garrad, M., Rossiter, J., Conn, A. T. (2019). RUBIC: An Untethered Soft Robot with Discrete Path Following. *Frontiers in Robotics and AI*, vol. 6.

Peer-reviewed Conferences

- **Simons, M. F.**, Haynes, A. C., Gao, Y., Zhu, Y., Rossiter, J. (2020). In Contact: Pinching, Squeezing and Twisting for Mediated Social Touch. *CHI EA '20: Extended Abstracts of the 2020 CHI Conference on Human Factors in Computing Systems*, pp. 1-9.

- **Simons, M. F.**, Digumarti, K. M., Conn, A. T., Rossiter, J. (2019). Tiled Auxetic Cylinders for Soft Robots. *2019 2nd IEEE International Conference on Soft Robotics (Robosoft)*, pp. 62-67.

1.7 Outline of Thesis

This thesis covers the following:

Chapter 2: This chapter details the relevant background information, with a critical evaluation of the papers read and concepts encountered. It provides an overview of the skin anatomy, exploring the challenges of skin interfacing with a device, and how we can utilise skin properties to our advantage. An introduction to some smart materials and structures are given, including haptic devices, auxetic structures, and auxetic textiles, which may be suitable for addressing the challenges identified at the body-device interface.

Chapter 3: This chapter considers the fit of prosthetic devices, addressing objective 1 (section 1.5). It explores the use and characteristics of auxetic structures as a metamaterial for potential wearable applications. The concept of Tiled Auxetic Cylinders (TACs) is presented, including their design, fabrication and characterisation.

Chapter 4: This chapter focuses on emotive touch in the form of haptic feedback, addressing objective 2 (section 1.5). TACs were used to create haptic interfaces and the emotive responses to these devices was recorded and presented here. We look at the use of these devices for everyday life.

Chapter 5: This chapter considers the lack of sensory feedback in prosthetic devices, addressing objective 3 (section 1.5). A new wearable tactile device is presented that relays pressure feedback to the user with use of simple non-silicon computation. Its potential use in prosthetic devices is explored.

Chapter 6: This chapter is an early study in investigating fit and comfort of smart wearable tactile devices, addressing objective 4 (section 1.5). We explore the potential of auxetic fabrics and how we can incorporate the auxetic structures explored throughout the previous chapters

into more wearable and comfortable designs. An attempt is made at fabricating auxetics fabrics and the difficulties encountered are discussed.

Chapter 7: This chapter concludes the overall findings of this thesis and considers developments for the future.

The order of the work presented here reflects the progression of the technology developed. In chapter 3, auxetic structures were considered due to their various inherent properties that make them desirable for wearable applications. These auxetic structures were considered in a cylindrical configuration to represent a piece of clothing worn on the body. These Tiled Auxetic Cylinders (TACs) actuate passively in reaction to the environment. In chapter 4, we consider these cylindrical auxetic structures with active actuation using the smart material shape memory alloys (SMAs), and investigate their interaction with the skin. We develop these haptic devices further in chapter 5 by considering their potential application to upper limb prosthetic devices. Lastly, in chapter 6, we consider the wearability of the devices presented and explore the fabrication of auxetic textiles.

CHAPTER 2

BACKGROUND

To fully understand the issues that occur at the body-device interface as summarised in chapter 1, more detail is provided of the biological (body) aspect. This chapter will investigate the problems associated with the body-device interface, along with innovative technology that has the potential of overcoming these. In addition, we discuss how this interface can also be used to its advantage in the form of sensory feedback, and explore some smart materials and structures that can be used for this.

2.1 Somatosensory System

The somatosensory system encompasses four sensory modalities; touch, temperature, proprioception and nociception. These somatosensory receptors are spread across and throughout the whole body including the skin, subcutaneous tissue, skeletal muscles, bones, tendons, and other internal organs [48].

2.1.1 Skin Anatomy

The skin is the largest organ of the human body and covers a surface area of approximately 1.5 – 2 m^2 for an adult. It provides us with the ability to perceive and interact with our surroundings and is a vital mediator for social interactions [49].

The skin can be divided into two categories; glabrous (hairless) skin found on the palms of our hands, fingertips, soles of our feet and pads of our toes, and hairy skin found essentially everywhere else. Skin is made up of an outer layer (epidermis) and inner layer (dermis) under which lies the subcutaneous tissue, all of which contain different receptors [48].

The three main categories of skin receptors are: mechanoreceptors for detecting physical changes of the skin such as that produced by pressure vibrations, stretch or light touch; thermoreceptors that can sense changes in temperature; and chemoreceptors which respond to chemical stimuli.

Fig. 2.1 illustrates the anatomy of the skin. Fig. 2.2 details the characteristics of the different mechanoreceptors found in the skin, including their location within the skin, the stimulus each senses and the perceptual function of this sense. It also provides a rough comparison of their receptive fields and indicates the receptors' stimulation threshold and adaptability. The diversity of mechanoreceptors which are distributed through the skin, in addition to the great surface area of the skin, makes it ideal for its potential use as a communication channel.

2.2 Haptic Perception

Haptic perception is directly related to the somatosensory system, described in section 2.1. It is the perception of the combined sensations received by the different somatosensory receptors present throughout the body. It can be divided into two categories: kinesthetic and tactile sensation [52].

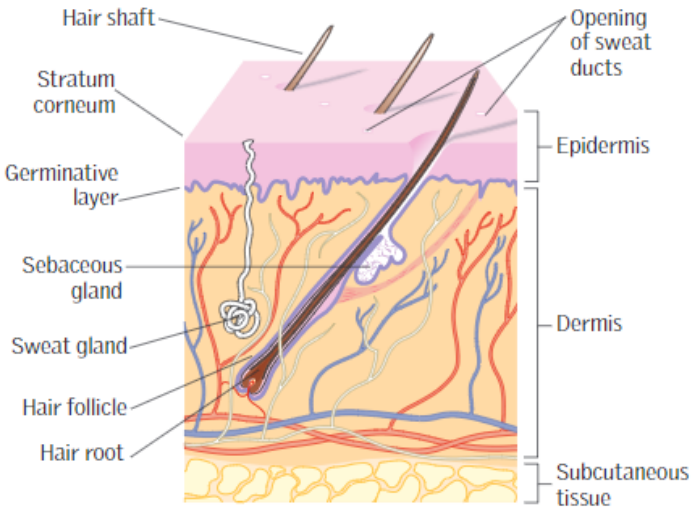

FIGURE 2.1. Diagram of skin anatomy illustrating the different layers of skin. Figure reproduced from [50].

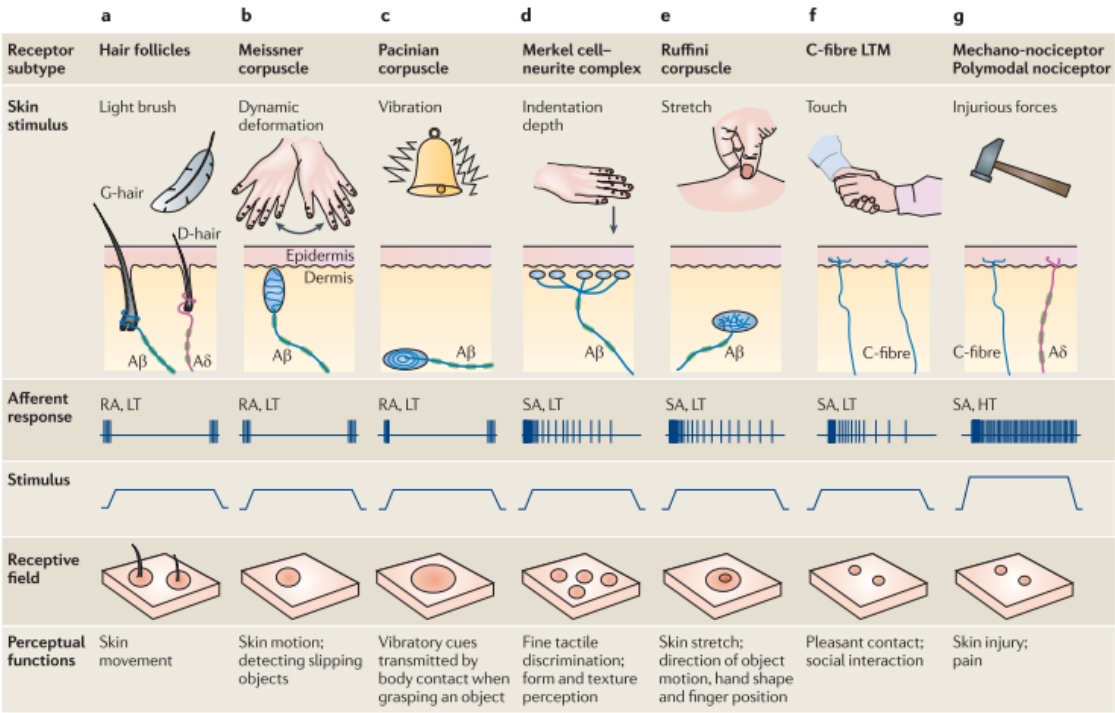

FIGURE 2.2. The characteristics of the different mechanoreceptors found in the skin. RA = Rapidly adapting; SA = Slowly adapting; LT = Low-threshold; HT = High-threshold; LTM = LT Mechanoreceptors; G-hair = Guard hair; D-hair = Down hair. Figure reproduced from [51].

Kinesthetic sensation refers to the movement of the body and the information received by receptors distributed in the muscles, tendons and joints; the dynamic attributes. When interacting with an object, the kinesthetic aspect relates to the position of, for example, a limb in space relative to the body and the size and weight of this object.

Tactile sensation, on the other hand, refers to touch and the information received by the receptors found in or just under the skin (fig. 2.2); the static attributes. This relates to the object itself, how it feels to touch, for example, in terms of texture and temperature.

The haptic interface is one which has been studied for many years in an attempt to exploit it as a means of manipulation or sensory feedback. For example, force feedback systems are used in robot-assisted surgeries to augment the virtual reality and increase outcomes by allowing the surgeon to 'feel' what they are doing [53]. This kinesthetic technology can also be used in exoskeletons to aid movement for, for example, rehabilitation therapy or people with muscle weakness [18] (section 1.1.2, fig. 1.6).

The majority of tactile feedback systems are vibrotactile. They are used successfully for many different applications, such as phone alerts or in virtual reality games [54] [55]. These sensory feedback devices predominantly target and activate the Parcinian corpuscles responsible for detecting vibrations (fig. 2.2c). However, the other receptors of the skin with different characteristics might be more desirable to target, depending on the application for the sensory feedback. The Parcinian corpuscles have a relatively large receptive field compared with the other mechanoreceptors of the skin. Hence when relaying sensory feedback to the skin where the user should be able to accurately pin-point the location of the source, Merkel cell-neurite complex (fig. 2.2d) or C-fibre LTM (fig. 2.2f) receptors could be more appropriate to target. In addition, Pacinian corpuscles are rapidly adapting, meaning that you are likely only to notice when the vibrations start and stop, but not during activation.

Sensory feedback for prosthetic use is also predominantly vibrotactile. Vibration motors are small and lightweight making them easy to incorporate into prosthetic devices. It has been utilised for different sensory modalities such as relaying grasping force [56] or used as a means to provide the user with a status of their prosthetic device, such as in the Hero Arm by Open Bionics™. Other methods used for providing sensory feedback include electrotactile feedback, mechanotactile pressure, temperature feedback, audio feedback and augmented reality [57].

The ideal characteristics for a sensory feedback technology would be portability, low weight, thinness, flexibility, durability, low cost and ease of manufacture. Wearable devices made from smart materials or fabrics may provide some, if not all, of these desired characteristics.

2.3 Emotive Touch

Touch is a predominant sense, not only for perceiving our environment, but also for social interactions. Our skin is a multimodal sensor capable of detecting touch, stretch, temperature, texture, vibration, pressure and pain [51, 54]. Haptic feedback as a form of sensory feedback has long been an area of interest and is still being explored. Applications include force feedback in virtual reality surgery [58], improving prosthesis-body interfaces in the medical field [57], and enhancing military training, augmented reality and immersive experiences in gaming [55]. A major challenge in current wearable tactile devices is the trade-off between the cost, comfort, and portability of the device, and its provision of a realistic feeling of touch [59].

Haptic wearable devices come in a wide range of shapes, sizes and interaction modalities, including insoles that aid navigation for the visually impaired [60], kinesthetic haptic feedback to guide a user's hand [61] and active pin arrays for laterotactile stimulation [62]. The majority are vibrotactile, where sensory information is relayed to the body by the use of vibrations with

differing frequency, amplitude, duration, and/or waveform [54, 63, 64].

Although an effective tactile interface modality, vibrations produced by motors are not a natural sensation, nor are they very localised. Vibrotactile stimuli activate the fast-acting mechanoreceptors (the Meissner and Pacinian corpuscles) within the dermis which have a relatively large perceptive field. Efforts have been made to anthropomorphise vibrotactile feedback such as the CheekTouch [65] and ForcePhone [66] which use vibration patterns to signify different social interactions. The TaSST is a vibrotactile sleeve used for mediated social touches [67] such as for conveying squeezing and stroking. Tsetserukou *et al.* [68] created a number of devices to elicit various human feelings. They used vibration to simulate tickling, shivering and butterflies in the stomach and a speaker on the chest conveyed the other person's heartbeat.

Despite these efforts to 'anthropomorphise' vibrotactile stimulation, these characteristics make them unfavourable for inter-person communication, where a more natural sensation of touch is needed. The importance of haptic feedback for inter-person communication has long been known [69, 70] and there is evidence to suggest that mediated social touch is processed in a similar way to real physical contact [71]. Applications include augmenting long-distance phone calls by enabling users to send and receive a "hug", aiding rehabilitation where the patient can feel the physiotherapist demonstrating the desired movement, and delivering non-interruptive notifications. Devices which deliver more natural, affective touch could also improve engagement in human-robot interaction.

Over the past decade, a number of devices have utilised skin stretching methods as alternatives to vibratory stimulation. Of these devices, those that were designed for affective touch or mediated social touch have aimed to simulate real human interactions. Stanley and Kuchenbecker [72] created wrist-worn devices to simulate four types of human touch; tapping, dragging, squeezing, and twisting. The sensations were generally found to be comparable to human touch

and participants reported that squeezing in particular felt natural and pleasant. Wang *et al.* created a servo-motor driven device that squeezes a listeners arm at specific times during a story. They found that it increased the listener's sense of connectedness with the storyteller [73]. Knoop and Rossiter [74] created a wearable wristband designed to gently stroke the user's skin as a method of conveying affection and emotion. Hamdan *et al.* [75] used SMAs attached to pads adhered to the skin in a number of ways to generate six different tactile sensations: pinching, directional stretching, pressing, pulling, dragging, and expanding.

Skin stretching has been shown to be superior to vibratory feedback to convey proprioception information [76] and all of these devices demonstrate the effectiveness of non-vibrational tactile sensations as an information channel. Skin stretching sensations activate the slow-acting mechanoreceptors (Ruffini endings and Merkel's disks) [76, 77] that have smaller receptive fields and process localised force information. Skin stretching is also capable of activating the CT afferents in human hairy skin which process social and affective touch [78]. This evidence suggests that vibrotactile stimuli alone may not be sufficient to simulate diverse and meaningful affective touch sensations. While skin stretching devices show considerable potential, the majority are powered by servomotors which are often bulky and noisy. In addition, the analyses of these devices do not explore the affective response of users to the device, such as the pleasantness of the sensations.

In chapter 4, we explore the use of Shape Memory Alloys (SMAs) to generate a more delicate and subtle haptic feedback mechanism. SMAs are lightweight, flexible and actuate silently, beneficial properties for use in an unobtrusive wearable device as exploited in tactile pin-arrays [79–81] and fingertip-mounted skin stretching devices [82].

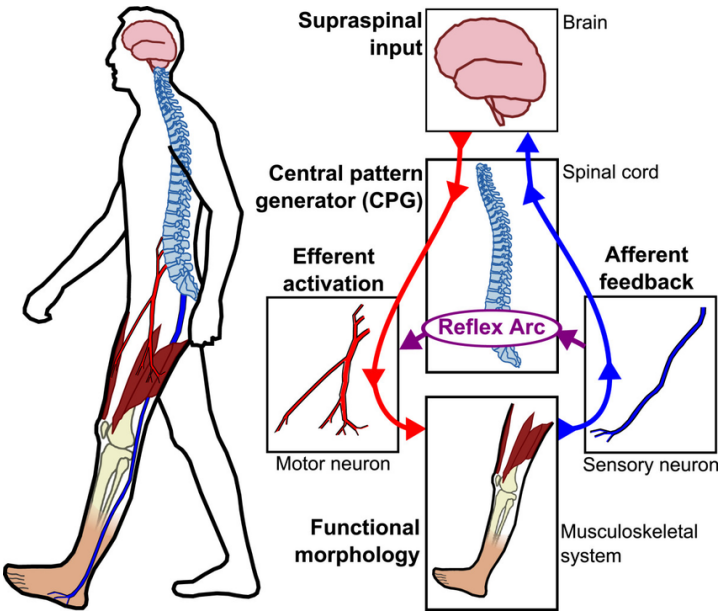

FIGURE 2.3. The human sensory-motor control loop. The efferent pathway is responsible for movement of the limb, and sensory information from the limb is sent to the brain via the afferent pathway. Figure reproduced from [83].

2.4 Sensory Feedback for Upper Limb Prostheses

The sensory-motor loop is a closed loop feedback system (fig. 2.3). An efferent pathway runs from the brain to the limb and is responsible for motor control (e.g. movement). Complementary to this is the afferent pathway which relays sensory signals from receptors in the limb to the brain and is responsible for sensory control [83].

Amputation leads to the disruption of this closed-loop system of the amputee. Both the motor and sensory functions are lost, significantly limiting their ability to perform daily activities and affecting their quality of life [84]. They may require physical and financial support, extending the impact on their family and friends.

Most prosthetic devices currently focus on reinstating the motor part of the missing limb, with less consideration of the sensory feedback that is a crucial part of the sensory-motor loop. For upper limb amputees, motor functions can be partially re-established by means of body-

powered or myoelectric devices (described in chapter 2). Restoring natural sensory functions remains challenging and the lack of sufficient sensing is a contributing factor to prosthetic devices generally being very poorly accepted by the user. Average rejection rates for upper limb prostheses range between 23% to 39% for adults and 32% to 45% for children, depending on their type of device. Electric devices are generally better accepted over passive or body-powered prostheses due to their increased aesthetic appeal and pinch strength, ease of operation, and lack of harness [47].

Lack of sensory feedback may also be a contributing factor to phantom limb sensation experienced by 60-80% of amputees [85–87]. This is where the person can 'feel' their limb despite it not being there and can become the site of phantom limb pain which is extremely difficult to treat. Although prevalence rates for phantom limb pain is higher for surgical amputees, interestingly this phenomenon is also experienced by congenital amputees (i.e. those born with a limb difference) [85]. Restoring this sensory feedback system and thereby closing the sensory-motor control loop could aid in reducing phantom limb pain, in addition to improving control of the prosthesis, and therefore increase acceptance [88, 89].

To address this lack of sensory feedback, efforts have been made to bridge the robot-body gap and deliver natural two-way communication between the amputees and their prostheses [57, 90]. A common technique to reinstate intuitive motor control of a myoelectric prosthesis is by electrodes placed on the skin of the residual limb which pick up electromyography (EMG) signals produced by the muscles when they are activated. For example, for a transradial amputee, surface electrodes can be placed on the skin overlying the flexor and extensor muscles of the wrist to control closing and opening of the electric prosthetic hand respectively. Targeted Muscle Reinnervation (TMR) is a technique where the severed motor and sensory neurons are redirected to muscles in the residual limb and chest. The reinnervated muscles act as amplifiers of the

original muscle signals sent from the brain to the missing limb. Additionally, this skin can be stimulated with sensory information which the amputee will perceive to be experienced on their missing limb [91]. This approach has been shown to increase embodiment and acceptance in upper limb amputees [89], however it is invasive and requires surgical interventions which could lead to complications.

The skin is a suitable target to act as a portal for direct communication with the pathways to and from the missing limb (shown in fig. 2.3). It is the largest sensory organ of the body and contains a range of cutaneous mechanoreceptors. These are widely distributed and are capable of detecting a multitude of stimuli including touch, vibrations, stretch, temperature, texture and pain [51] as described in chapter 2.1.

Many haptic interfaces currently focus on vibrotactile feedback. In upper limb amputees this increases their ability to grasp objects with their prosthetic arm without the need to rely on their vision [92, 93]. However, vibration receptors have a large receptive field (fig. 2.2), which severely limits spatial resolution and activity [51, 94]. Furthermore, vibrotactile feedback is disruptive to user concentration and may be less suitable for long-term stimulation [95, 96]. Research has therefore turned to other modes of cutaneous stimulation that can simulate more natural and localised sensations.

Receptors that respond to pressure have a much smaller receptive field than vibration receptors (fig. 2.2) [94] and can distinguish between closer stimulation sites on the skin [97]. Simple, purely mechanical designs have been created where the pressure experienced at the fingertips of the prosthesis are directly transmitted to the residual limb by use of air [98] or water [27]. When the prosthetic fingertip is deformed due to touch, the pressure inside the connected channels increase and result in deformation of specific membranes in contact with the skin. These direct pressure feedback systems can also be integrated into a prosthetic liner that sits between

the socket and the skin [99]. This prevents the need to cross through the prosthetic liner and potentially compromise on the suction required to keep the device fixed to the body.

Another modality of skin stimulation that has seen recent interest is skin-stretching. This can be achieved not only in the lateral direction - where orientation on the skin does not affect accuracy of stimulus detection [100], but also by twisting [101] or rolling something across the skin [102]. Skin-stretching can be used to provide proprioceptive information about the opening/closing of the prosthetic hand as seen in the Rice Haptic Rocker [103, 104]. The use of shape memory alloy (SMA) actuators for stretching the skin has become more common over recent years as they are lightweight, small, flexible and quiet and provide less intrusive feedback compared to vibrotactile stimulations [96]. They can be used in a variety of configurations to provide different tactile sensations, such as pinching, directional stretching, pressing, pulling, dragging, and expanding [75]. They can be used to provide squeezing pressure feedback in the form of tangential and shear forces, for example when wrapped around the wrist and finger [105]. The Tickler [74] is also worn around the wrist but utilises SMAs to move parallel bars laterally across the skin to generate natural and pleasant sensations.

2.5 Body-Device Interface

As mentioned in chapter 1, the main issues that arise from prolonged contact between soft tissue and hard devices include the formation of pressure points and the presence of excessive heat and perspiration. Other significant problems specific to prostheses users include improper fit of the prosthetic socket due to fluctuating residual limb volume changes, weight of the prosthetic device, and lack of device functionality [36]. We will now look at some of these problems in more detail, along with current solutions which aim to overcome these.

2.5.1 Pressure

One of the main problems with prolonged body-device contact is pressure. This is especially the case for those in hospital on prolonged bed rest, wheelchair users, and lower limb prosthesis users. Pressure and shear on the skin results in occlusion of the blood vessels and consequently necrosis (tissue death) due to the lack of oxygen and nutrients being supplied to the tissue. Furthermore, obstruction of the lymphatic system results in the added effect of being unable to remove metabolic waste products, which accumulate and also contribute to tissue damage. It is thought that pressure is accumulative, where a large amount of pressure applied for a relatively short amount of time could result in the same amount of damage as a small amount of pressure applied for a longer period. This tissue damage could ultimately lead to the formation of a pressure ulcer [106].

The progression of pressure ulcer formation can be seen in fig. 2.4. Stage 1 (2.4a) is characterised by redness of the skin that may feel hot. The skin is still intact. Once the skin breaks open, it has reached stage 2 (2.4b). At this point it may look like a blister and feels tender. Stage 3 (2.4c) is when this pressure sore progresses into the deeper tissue layers underneath the skin. Once the pressure injury reaches the underlying muscles, tendons and bones, it has reached stage 4 (2.4d).

The best solution to pressure ulcers is prevention, where the most successful technique is pressure relief. In order to restore tissue oxygen levels, the tissue needs to be completely unloaded for at least 2 minutes [107]. In UK hospitals this is done every hour for patients on prolonged bed rest and therefore at high risk of developing a pressure ulcer. Visual inspection of the skin is still the most commonly used method for early detection. Other technology does exist, however these prove to be too expensive to buy or to train medical staff, with no additional benefits

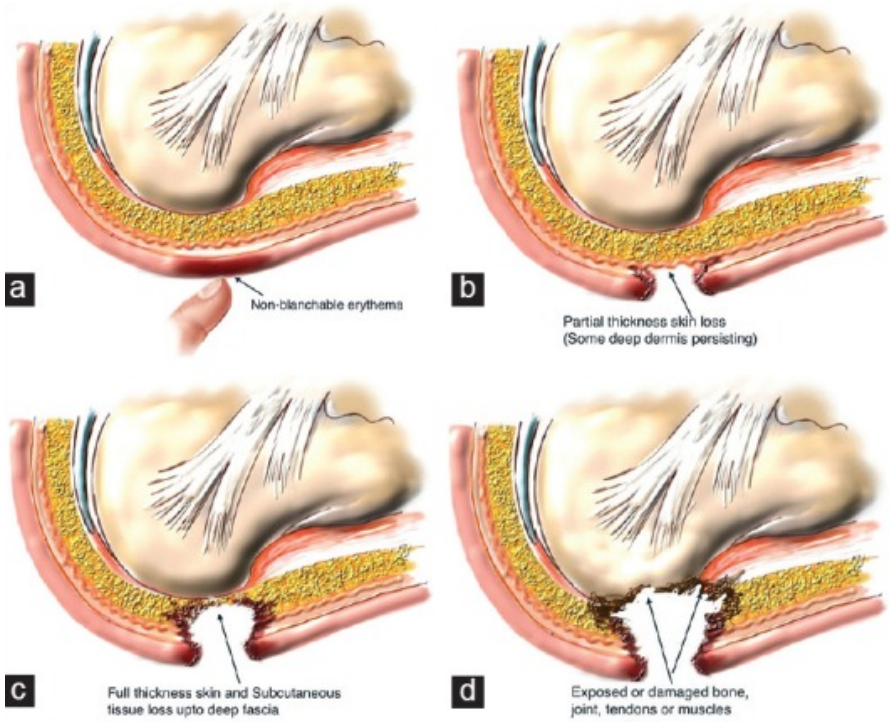

FIGURE 2.4. Diagram of the progression of pressure ulcers, from stage 1 to stage 4 (a-d). Figure reproduced from [106].

(verbal discussion with consultant at the Spinal Cord Injury Unit in London). For example, subepidermal moisture (SEM) scanners have been developed which measure localised oedema. This is particularly beneficial over visual inspection in patients with darker skin tones where redness of the skin, a marker of stage 1 (fig. 2.4a), is more difficult to detect [108]. However, the order, angle and site at which the measurements are taken can significantly affect the reading outcomes [109]. For example, transepidemal water loss is particularly noticeable in the skin of the heels after prolongoned loading, however there is no significant change at the sacral skin (at the bottom of the spine) [110].

Specialised hospital beds have also been developed to reduce the risk for patients of developing pressure ulcers, such as the Dolphin Fluid Immersion Simulation® system (Joerns Healthcare LLC) [111]. This mattress simulates fluid immersion by redistributing pressure with the use of

air to prevent compression of the tissue and occlusion of blood flow. Problems associated with this type of technology are their bulkiness, making them unfavourable for transport, and lack of postural control, making them unsuitable for translation into wheelchair cushioning.

For prosthetic devices, socket liners have been developed, predominantly made of silicone, such as Össur's Iceross® liners. These are designed to increase comfort and reduce friction of the socket with the skin. Newer technology includes moisture wicking capabilities, such as Blatchford's Silcare Breathe liners, which incorporate laser drilled perforations to allow moisture and heat to escape.

Another way to prevent pressure, heat and moisture build up is discarding the body-device interface all together. This has been achieved for prosthetic devices with osseo-integration, as mentioned in chapter 1. This technique consists of surgically embedding a rod-shaped implant into the length of the bone of the residual limb. The implant sits percutaneously, penetrating through the skin barrier, onto which a prosthetic device can be attached (fig. 2.5) [112]. This results in the prostheses being directly connected to the bone and therefore eliminates the need for a socket and eradicates the body-device interface and the problems associated with it. [113] found that compared with socket prosthesis users, those with osseointegration reported a higher prosthesis-related quality of life.

Unfortunately, osseointegration does have its own limitations, predominantly the high risk of infection at the site of the stoma, due to the skin being unable to heal and create a sealed barrier to the environment [115]. However, researchers have been turning to biological examples such as deer antlers which naturally cross the skin-barrier without the complication of infections, to investigate overcoming this [116].

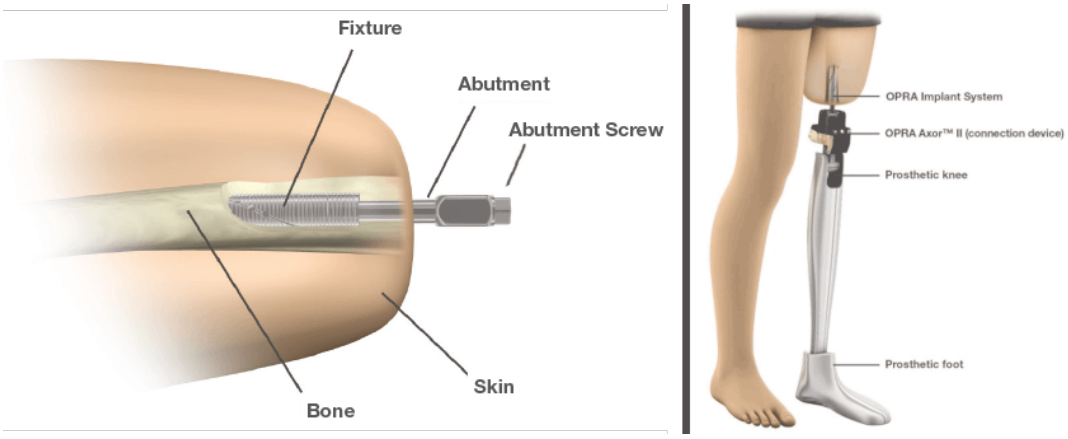

FIGURE 2.5. Image illustrating an osseointegrated implant (left) for attachment of a prosthetic device (right). Figures reproduced from [114].

2.5.2 Perspiration

Thermoregulation of the human body includes heat transfer by convection, radiation, evaporation, and conduction. Vasodilation of the cutaneous blood vessels results in increased heat dissipation to the environment. In addition, evaporation of sweat released from sweat glands in the dermis layer of the skin (fig. 2.1) causes a decrease in skin temperature. Unfortunately, these methods of temperature regulation can be disturbed when in contact with another surface, especially when this surface is made of non-breathable materials which is generally the case for mobility aids. Prosthetic sockets for example tend to be constructed from thermoplastics. In the case of amputees, the reduced surface area of their skin can also impact their body's ability to regulate its temperature [117, 118]. This increase in temperature and moisture can lead to numerous dermatological conditions, including maceration of the skin, friction blisters and unpleasant odours, and it creates a favourable environment for bacterial growth that could lead to infection. The issue with thermoregulation of the residual limb can be particularly problematic for those that live in hot and humid environments, as is the case for most developing countries [119].

Innovative prosthetic sockets have been generated that aim to restore temperature regulation

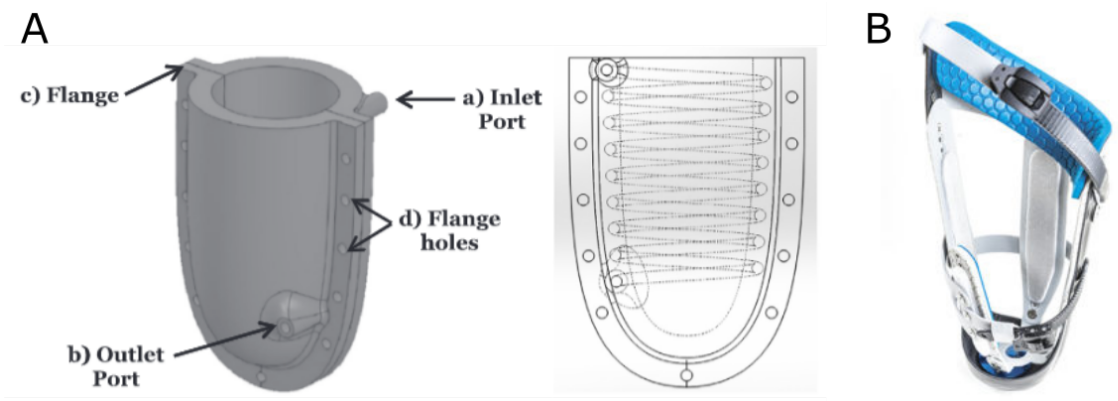

FIGURE 2.6. Innovative prosthetic sockets aimed to reduce temperature and perspiration of the residual limb. (A) A helical channel throughout the prosthetic sockets allows greater heat exchange with the environment with cross-sectional view (A). The socket-less socket by Martin Bionics (B). Figures reproduced from [120] and [121] respectively.

of the residual limb. [120] created a prosthetic socket that included a helical cooling channel that was shown to create a greater temperature drop across the socket wall compared with the control (fig. 2.6A). Other developments include the "socket-less socket" which is an open socket design. It is constructed from minimal material with open panels to allow heat exchange (fig. 2.6B) [121]. This simultaneously makes it very light-weight, addressing another issue discussed in more detail in section 2.5.4.

2.5.3 Limb Volume Fluctuation

The lymphatic system works to maintain fluid balance in the tissues of the body by providing a transport system between the blood vessels and the interstitial space of the tissues. It also aims to support the body's immune system to help fight infections [122, 123]. After amputation, the lymphatic system is compromised and cannot perform its functions adequately. This can lead to oedema in the residual limb and results in significant fluctuations in the residual limb volume [124]. An increase in residual limb volume would lead to high pressure inside the socket and a

decrease in residual limb volume would lead to displacement and pistoning within the socket [125].

The prosthetic socket mechanically couples the body to the prosthetic device. It requires a perfect fit with the residual limb to ensure the best level of control. Conventional prosthetic sockets constructed from thermoplastics are hard structures and therefore cannot accommodate any change in volume of the residual limb, affecting both control of the prosthetic device and comfort. To accommodate these fluctuations in residual limb volume, amputees tend to add or remove liners or socks from their residual limb. More adaptive sockets would improve everyday use. Bladders can be inserted into the prosthetic socket that can be filled with air or water to adjust the fit without the need for taking off the socket [119, 126]. Other solutions include using an open socket design, like mentioned in section 2.5.2, that allows tightening or loosening of the socket with the use of straps (fig. 2.6B) [121]. Research is currently being undertaken exploring the use of auxetic materials to accommodate fluctuations in residual limb volume [127]. This will be explored further in chapter 3.

2.5.4 Prosthesis Weight

[36] found that prostheses wearers ranked 'reducing prosthesis weight' as the top design priority. More recent developments in prosthetic devices recognise this need. The Hero arm developed by Open Bionics weighs less than 1kg for a full trans-radial prosthetic arm (fig. 2.7A) [128]. This arm is 3D printed from plastics which make it lightweight. Another material that is becoming popular is carbon-fibre, such as seen in Össur's Re-Flex prosthetic foot (fig. 2.7B) [129]. Carbon fibre is favourable as it is lightweight, strong and durable, however it is more expensive compared with conventional materials [130].

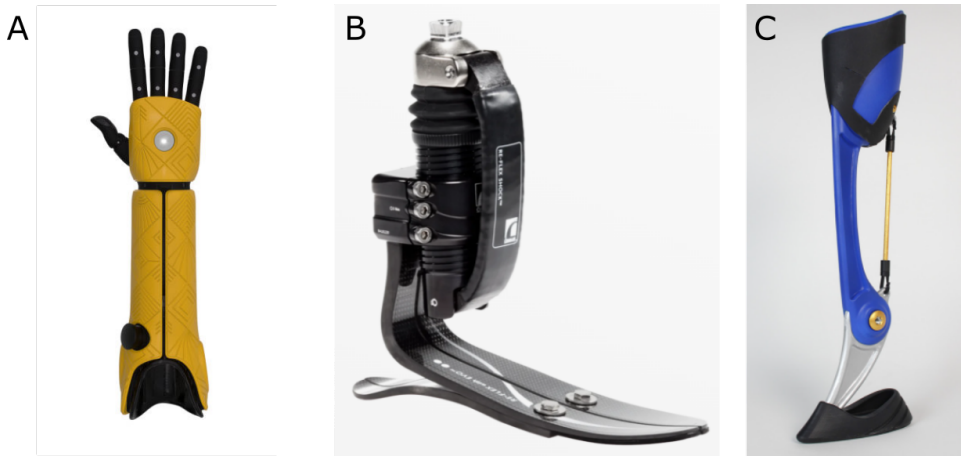

FIGURE 2.7. Lightweight prostheses (A and B) and sport-specific prosthetic leg (C). (A) Hero Arm by Open Bionics which is 3D printed from plastic. (B) Össur Re-Flex prosthetic foot constructed from carbon fibre. (C) KLIPPA prosthetic leg for rock climbing, inspired by mountain goats. Figures reproduced from [131], [129] and [132] respectively.

2.5.5 Prosthesis Functionality

The desired functionality of prosthetic devices depends on the type of device. For example, [36] found that upper limb amputees with active prostheses desired the gripping function of the prosthetic hand the most, followed by steadying and manipulation. Whereas, those with passive prostheses favoured appearance the most. Therefore, trying to address the lack of functionality in prosthetic devices needs to be tailored to the type of device. Custom prosthetic devices have also been made for specific sports or hobbies. The KLIPPA prosthetic leg is designed for rock climbing, inspired by mountain goats (fig. 2.7C) [132]. However, it is currently a proof-of-concept and not yet available commercially.

2.6 Auxetic Structures

Auxetic structures are a class of metamaterials, materials which are designed to possess specific desired mechanical characteristics. They have a negative Poisson's ratio and this auxetic effect

may be present in the macro-, micro-, or nano-structure [133].

The Poisson's ratio (ν) is the negative of the ratio between the lateral strain (perpendicular to the force) and the longitudinal strain (parallel to the force) (equation 2.1), where the strain (ε) is the change in length divided by its original length (equation 2.2). The Poisson's ratio for 3-dimensional isotropic solids ranges between -1 to 1/2 [134]. This can be used to determine whether a structure is auxetic or non-auxetic, where an auxetic behaviour is characterised by a negative Poisson's ratio as the lateral strain increases with increasing longitudinal strain [135].

$$\nu = -\frac{\varepsilon_{lateral}}{\varepsilon_{longitudinal}} \tag{2.1}$$

$$\varepsilon = \frac{\Delta L}{L} \tag{2.2}$$

2.6.1 Categorisation

There are many different shapes and structures that can give this auxetic effect. These can be broadly classified into three sub-groups, depending on their mechanism of deformation; re-entrant, rotating, and chiral [136].

2.6.1.1 Re-entrant

The re-entrant types are created when certain beams of the structure are folded in on themselves on loading. One of the most common type is the re-entrant hexagon seen in fig. 2.8. When stretched, the beams unfold and the angle of these beams with the vertical (θ) will decrease, effectively increasing the area of each auxetic unit. Fig. 2.8 (left) illustrates the overall behaviour

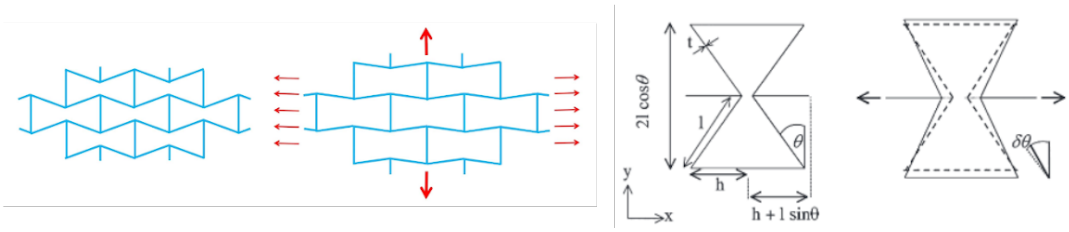

FIGURE 2.8. (Left) The overall behaviour of the re-entrant hexagon. (Right) The behaviour of a single re-entrant hexagon unit as modelled by Masters & Evans [138]. Figures reproduced from [137] and [139] respectively.

of a re-entrant hexagon structure [137]. This behaviour was first modelled by Masters & Evans [138] and is shown in fig. 2.8 (right) [139].

2.6.1.2 Rotating

In rotating auxetics, the rotating geometries do not change shape in themselves as seen with the re-entrant types. Instead, they rotate around a hinge point where two geometries meet. Fig. 2.9 illustrates the model of the rotating squares [140]. One auxetic unit is depicted by four rotating squares, illustrated by the dark grey in fig. 2.9. The length of the sides of the squares (l) remains constant, however the angle between two connecting squares (θ) changes as the structure is being stretched. A prototype of a rotating auxetic structure was created and shown in fig. 2.10. The beams are made from bending straws with slits to pre-determine bending location.

2.6.1.3 Chiral

Chiral structures work by beams curling around a central node and elongating when stretched to create a longer gap between the nodes. Fig. 2.11 illustrates the model for the hexachiral honeycomb [134] (taken from [141]). A range of n-chiral auxetics are possible by altering the number of node-to-node connections.

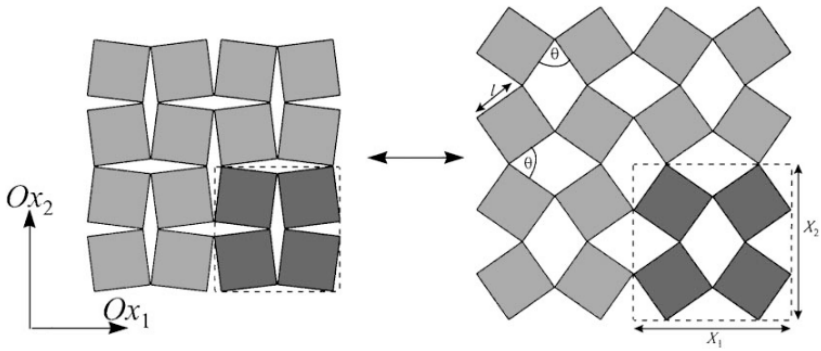

FIGURE 2.9. Model of the rotating squares structure. The length of the sides of the squares (l) remains unchanged, whereas the angle between two connecting squares (θ) changes with tension, increasing the size of one auxetic unit (shaded in dark grey). Figure reproduced from [140].

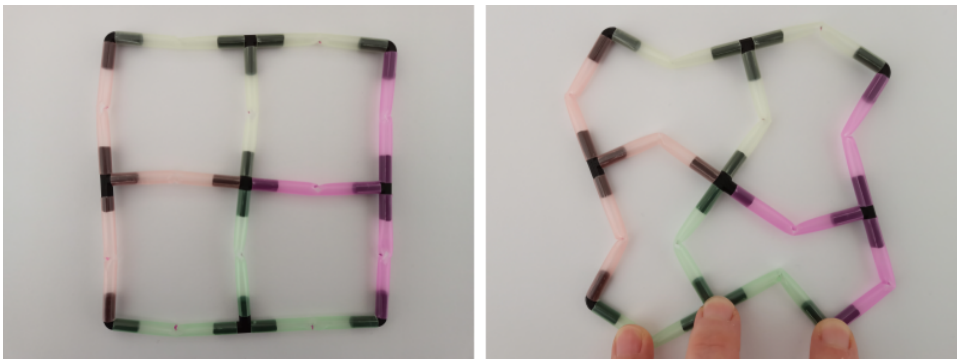

FIGURE 2.10. Rotating auxetic prototype at rest (left) and when compressed (right).

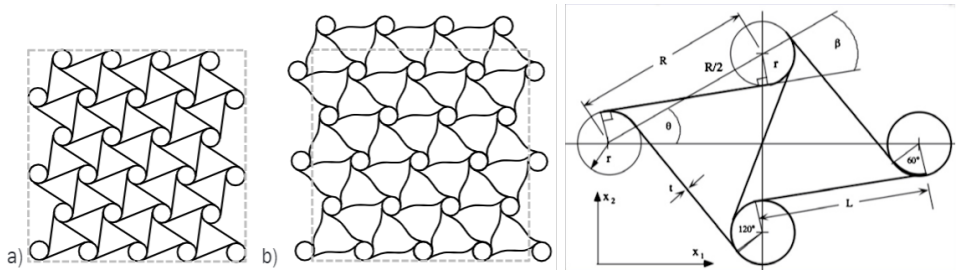

FIGURE 2.11. (Left, a and b) Chiral honeycomb behaviour and (right) parameters as modelled by [134]. Figures reproduced from [11] and [141] respectively.

2.6.2 Applications

The negative Poisson's ratio of auxetics embodies interesting behaviours which can be applied in a number of different fields. In the medical field, auxetics have been used to create cardiovascular stents. These are small structures which open up or support a blood vessel and therefore need to be strong and easily transportable through blood vessels for placement. [142] developed a self-deployable stent which achieved its auxetic nature by the use of origami. Auxetics can also be beneficial in the creation of prosthetic blood vessels. When a weak point presents itself along a blood vessel, the blood inside the blood vessel causes the vessel walls to distend. In the normal (non-auxetic) case, this stretch of the vessel walls would result in them becoming thinner and therefore even weaker. In an auxetic blood vessel, this distension would result in the vessel walls thickening and creating more support (see fig. 2.12, 1) [143].

Another area in which auxetics have proved to be useful is in the use of various construction components. An auxetic nail created by Ren *et al.* [144] uses the auxetic nature to make the nail easier to push in as the nail narrows, but harder to pull out as the nail widens (fig. 2.12, 2). This same mechanism is why corks are used for bottles. They have a Poisson's ratio that is very near 0 and therefore as it is pushed in to plug the bottle, it does not expand sideways which would make it more difficult [145, 146]. Filters have also been made using auxetic structures with the advantage that they are easier to unclog from any dust or dirt [147, 148]. This mechanism can also be used for bandages to cover wounds or swelling [149], where the auxetic units prevent the passing through of particles until stretched on cleaning or with swelling respectively (fig. 2.12, 3).

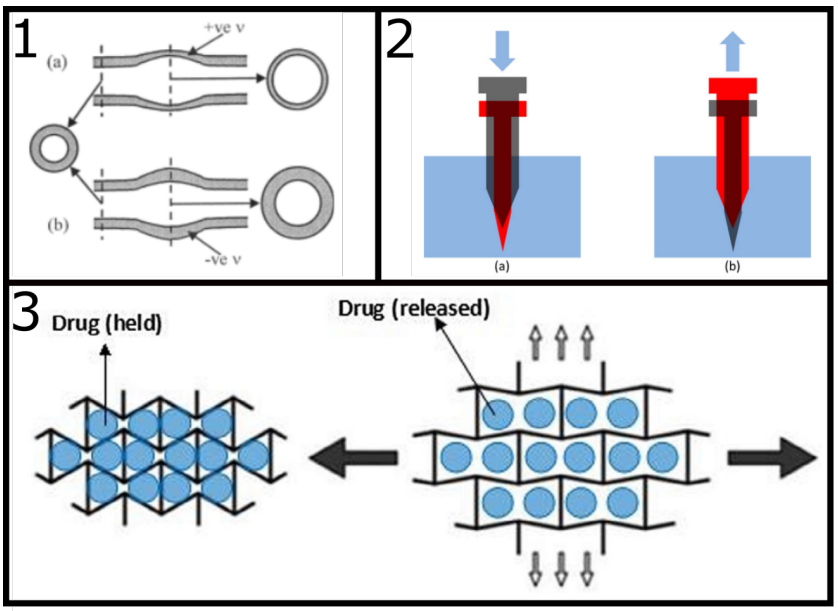

FIGURE 2.12. 1) Illustration of a non-auxetic prosthetic blood vessel (a) and an auxetic one (b). As blood distends the vessel wall, the non-auxetic wall becomes thinner and therefore weaker, whilst the auxetic wall becomes thicker and therefore stronger meaning it is less likely to rupture at this weak point. 2) Illustration of how an auxetic nail may make it easier to push in (a) but harder to pull out (b). Grey = before deformation, red = after deformation. 3) Illustration of how an auxetic can be used as a filter or medical bandage for easy cleaning or release of drugs on swelling respectively. Figures reproduced from [143], [144], and [149] respectively.

2.6.3 Additional Properties

In addition to this counter-intuitive auxetic effect, auxetics have a number of other properties, including high indentation resistance, synclastic (dome) shaping abilities, and enhanced acoustic absorption [133, 150].

2.6.3.1 Indentation Resistance

The indentation resistance of auxetic structures increases when exposed to an external force, as opposed to non-auxetics where the opposite occurs. As explained in [143], the indentation resistance (H) is proportional to $[(1-\nu^2)/E]^{-x}$, where ν is the Poisson's ratio, E is the Young's modulus, and x depends on the pressure distribution which is equal to 1 when this pressure

distribution is uniform. Therefore, the indentation resistance is the same for non-auxetic and auxetic solids with the same Young's modulus when ν tends to 1/2 or -1/2 respectively. ν=1/2 is the limit for non-auxetic samples, whereas auxetics can decrease their Poisson's ratio further to -1. As ν tends to -1, the indentation resistance will tend to infinity. Hence increased indentation resistance of auxetics compared to non-auxetics occurs at $-1 \leq \nu \leq -1/2$. Fig. 2.13 (A) shows an illustration of the indentation resistance behaviour of a non-auxetic compared to an auxetic material [12].

[151] measure the different characteristics including stiffness, energy absorption, indentation and impact stiffness of auxetic and non-auxetic structures and clearly shows the auxetic (specifically the re-entrant honeycomb) outperforms the other structures in terms of resisting indentation. This increased indentation resistance gives auxetics a shock absorbing nature, making them ideal for use in the sport industry in protective equipment [152]. They can be made into auxetic foams and incorporated into helmets and the soles of running shoes [145, 153]. Auxetic foams can also be used for seating furniture for use in offices or in the healthcare sector, such as wheelchairs or mattresses, especially for those who require them for long-term use [154, 155]. Fig. 2.13 (B) illustrates the forces involved in sitting on a conventional and auxetic foam respectively. In a conventional foam, the internal forces (P_i) are directed outwards. This creates shear forces (T) on the body that can lead to skin degradation as explained in chapter 2. In contrast, the internal forces in the auxetic foam are directed inwards and eliminate these undesirable shear forces.

2.6.3.2 Synclastic Formation

The synclastic nature of auxetics is shown in fig. 2.14. In a non-auxetic structure, out of plane bending in one axis will result in curving of the perpendicular axis in the opposite direction i.e.

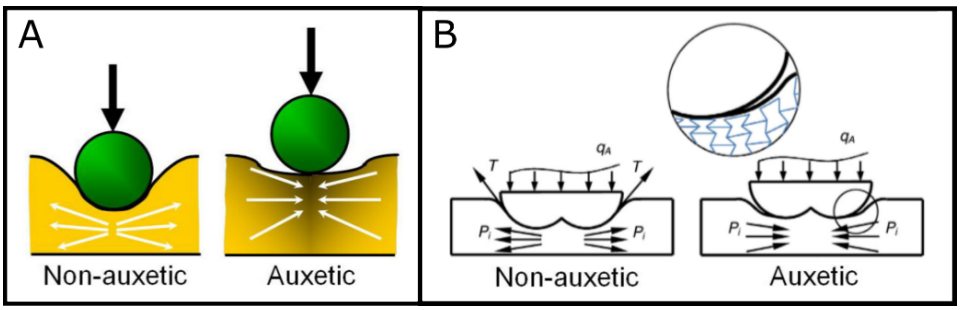

FIGURE 2.13. (A) Illustration of the indentation resistance behaviour of a non-auxetic compared to an auxetic material. As the material is being subjected to an indenting force, the non-auxetic material moves laterally, making it easier for the force to indent, whilst the material of the auxetic comes in, creating a more dense area and preventing the force from indenting as much. (B) Illustration of the forces involved in a seat support constructed from conventional foam compared to auxetic foam. q_A=Indent force, P_i=Internal foam forces, T=Shear force. Figures reproduced from [12] and [154] respectively.

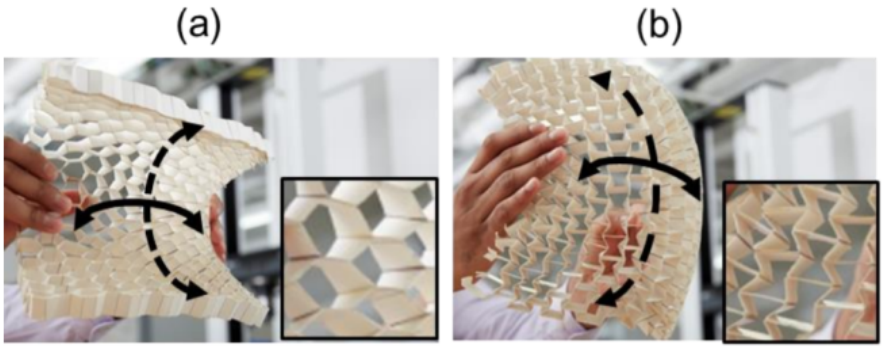

FIGURE 2.14. Image showing saddle curvature of a non-auxetic structure (a), and dome or synclastic curvature of an auxetic structure (b). Figure reproduced from [156].

a saddle shape is formed. In the case of auxetics, the second axis bends in the same direction as the first, created a dome shaped structure. This is beneficial for wearable items as they can easily conform to shapes around the body [156]. This out-of-plane bending can also be tuned by varying the thickness or infill of the linear beams of the auxetic elements along a planar sheet [157]. This auxetic behaviour is not only functional but also aesthetically pleasing and has been seen in architecture [157, 158] and fashion (such as in shoes [159] and clothing [149]).

2.6.3.3 Acoustic Absorption

The acoustic behaviour of auxetic foam is quantified in numerous papers [160, 161]. [162] showed that higher convoluted foam (e.g. auxetic foams) showed lower cut-off frequencies (i.e. where the phase velocity of acoustic waves tends to zero as frequency increases). This means they are better are absorbing sound and illustrates the potential use of these for noise dampening applications.

2.6.4 Tunability

To increase the scope of auxetic applications further, auxetic structures are also highly tunable. For example, they can be combined with non-auxetic structures to generate a Poisson's ratio of 0. This means that the width remains constant when stretched along its length. Fig. 2.15 illustrates the individual and combined effects of a hexagon and a re-entrant hexagon unit [13].

One such application of this hybrid effect can be seen in a medical setting where they are used for cardiovascular stents (fig. 2.16) [13]. Non-auxetic diamond shaped stents shorten in length on expansion of the structure. Incorporating an auxetic structure to create a hybrid stent results in the negative Poisson's effect of the auxetic structure cancelling out the positive Poisson's effect of the non-auxetic structure and therefore the length of the stent remains unchanged after expansion. This is beneficial to reduce stresses in the stent and therefore the blood vessel walls and reduces the risk of the blood vessel narrowing again.

In a similar vein, a programmed hybrid planar sheet was designed in [163] to conform to objects of varied shapes which could be beneficial for wearable applications as anatomical shapes will vary per person.

In [164], a 3D auxetic lattice was used in combination with a non-auxetic lattice to create soft locomotion in a pipe-climbing robot (fig. 2.17). As the linear actuator pushes on both 3D lattices,

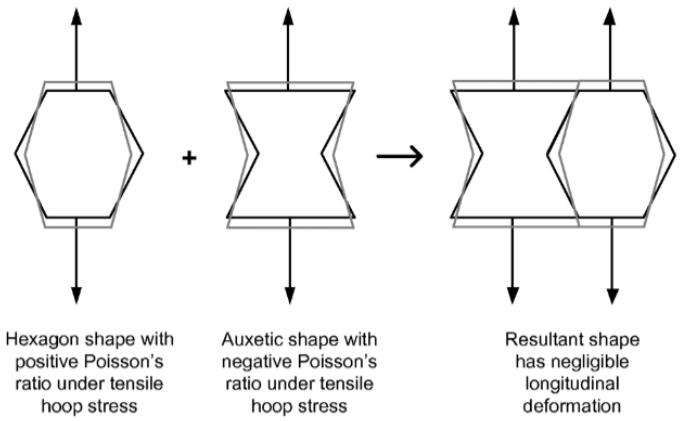

FIGURE 2.15. Illustration of the configurational changes experienced by a non-auxetic and auxetic unit and a combination of the two. Figure reproduced from [13].

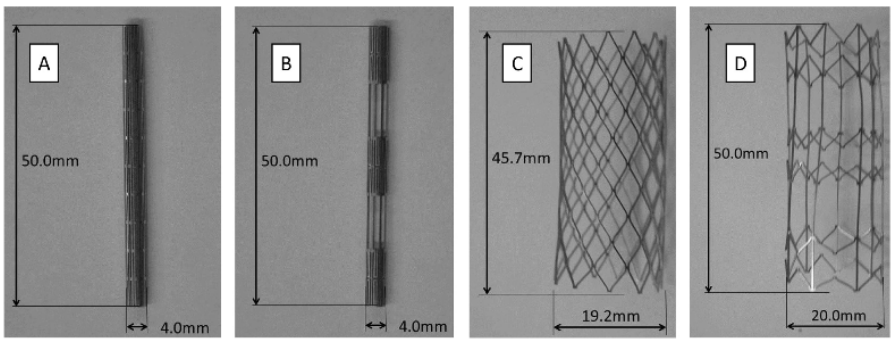

FIGURE 2.16. Cardiovascular stents. Comparison of a non-auxetic diamond shaped stent (A & C) with a hybrid auxetic stent (B & D) before and after expansion respectively. Note that the non-auxetic stent shortens in length, whereas the auxetic hybrid remains constant. Figure reproduced from [13]

the non-auxetic structure expands and acts as a clamp whilst the auxetic structure compresses down to allow it to be pushed through the pipe. Conversely, as the linear actuator pulls on both 3D lattices, the auxetic structure now acts as a clamp whilst the non-auxetic structure compresses to allow it to be pulled up the pipe.

The stiffness of auxetic structures can also be tuned by a variety of different methods. In [165], stiffness of a chiral auxetic structure can be altered by varying the angle of inter-hub connections. Kirigami and origami techniques have also been shown to allow the tuning of stiffness of auxetic

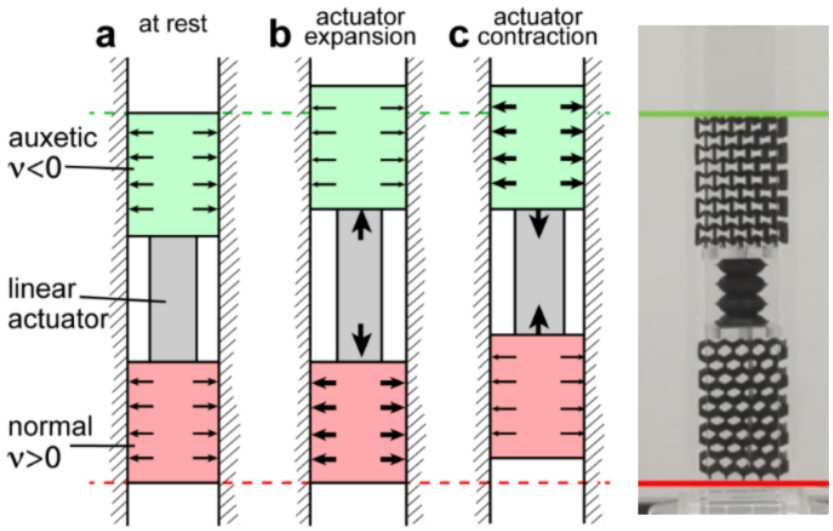

FIGURE 2.17. Soft robot with auxetic and non-auxetic lattices for climbing through a cylinder. (Left) Schematic of the concept; (Right) Prototype of soft robot. Figures reproduced from [164].

patterns, where stiffness can be tuned in specific isolated regions. This can be particularly useful in biomedical applications such as for minimally invasive surgeries [166].

Tunability of auxetics can also be achieved by modifying the location and angle of the hinges. Using dual material to create auxetic structures, where the hinges are made of a flexible material and the beams are made of a rigid material, allows for specifying the exact bending configuration. Fig. 2.18 illustrates the different types of transformation generated using this technique by [15]. By combining various transformations together they managed to create structures with higher-level deformations, such as encoded displays, a self-folding cube with a single direction of force, and the generation of a helmet that fits neatly around the head. Dual material auxetics have also been shown to increase the stability of the negative Poisson's ratio over single material auxetics as buckling of the beams are prevented [167].

Another mechanism to tune auxetics is by specifying which auxetic units buckle on loading which can generate desired deformations [168, 169]. More recently, sets of handed auxetics

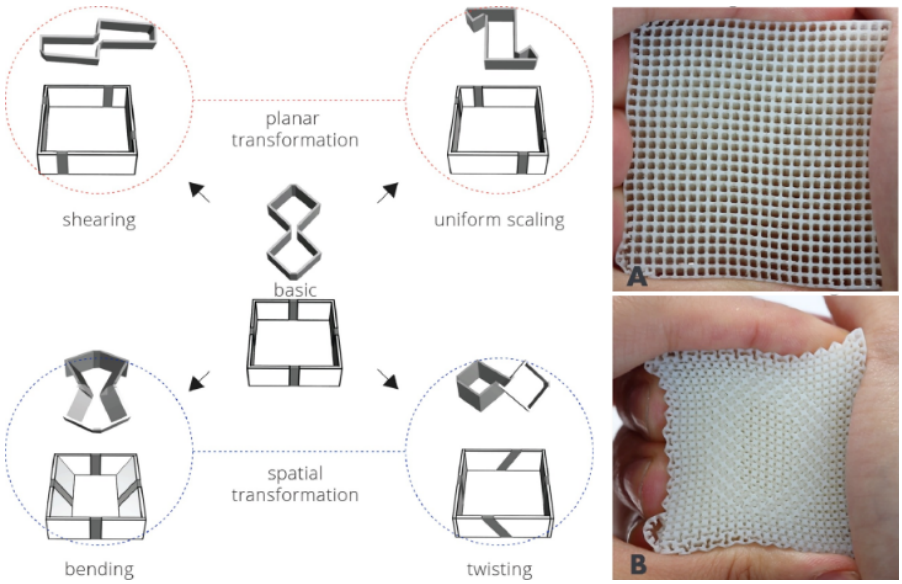

FIGURE 2.18. Auxetic structure with tunable shape-changing technology. Figure reproduced from [15].

[170] have been proposed which can bend in opposing directions as a possible alternative to conventional soft robot actuators such as pneumatic networks [171].

Altering certain parameters of single auxetic units within a structure, such as the length of the beams and the angle between them, can also enable tuning. Especially when combined in parallel or series with other units, certain behaviours such as localised bending and radial expansion can be achieved [172].

Lastly, bistability can be introduced to auxetic structures. This is where there are two stable low energy states, for example when the auxetic structure is fully contracted and fully expanded [14, 173, 174]. This can be especially advantageous for deployable applications.

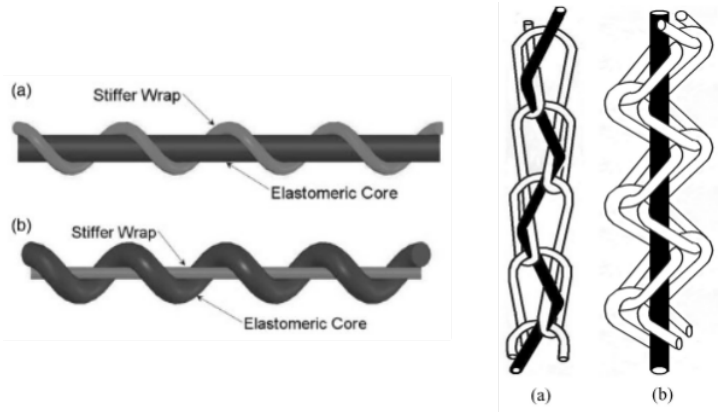

FIGURE 2.19. Mechanism of action of auxetic yarn (left) and warp-knitted fabric (right); relaxed (a) and stretched (b). Figures reproduced from [175] and [176] respectively.

2.7 Auxetic Textiles

Smart fabrics have generated a lot of interest recently. They are fabrics which can react to the environment, either passively or actively. Many different mechanisms and materials can be used to make fabrics "smart", and the resulting materials have many different applications.

The auxetic nature of auxetic textiles can be achieved either on the micro- or macro-scale. Auxetic yarns have been studied that use two fibres of different elasticity, where the stiffer one is wrapped around the elastic core. As the stiffer fibre gets pulled, it straightens and the softer fibre stretches so that it is now wrapped around the stiffer one (fig. 2.19, left) [175]. In a similar vein, [176] created a warp-knitted structure consisting of loops through which another yarn is threaded. As this yarn is pulled, the loops extend laterally as they become wrapped around it (fig. 2.19, right).

On a larger scale, auxetic textiles can also be created by generating auxetic geometries (such as those seen in chapter 3 or origami/kirigami patterns with auxetic effects) out of conventional non-auxetic yarn or fabric (see fig. 2.20).

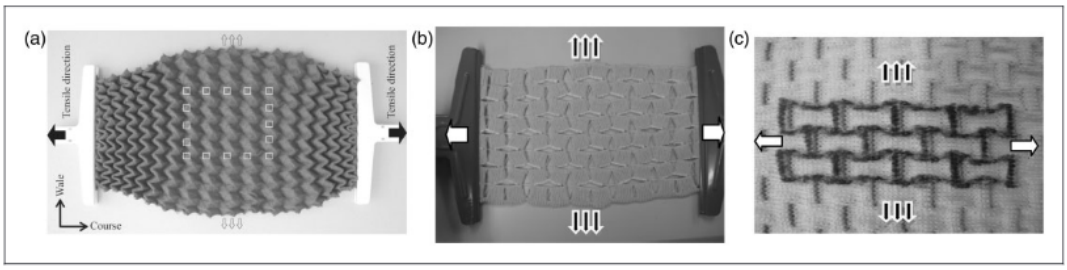

FIGURE 2.20. Auxetic textiles generated with the use of different auxetic geometries; miura ori origami pattern (a), rotating squares kirigami pattern (b), and re-entrant hexagons (c). Figure reproduced from [175].

FIGURE 2.21. Auxetic t-shirt generated by using conventional material to create an auxetic geometry that can grow with the wearer. Figure reproduced from [149].

2.7.1 Applications

The techniques described above can be used to create auxetic textiles which in turn can be developed into wearable clothes. This can be especially beneficial for children's clothes or maternity wear to accommodate the fast growth of children and reduce pressure on the abdomen of pregnant women that can be experienced with the elasticated clothing generally worn (fig. 2.21) [149].

Due to the synclastic nature of auxetics, auxetic fabrics can also be used to create clothing that tailors to the curvature of the body. [159] cut thin kirigami slits into a sheet of leather to create triangular linkanges that can rotate to give the desired auxetic property. As can be seen in

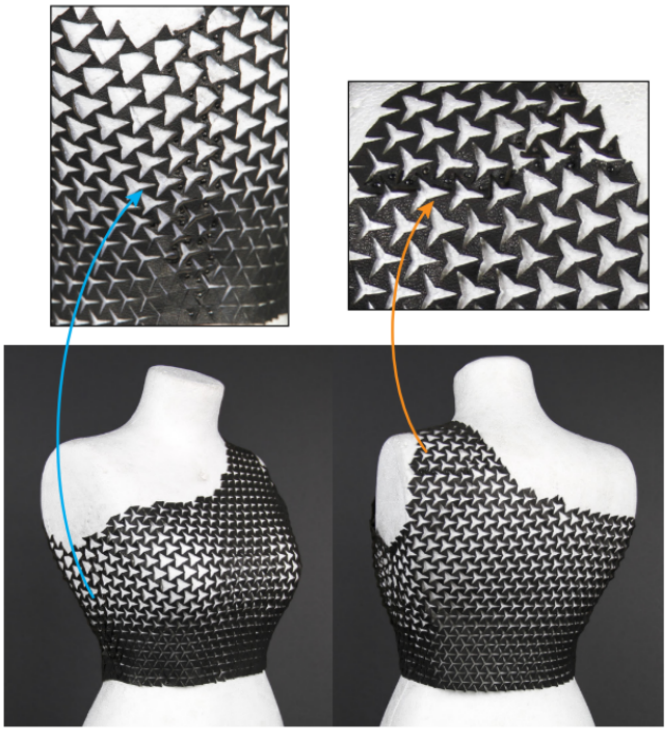

FIGURE 2.22. Top with a triangular linkage auxetic design that allows it to tailor to the wearer's curves. Figure reproduced from [159].

fig. 2.22, the auxetic top fits neatly around the bust and waist, both with significantly different circumferences.

Other applications of auxetic textiles include those within healthcare. Auxetic fabric could be used to create a medical bandage that contains a drug or medicine of some kind. This smart bandage can be wrapped around a wound, which will then expand as the wound swells, opening up the pores in the bandage and releasing the drug held within. Once the wound has healed and the swelling has gone down, the bandage will shrink and prevent any more release of the drug. Fig. 2.23 illustrates this sequence of events [175].

Chapter 6 explores the potential advantage of auxetic fabrics over conventional ones, specifically to increase comfort, and demonstrates a number of different fabrication methods.

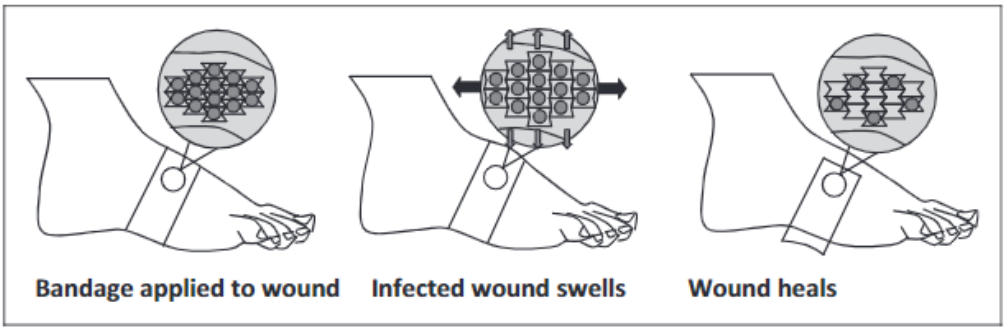

FIGURE 2.23. Auxetic medical bandage. As the wound swell, the auxetic nature of the bandage opens up its pores, allowing wound-healing drugs contained within the bandage to release. As the wound heals and reduces in swelling, the bandage contracts and prevents any further release of the drug. Figure reproduced from [175].

2.8 Summary

This chapter explored the background information relevant for the following chapters. An overview was given on the anatomy of the skin and its receptors. The use of the skin for haptic feedback was explored. Issues at the body-device interface were established and each issue was discussed, along with innovative technologies that could potentially overcome these. An introduction was given to auxetic structures and textiles, with a consideration of their properties that make them favourable for wearable applications. This serves as the background required for the following chapters which look at auxetics (chapter 3), emotive touch (chapter 4), sensory feedback (chapter 5), and auxetic textiles (chapter 6). A summary of the background information is presented in table 2.1, along with the chapters in this thesis to which this information is most relevant.

In the next chapter we will explore how comfort and fit of wearable devices, such as prostheses, can potentially be improved through metamaterials. More specifically, chapter 3 will focus on auxetics as a metamaterial, where we develop a tiled auxetic cylinder (TAC) as a first step towards a wearable auxetic sleeve.

Area of Literature Review	Summary	Relevant Chapters
Somatosensory System	Skin anatomy and its receptors	Chapters 4 and 5
Haptic Perception	Haptic perception overview and examples of devices in literature	Chapters 4 and 5
Emotive Touch	Review of haptic devices for affective touch in literature	Chapter 4
Sensory Feedback For Upper Limb Prostheses	Motivation for sensory feedback in upper limb prostheses	Chapter 5
Body-Device Interface	Challenges at the body-device interface where improvements need to be made	Chapter 5
Auxetics	Properties of auxetic structures which make them favourable for wearable applications	Chapters 3 and 6
Auxetic Textiles	Potential of auxetic textiles as a smart fabric	Chapter 6

TABLE 2.1. Summary of the different areas reviewed in the literature and the chapters in the thesis to which they are most relevant.

CHAPTER 3

ADAPTIVE METAMATERIALS FOR WEARABLES

Fit and comfort of prosthetic sockets is a critical issue which needs to be addressed, as discussed in chapters 1 and 2. The characteristics of metamaterials, specifically auxetics, that make them favourable for wearable applications were explored in section 2.6. Here we show a simple fabrication method for creating tiled auxetic cylinders (TACs) which we characterise to demonstrate the potential of auxetic structures in improving comfort and fit for prosthesis wearers. This chapter addresses objective 1 (section 1.5) and is based on the following publication:

> **Simons, M. F.**, Digumarti, K. M., Conn, A. T., Rossiter, J. (2019). Tiled Auxetic Cylinders for Soft Robots. *2019 2nd IEEE International Conference on Soft Robotics (Robosoft)*, pp. 62-67.
>
> *Contribution statement: Simons MF and Digumarti KM contributed equally to this publication and are joint first authors. All the authors were involved in conceptualisation of design, planning of experiments and writing the final manuscript. Simons MF fabricated the structures. Simons MF and Digumarti KM performed the experiments, analysed the data and wrote the first draft.*

3.1 Tiled Auxetic Cylinders

Auxetic designs are rarely seen in nature [177] and hence most designs are hand-crafted (inspired for example from ancient motifs [173]) to suit a specific application. In this chapter, we take a tiling based approach for the design of auxetics which has been studied in [178]. In particular, we focus on isohedral tiling patterns [179]. These patterns are categorised into classes based on the shape and dimensions of an individual tile. They are further classified into families defined by the pattern of repetition of the minimal repeating unit. A study of mechanical properties (Young's modulus, Poisson's ratio and bending stiffness) of sheet materials designed using isohedral tilings is presented in [180]. Though the study provides indication of the auxetic property of certain patterns, this behaviour was not explicitly investigated. An advantage of the tile based approach is that it is conducive to parameterisation. This implies that the structures can be tuned to achieve desirable mechanical properties. Indeed, we demonstrate this change in behaviour in our work.

Most auxetic structures that are currently being studied have focused on two dimensional sheets and three dimensional lattices. A comparison of various different auxetic configurations in terms of their computational estimation of mechanical properties is presented in [181] and an experimental verification of properties in 2D hexagons is presented in [182]. There has been some fabrication of auxetic cylinders in the literature. [183], for example, created an auxetic cylinder by 3D printing a wax version of the auxetic cylindrical structure around which a mould could be generated. Moulten brass was then poured into the mould to create the final auxetic cylinder which they then characterised. Another method described by [184] uses 3D printing of silicone to print an auxetic hexichiral structure directly onto a tubular elastomer balloon to produce a seamless auxetic cylinder. However, both of these methods require multi-step processes with

complex computation.

The behaviour of auxetics when in a cylindrical shape seen in the literature, such as for use as cardiovascular stents or nails as described in chapter 2, predominantly considers their behaviour relative to gripping on the outside of the cylinder. In the case of wearables, however, we need to consider the behaviour of the inside of the auxetic cylinders gripping on the body. This is explored in chapter 6. As a first step towards realising this, we need to characterise the mechanical properties of elastomer auxetic cylinders.

This chapter describes a simple fabrication method for fabricating elastomer auxetic cylinders by 3D printing planar auxetic sheets with thermoplastic polyurethane (TPU) and rolling them up into a cylindrical configuration. We call these Tiled Auxetic Cylinders (TACs). We record the characterisation of these cylindrical auxetic structures and compare four different auxetic designs (fig. 3.1). The elongation force required to stretch the auxetic structure in length and the change in diameter are analysed. Comparisons are made between the various auxetic designs in terms of changes in these properties and the implications of these changes relative to wearable applications is considered.

3.2 Design

3.2.1 Fabrication

The auxetic structures presented in this work were 3D printed in a single plane on a desktop 3D printer (Wanhao Duplicator i3) with thermoplastic polyurethane (TPU, rigid.ink, Youngs modulus = 15.5MPa [180], Poisson's ratio = 0.48 [185], Shore A Hardness: 94A). The thickness of each sheet was 1mm. They were then rolled up to form a cylindrical structure that was bonded together with adhesive (Ethyl 2-cyanoacrylate, Loctite superglue). The flexible nature of the

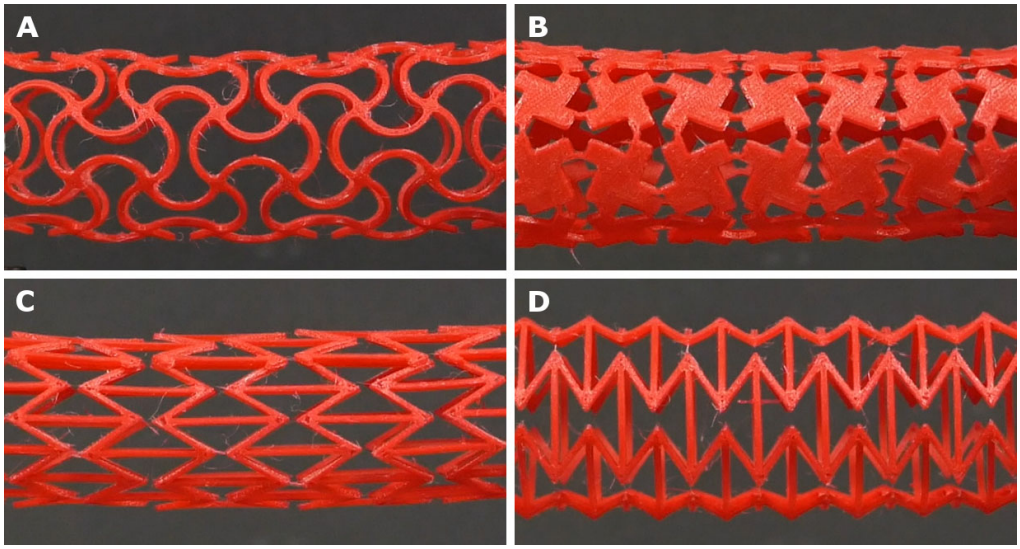

FIGURE 3.1. The four Tiled Auxetic Cylinder designs studied are (A) re-entrant sinusoid, (B) modified re-entrant sinusoid, (C) re-entrant hexagon oriented along the axis and (D) re-entrant hexagon oriented perpendicular to the axis.

material facilitated the construction of a 3D structure from a 2D sheet. Loops were printed on the structure so that the free ends of the cylinder could be suitably clamped in the experiments that characterise their mechanical properties.

3.2.2 Auxetic Design

Four different auxetic designs were studied, which were all re-entrant structures. The first two designs (A and B in fig. 3.1) are re-entrant sinusoids [186] and the second two (C and D in fig. 3.1) are re-entrant hexagons [187]. The difference between the two hexagons is the orientation of the pattern with respect to the axis of the cylinder. The designs are referred to as being oriented along the axis (C in fig. 3.1) and perpendicular to the axis (D in fig. 3.1) based on the angle that the parallel rods make with the longitudinal axis of the cylinder.

The re-entrant sinusoid designs belong to the same family of isohedral tiling [188], which can be described as a pattern of square tiles (fig. 3.2a). They are effectively the same design, the

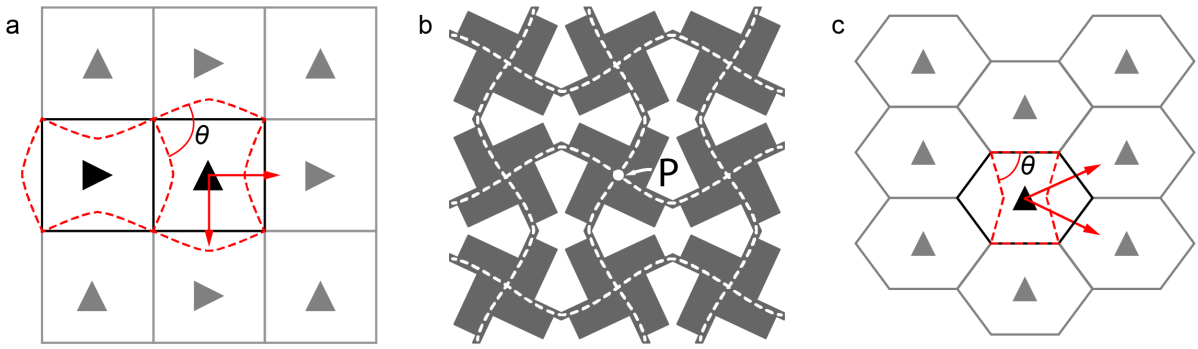

FIGURE 3.2. (a) Isohedral tiling pattern with square tiles. Triangles indicate orientation of tiles. Arrows indicate tiling directions. Dotted line shows a re-entrant sinusiod on the minimal repeating unit. (b) Re-entrant sinusoid (dotted line) overlaid on the modified re-entrant sinusoid (grey) showing that both the structures belong to the same isohedral tiling family. The point P that is common to four neighbouring tiles is the point of rotation. (c) Isohedral tiling pattern with hexagonal tiles. In this case, all the tiles have the same orientation. The re-entrant hexagon is shown with a dotted line. θ denotes the re-entrant angle.

difference being that the latter, referred to here as the modified re-entrant sinusoid, has enlarged rotation points that makes it stiffer than the simple re-entrant sinusoid (point P in fig. 3.2b). The smallest repeating unit in the pattern is a pair of adjacent tiles oriented perpendicular to each other (fig. 3.2a).

The hexagonal designs belong to a family with hexagonal tiles which are arranged next to each other in the same orientation (fig. 3.2c) rather than perpendicular to its neighbouring tile as seen in the sinusoidal designs. The re-entrant hexagon structure was orientated in two different ways to create the cylindrical structure: along the axis and perpendicular to the axis.

These four designs have been selected to illustrate the effect of change in geometry and orientation of patterns on mechanical properties when they belong to the same family of tilings. The re-entrant sinusoid and re-entrant hexagon auxetic families both have relative large negative Poisson's ratios (<-0.8) compared to other common auxetic structures studied [181], such as arrowheads [12], stars [181] and chiral geometries [165], [12], [181]. This makes it easier to

characterise their behaviour and measure any change in behaviour when altering their designs. In addition, these auxetic structures have relatively simple configurations which should not be discounted for easy fabrication. Our hypothesis is that the two auxetic designs belonging to the re-entrant hexagon family will show stiffer behaviour compared with the re-entrant sinusoid family, as the latter relies on simple rotation of the material whereas the former requires bending of the material where the material may resist this to a certain extent.

3.3 Experimental Method

To measure the relationship between elongation force and length, a similar setup was used as seen in [189]. The cylindrical structures were held in a linear stage with the axis parallel to the horizontal (fig. 3.3). One end of the cylinder was fixed to a load cell (Model no. 1022, Tedea-Huntleigh, max. load 5kg, calibrated with 0, 100g, 200g, 500g, and 1000g weights) while the other end was connected to the moving carriage which moved at a constant rate of 0.45mm/s imposing an elongation in length. Two wooden supports were inserted into the diametrically opposite loops at each free end of the cylinder, oriented perpendicular to one another and to the axis of the cylinder resulting in four points of contact at either end. The rotation of the structure was thus constrained, while allowing it to freely increase in diameter upon elongation in length. The position of the carriage was measured using a laser displacement sensor (LK-G512 and LKGD500, Keyence). Both elongation force and displacement readings were recorded using a data acquisition system (USB-6001, National Instruments) at a frequency of 1000Hz. The experiment was repeated 10 times for each design.

Each experiment was recorded on video (DMC-G80, Panasonic) with a resolution of 1920x1080 pixels and at a constant rate of 60fps. Individual frames from the video were then analysed

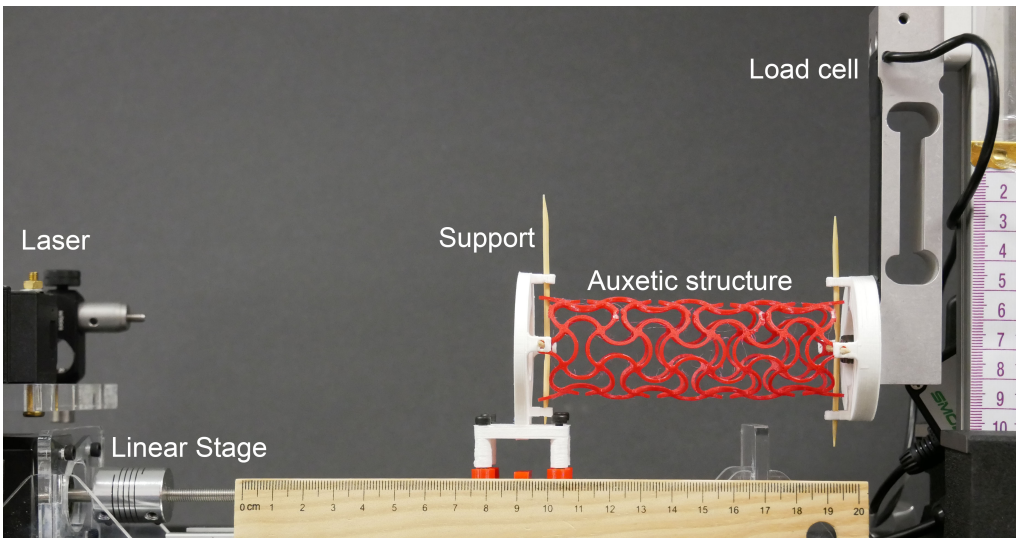

FIGURE 3.3. The experimental setup used to determine the relationship between elongation force and elongation in length of a cylindrical auxetic structure.

in MATLAB using MATLAB's Image Processing Toolbox add-on to extract the diameter of the complete structure (defined as the maximum span of a 2cm wide region in the middle of the structure) as it changed with its entire length.

3.4 Results

3.4.1 Deformation of the Structure

A close up of the structure's deformation upon elongation in length for the four designs is shown in fig. 3.4. In the case of the re-entrant sinusoids (A and B in fig. 3.4), the curved edges straightened out during elongation. This can be seen as a rotation of the square patches in the case of the second design. In the third design, a three-dimensional buckling of the structure was observed. In the final design, curving of elements forming the re-entrant portion of the structure was seen.

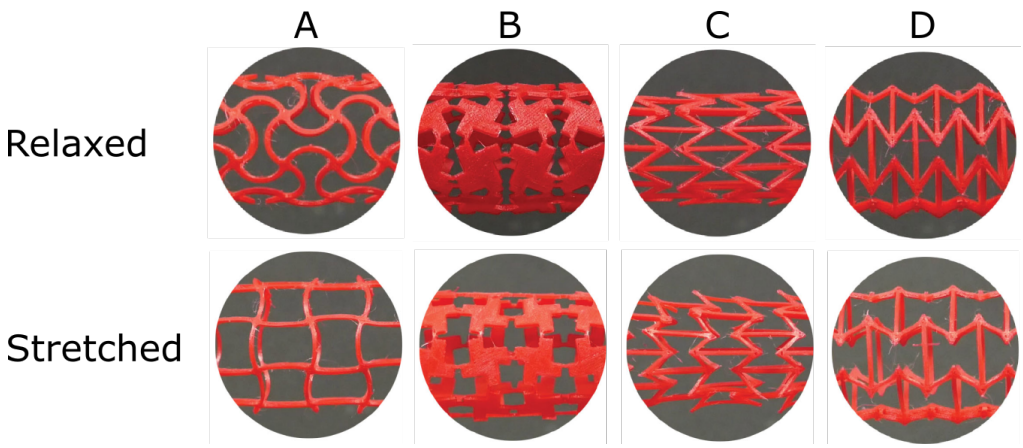

FIGURE 3.4. Configuration of the structure at rest (top) and after elongation (bottom) for the four designs considered: (A) re-entrant sinusoid, (B) modified re-entrant sinusoid, (C) re-entrant hexagon oriented along the axis and (D) re-entrant hexagon oriented perpendicular to the axis.

3.4.2 Force-Elongation Relationship

The relation between elongation force and elongation in length is shown in fig. 3.5. Both the re-entrant sinusoid (A) and modified re-entrant sinusoid (B) exhibit stiffening, with the latter stiffening more at a smaller elongation. This is expected as the points of rotation (P in fig. 3.2b) were designed to be stiffer in B. In the case of the re-entrant hexagons, two distinct behaviours are observed based on the orientation of the pattern in the cylinder. In the case of the pattern oriented along the axis of the cylinder (C), a stiffening behaviour is observed initially, followed by a softening of the structure. This can be attributed to the out of plane deformation that was observed in the structure (C in fig. 3.4, bottom). The relation between elongation force and elongation in length is approximately linear in the final case (D) where the structure was oriented perpendicular to the axis. A gentle stiffening was observed at larger elongations due to deformation of the re-entrant beam elements (D in fig. 3.4, bottom). The low standard deviation in all the cases demonstrates that the behaviour is repeatable.

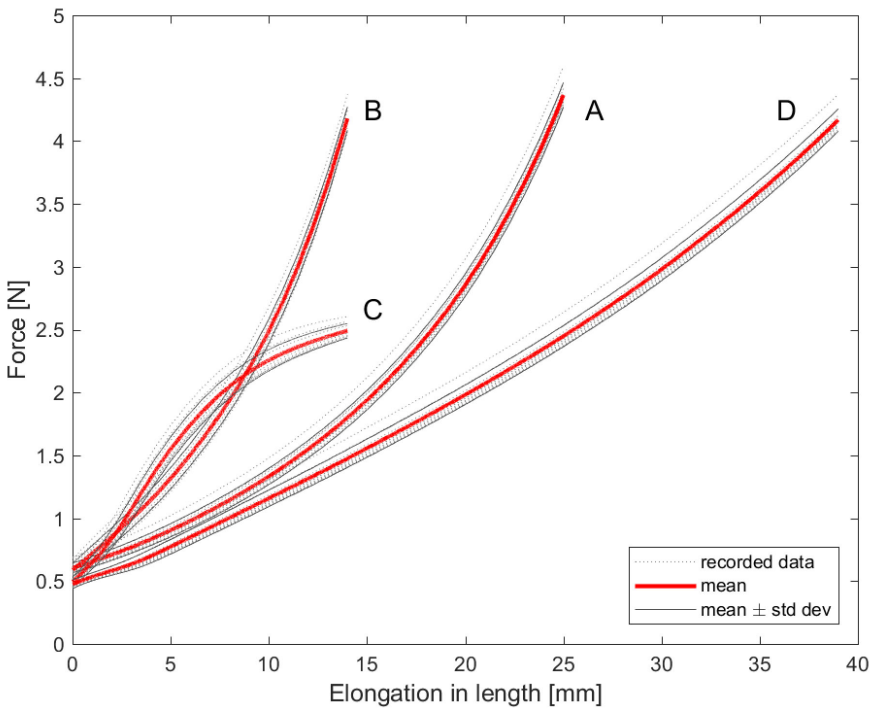

FIGURE 3.5. Relation between elongation force and elongation for the four auxetic designs considered: (A) re-entrant sinusoid, (B) modified re-entrant sinusoid, (C) re-entrant hexagon oriented along the axis and (D) re-entrant hexagon oriented perpendicular to the axis. The dotted lines indicate recorded data, the solid red line indicate the mean of 10 trials and the thin solid lines indicate one standard deviation away from the mean.

3.4.3 Diameter-Length Relationship

The relation between normalised change in diameter and normalised change in length for the four auxetic structures is shown in fig. 3.6. In all the cases, the relation was found to be linear. The negative of the slope of the curve can be interpreted as an equivalent Poisson's ratio for the structure since the Poisson's ratio defined for non-auxetic structures considers a decrease in dimension perpendicular to that of extension rather than an increase as seen here. These values are reported in table 3.1.

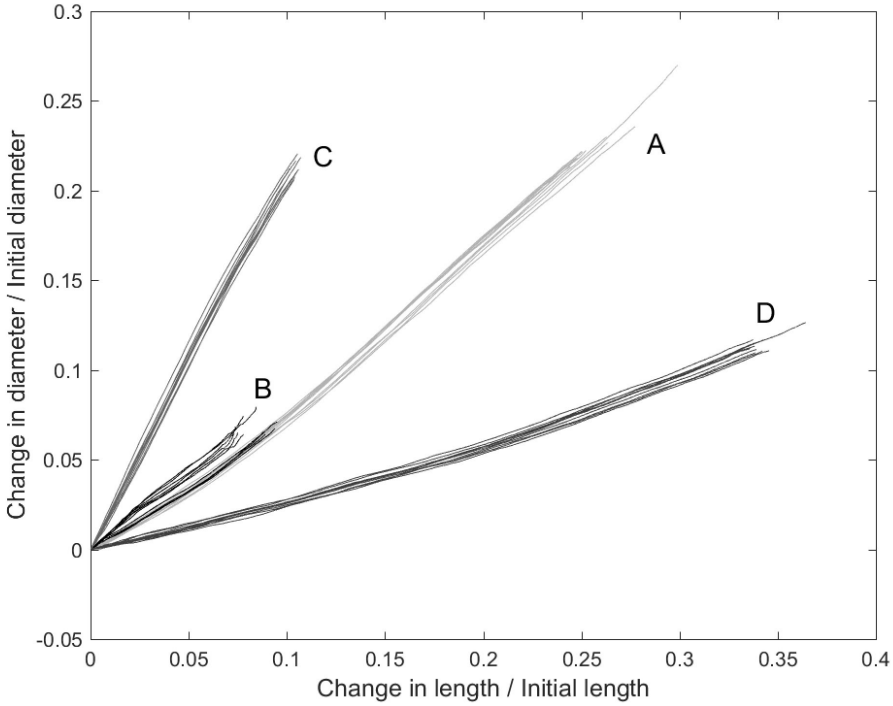

FIGURE 3.6. Relation between normalised change in diameter and normalised change in length for the four auxetic designs considered: (A) re-entrant sinusoid, (B) modified re-entrant sinusoid, (C) re-entrant hexagon oriented along the axis and (D) re-entrant hexagon oriented perpendicular to the axis.

Design	Equivalent Poisson's ratio
(A) Re-entrant sinusoid	-0.90 ± 0.01
(B) Modified re-entrant sinusoid	-0.76 ± 0.08
(C) Re-entrant hexagon ∥ axis	-2.09 ± 0.05
(D) Re-entrant hexagon ⊥ axis	-0.33 ± 0.01

TABLE 3.1. Equivalent Poisson's ratio for the four Tiled Auxetic Cylinder structures.

3.5 Discussion on TACs

The behaviour of the four different TAC structures studied show similarities as well as differences. The relation between elongation force and displacement (fig. 3.5) is an indication of the effective Young's modulus. Here we present the elongation force instead of the stress because it is not trivial to determine the area of cross section, which changes as the structure elongates and the material is stretched. The relation between the normalised change in diameter and normalised change in length (fig. 3.6) is an indication of the Poisson's ratio.

The two re-entrant sinusoid structures (A and B in fig. 3.1) showed the most similarities. In the case of the elongation force measurement with elongation of the structure (fig. 3.5), the shape of the curves are the same, but with a steeper curve seen for the modified re-entrant sinusoid (B) compared with the original re-entrant sinusoid (A). This is due to the enlarged rotation points (point P in fig. 3.2) making the structure stiffer overall. It may be deduced that structures with stiffness in the range between these two curves can be obtained by changing the amount of material at the points of rotation. The equivalent Poisson's ratios (table 3.1) for both are similar at a value close to -1. In fig. 3.6 the curves follow the same trajectory which reinforces this similarity, where the modified re-entrant sinusoid shows a smaller change in length and diameter, again due to its increased stiffness.

The larger proportion of solid surface area in the modified re-entrant sinusiod (B) relative to (A), also highlights the potential for design control over relative areal porosity change during expansion. For example, a 10% extension in length generates a relative surface porosity increase of 12% in B and 5% in A.

The two re-entrant hexagonal structures (C and D in fig. 3.1), though they are the exact same structure, show very different properties due to their different alignment relative to the

axis of the cylinder. The re-entrant hexagon orientated perpendicular to the axis (D) is most comparable to the re-entrant sinusoid designs, where the relation between the elongation force and elongation (fig. 3.5) is slightly more linear. The re-entrant hexagon orientated along the axis (C), however, shows a rather different relation between elongation force and elongation. Initially it shows stiffening similar to the modified re-entrant sinusoid (B). The structure then softens owing to the out of plane deformation of the parallel rods (C in fig. 3.4, bottom). This could be attributed to high stress concentration in the angular joints and the curving out of the structure to attain a minimal energy state. This is an interesting behaviour and can potentially be exploited for locomotion [7]. This is not observed in the other structures due to the nature of the design which provides a continuous beam from one end to the other, thus preventing out of plane deformation. A detailed investigation will be addressed in a future work. The equivalent Poisson's ratios are also very different. The former (C) demonstrates a large equivalent Poisson's ratio at -2, approximately twice that of the re-entrant sinusoid structures. When the same structure is orientated at 90° (D), the equivalent Poisson's ratio is less than a quarter at -0.33.

The equivalent Poisson's ratio for the samples studied listed in table 3.1 are comparable to those presented in [181] for flat sheets; -0.81 for the re-entrant sinusoid and -0.34 for the re-entrant hexagon when the orientation is perpendicular to the axis. Elastomers are the predominant soft robotic material and are widely considered to have a bulk material Poisson's ratio approximately equal to 0.5.

Interesting to note are the behavioural differences between the two tiling families. Elongation in structures A and B is due to the points of rotation (point P in fig. 3.2) where the re-entrant angle (θ in fig. 3.2) remains constant. Elongation of structures C and D however is due to a change in the re-entrant angle. This relationship between re-entrant angle and elongation of the structure will be investigated in future work.

Throughout analysis of the experimental results, it was assumed that the behavioural properties were as a result of the hinges in the structural design alone. Future work will look at the combined behaviours of structural expansion and material extension.

A factor to consider when analysing the results is the frame-rate and resolution at which the videos of the samples were taken and processed throughout the experiment, along with the resolution of the data recordings. The measurement of the change in diameter and length of the samples is achieved by converting the number of pixels from the images to mm, hence the resolution of the experimental recordings could greatly impact the end results. [189] performed tensile tests on 2D auxetic planar sheets with a similar set-up to the one demonstrated here. Their samples were stretched as a speed of 0.05mm/s, recorded with a video frame-rate of 1 frame per 5 seconds. Our sample was stretched at a slightly faster speed of 0.45mm/s and we therefore used a faster frame-rate of 60fps to ensure no data was lost. As the rate of movement is slow for the samples in this experiment, the frame-rate does not need to be too high.

We have demonstrated a simpler process of fabrication compared to that seen in the literature. Our method only requires two-steps (3D printing and rolling into a sheet), whereas the fabrication method used by [183] requires the fabrication of a mould first which can then be used to create the auxetic cylinder and therefore requires more steps compared to our method of fabrication. [184] 3D print the auxetic structure directly into a cylindrical configuration. This was done by 3D scanning the balloon onto which the auxetic structure was to be printed and reconstructing the surface shape in software onto which the auxetic structure was calculated. The fabrication method described in our research 3D prints the auxetic structure in a 2D sheet which does not require any complex computation. It should be noted, however, that our final auxetic cylinder includes a seam at the point where the two sides of the 2D sheet are glued together, whereas this is not the case for the two other fabrication methods from the literature described here. Future

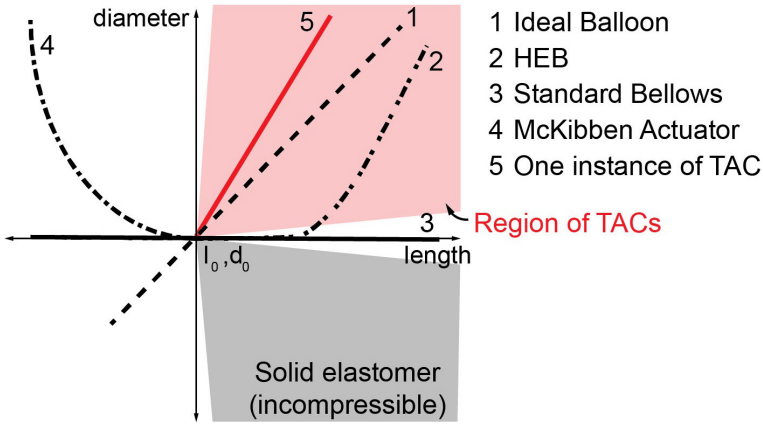

FIGURE 3.7. Comparison of TACs with various classes of structures showing the conceptual relation between diameter and length during actuation. All structures are assumed to have an initial length of l_o and diameter d_o. Adapted from [190].

work would need to consider whether this seam could potentially affect its behaviour.

The behaviour of the TACs can be compared to that of other classes of soft robotic structures. Here we compare the conceptual relation between diameter and length. The structures chosen for comparison are McKibben actuators, ideal balloon, standard bellows, hyperelastic bellows (HEB, [190]) and solid elastomers. This comparison is shown in fig. 3.7. The behaviour of the auxetic structure is linear and is similar to that of an ideal balloon. The slope of the curve can be tuned and various structures display varied magnitudes of steepness (fig. 3.6). Unlike in the case of the HEB, there is no region of decoupling between length and diameter. Both these dimensions increase or decrease simultaneously.

In the case of prosthetic devices, the TACs could be worn as a layer between the skin and the prosthetic socket to accommodate residual limb volume changes, as illustrated in fig. 3.8. The extensive range of TACs' dimensional behaviour as seen in fig. 3.7, allows them to be tuned to many applications and individuals. For example, a lower limb amputee may need a TAC structure with a higher maximum strain as their residual limb has a greater surface area than the residual limb of an upper limb amputee.

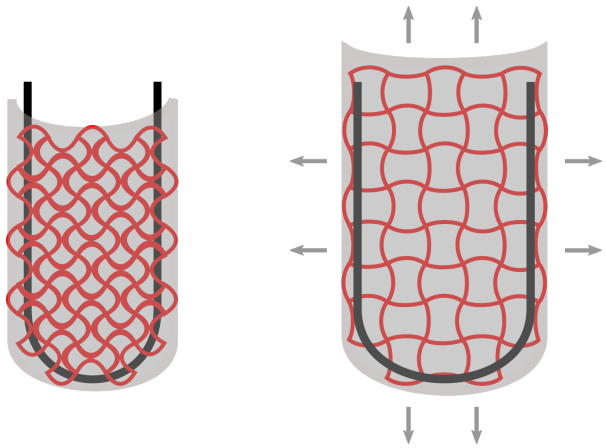

FIGURE 3.8. Future TAC sleeve design. The auxetic nature of the TAC sleeve could accommodate residual limb volume changes experienced by amputees.

3.6 Conclusion

In this chapter, we have investigated tiled auxetic cylinders (TACs); a tiling pattern based approach to the design of cylindrical auxetic structures. We present a simple method of fabricating these auxetic cylinders and focused on two particular designs, the re-entrant sinusoid and the re-entrant hexagon. We characterised the structures in terms of the elongation force and diameter as they change with elongation. Our analysis showed that a minor modification of the design within the same family of tiling can result in a significant difference in behaviour. In addition, we showed the emergence of variation in behaviour by simply altering the orientation of the pattern within the structure.

We have described the characteristics of auxetic structures that make them favourable for wearable applications in chapter 2, such as their resistance to indentation (section 2.6.3.1) and synclastic nature (section 2.6.3.2). In addition to the auxetic effect, this gives TACs the potential to be developed into a sleeve that could accommodate the limb volume changes seen in amputees' residual limbs, such as illustrated in fig. 3.8, and we have therefore demonstrated objective 1 (section 1.5). This is explored in chapter 6 where we aim to incorporate auxetics into

textiles to make them more comfortable and discreet to wear. In the next chapter we will look at characterising TACs' reaction and behaviour when in contact with the skin as a first step towards developing a comfortable and fitting sleeve for prostheses.

CHAPTER 4

EMOTIVE TOUCH

As described in chapter 2, the skin is a great target to act as a communication channel due to it being the largest sensory organ of the body and containing a range of cutaneous mechanoreceptors which are not only widely distributed, but are also capable of detecting a multitude of stimuli. In this chapter we look at how we can use smart structures, such as the Tiled Auxetic Cylinders presented in chapter 3, to generate sensations on the skin which could be used to convey a range of emotions (objective 2, section 1.5). This can be of particular importance for upper limb amputees. When someone wants to show them affection by holding or gently squeezing their hand, this sensation can be relayed from their prosthetic hand to the amputee. The addition of emotive touch to prosthetic devices can increase embodiment of the prosthetic device and consequently increase acceptance of the device.

This work is based on the following publications:

1. Haynes, A., **Simons, M. F.**, Helps, T., Nakamura, Y., Rossiter, J. (2019). A Wearable Skin-Stretching Tactile Interface for Human–Robot and Human–Human Communication. *IEEE Robotics and Automation Letters*, vol. 4, no. 2, pp. 1641-1646.

Contribution statement: Haynes A, Helps T, Nakamura Y, and Rossiter J were involved in conceptualisation of design and fabrication of the device. Haynes A and Simons MF planned and performed the experiments, analysed the data and wrote the first draft. All authors were involved in writing the final manuscript.

2. **Simons, M. F.**, Haynes, A. C., Gao, Y., Zhu, Y., Rossiter, J. (2020). In Contact: Pinching, Squeezing and Twisting for Mediated Social Touch. *CHI EA '20: Extended Abstracts of the 2020 CHI Conference on Human Factors in Computing Systems*, pp. 1-9.

   Contribution statement: Simons MF and Haynes AC contributed equally to this publication and are joint first authors. Gao Y and Zhu Y designed the devices based on concepts previously designed by Simons MF, Haynes AC, and Rossiter J. Gao Y and Zhu Y fabricated the structures aided by Simons MF. Gao Y and Zhu Y planned the experiments based on previous experiments by Simons MF, Haynes AC, and Rossiter J. Gao Y and Zhu Y performed the experiments and analysed the data. Simons MF, Haynes AC, and Rossiter J wrote the manuscript.

In this chapter, we use SMAs to generate lateral skin stretching by means of lightweight, wearable devices attached to the skin on the inner forearm. The forearm was chosen as an easily accessible region of the body which presents a large area of sensitive skin. The devices provide gentle stretching and squeezing of the skin with the goal of instigating a more localised and natural feeling. Each device aims to simulate a different human touch interaction as shown in fig. 4.1. The initial device (fig. 4.1, top left) acted as a design template on which the following three devices were based, with design alterations in an attempt to improve the initial device and alter the sensations provided to the wearer's skin. We present the following devices:

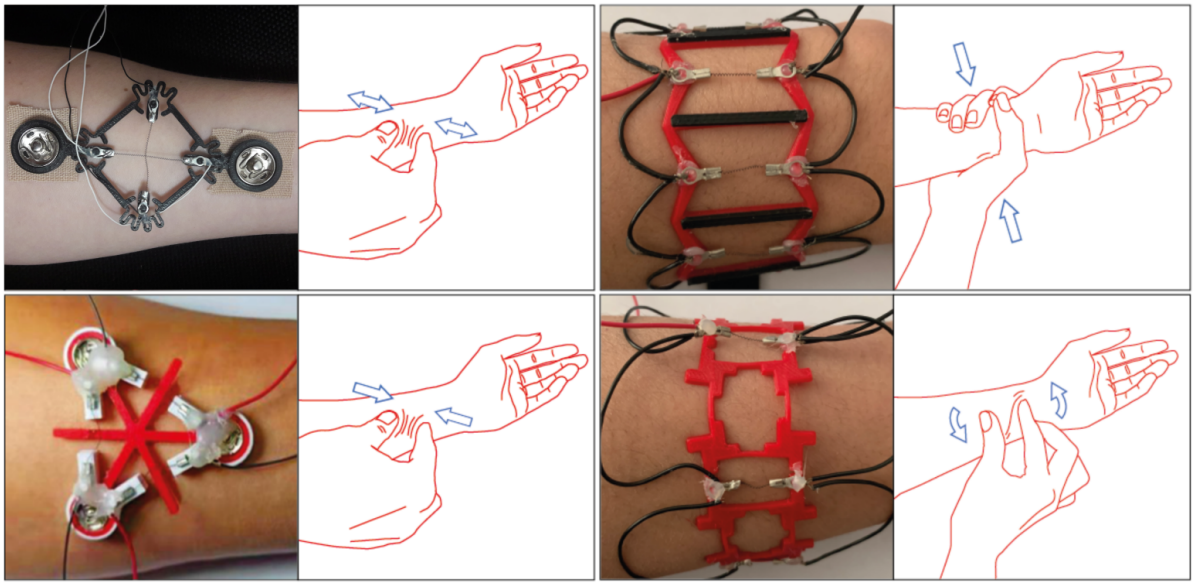

FIGURE 4.1. The four emotive touch devices fabricated and characterised as worn by a user, along with an illustration of the human touch interaction it simulates: SCWEES device (top left), Pinch device (bottom left), Squeeze wristband (top right), and Twist wristband (bottom right).

- Super-Cutaneous Wearable Electrical Empathic Stimulator (SCWEES) (section 4.1):

  This diamond-shaped device is adhered to the skin using two adhesive pads to provide gentle squeezing and stretching sensations on the skin (fig. 4.1, top left).

- Pinch device (section 4.2):

  This triangular-shaped device is adhered to the skin using adhesive pads to provide pinching sensations on the skin. It is based on the SCWEES device but provides more degrees of freedom (fig. 4.1, bottom left).

- Squeeze device and Twist device (section 4.3):

  These devices are worn with a strap around the wrist to provide squeezing and twisting sensations on the skin. The attachment method of the strap increases the practicalities of wearing these devices over adhesion to the skin as seen with the SCWEES and Pinch devices (fig. 4.1, top right and bottom right respectively).

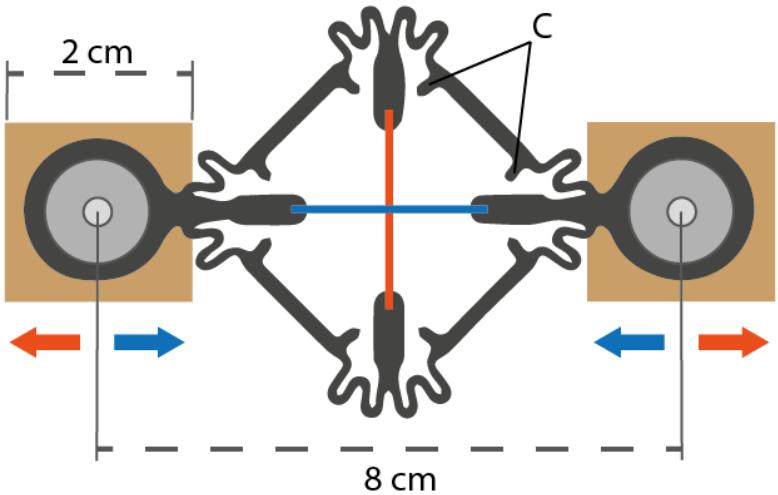

FIGURE 4.2. The SCWEES tactile stimulation device. On activation of the horizontal SMA (blue), the ends of the device are pulled closer together, compressing the skin. On activation of the vertical SMA (orange), the ends of the device extend, stretching the skin. Deformation limiters (C) constrain maximum displacement in both directions.

4.1 Super-Cutaneous Wearable Electrical Empathic Stimulator (SCWEES)

The Super-Cutaneous Wearable Electrical Empathic Stimulator (SCWEES) is shown in fig. 4.1 (top left), with its mechanism of action illustrated in fig. 4.2.

In this section we investigate three important characteristics:

1. The stretching/squeezing sensation in terms of affective response measured by pleasantness and strength,

2. The use of this device for inter-person interactions,

3. The use of this device for non-disruptive alerts when carrying out everyday tasks.

4.1.1 System Design

In this section we describe the SCWEES device. We define three core requirements for the design:

1. *Low visual and auditory disturbance to the user*. Many existing tactile devices use vibrational motors or servomotors which can be bulky and produce noticeable levels of sound. For this experiment we chose to use SMAs to generate movement as they are silent, lightweight and unobtrusive.

2. *Simple and quantifiable tactile sensations.* To reduce the ambiguity of sensations and obtain clear base-line psychometric results we designed the device with two specific and repeatable modes of stimulation; extension and contraction with predetermined displacements.

3. *Minimally intrusive for the user.* The device was designed for use on the inner forearm, an area easily accessible and commonly used for social touch. We also made the device as lightweight and unobtrusive as possible at this prototype stage by 3D printing a small frame for attachment to the skin while keeping the driver electronics separate and out of view of the user.

4.1.2 Hardware and Fabrication

The SCWEES device is a 3D printed (polylactic acid plastic) planar diamond-shaped structure (fig. 4.1, top left) with flexible elements at the four corners that act as hinges. Two SMA coils (Toki Biometals) are mounted orthogonally between opposite corners. As a safety measure, the SMA coils are suspended on raised pins 4 mm above the skin, minimising any risk of harm to the user or interference of the tactile sensation that could occur from the heat of the activated SMA wire (transition temperature 70 °C). The diamond structure couples the two actuators such that contraction of one SMA extends the counter SMA as shown in fig. 4.2. At each corner, deformation limiters cap the maximum stroke of the device to ± 5 mm, ensuring repeatability of stimuli. Two circular rings are connected at opposite corners into which female poppers are inserted. These connect to the adhesive pads on the skin via male popper fastenings allowing for easy application, modification and removal. The device was connected to a control system via four very thin and

flexible insulated multi-core wires. Each SMA was driven by up to 5 V using a power transistor controlled by an Arduino Nano. Voltage control was achieved using Pulse Width Modulation (PWM) from 0 to 100% duty cycle. The Arduino interfaced to a PC for high level control and data processing. The total weight of the device on the arm was 2.5 g and its height was 5 mm making it comfortable and unobtrusive to wear.

For comparison to existing vibrotactile devices such as smart watches, a low mass vibration motor was also used in experiments, attached with the same size adhesive pad next to the SCWEES device. The 3.3 V, 1 A motor had 3 mm thickness, 10 mm diameter, weighed 1 g and exhibited negligible spin-up time compared to the SCWEES device.

4.1.2.1 Device Characterisation

To characterise the device, the displacement was recorded while triggering the contracting SMA (blue in fig. 4.2) with a 1 V step function for 5 s. Voltage and current were recorded via a galvanostat connected to a National Instruments data acquisition device (NI-USB 6009). Results in fig. 4.3 show a delay of approximately 1 s as the SMA heated up and a maximum displacement of 2.3 mm at this voltage. The device was characterised while not attached to a human, free to move on a smooth surface, ensuring a controlled test environment. For comparison, the displacement of the device when mounted on the arm and actuated at 1 V is also shown.

The frequency response of the device was characterised by recording displacement while activating the contracting SMA with a 1 V square wave of increasing frequency. Five oscillations were recorded at frequencies ranging from 0.1 Hz to 10 Hz. The Bode plot is shown in fig. 4.4, from which the interpolated bandwidth (at the -3 dB level) was found to be 0.216 Hz.

Fig. 4.5 shows variation of blocking (maximum) force of the SCWEES device with displacement. In an idealised system, extensive force would reduce from maximum when the device is fully

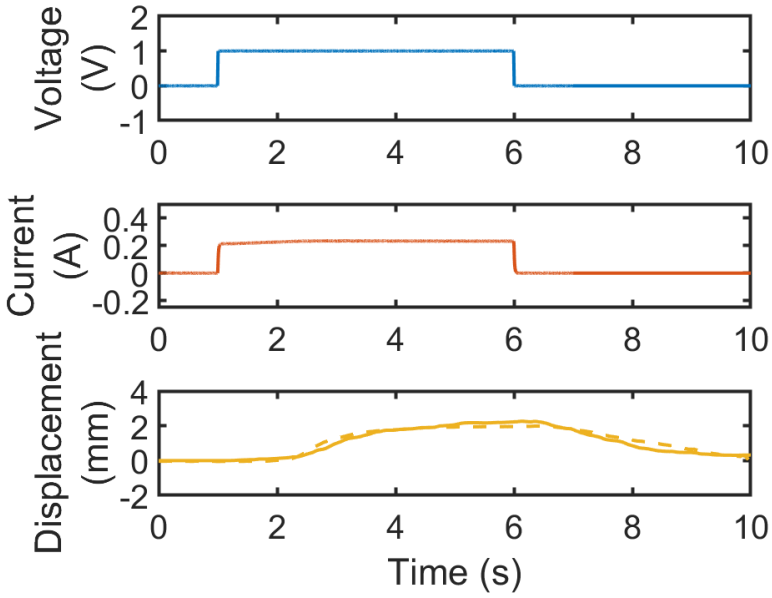

FIGURE 4.3. Device characterisation using a 1 V step input to the contracting SMA with the device free to move on a flat surface (solid), and displacement when worn on the forearm (dashed).

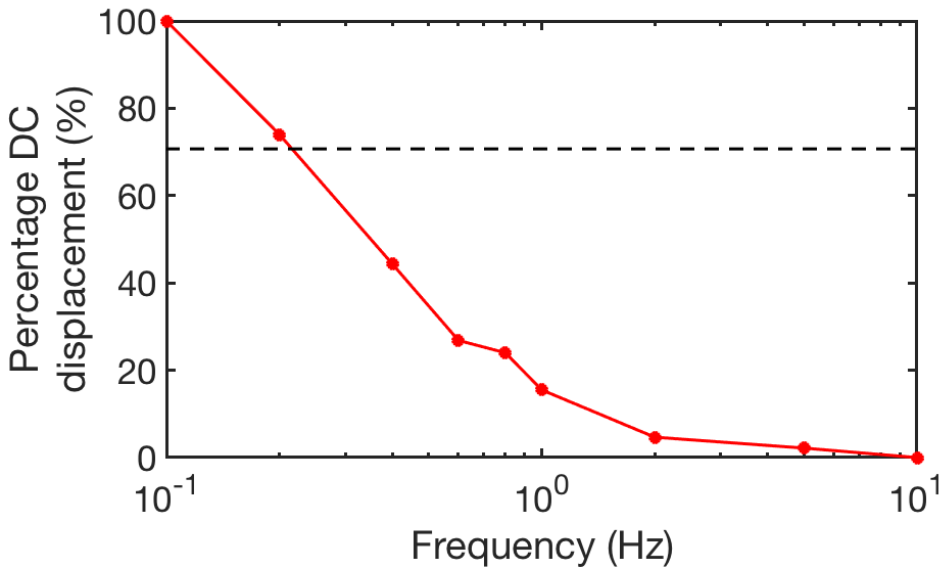

FIGURE 4.4. Bode plot for SCWEES device using a 1 V square wave input to the contracting SMA. 100% DC displacement corresponding to 2.3mm displacement shown in fig. 4.3.

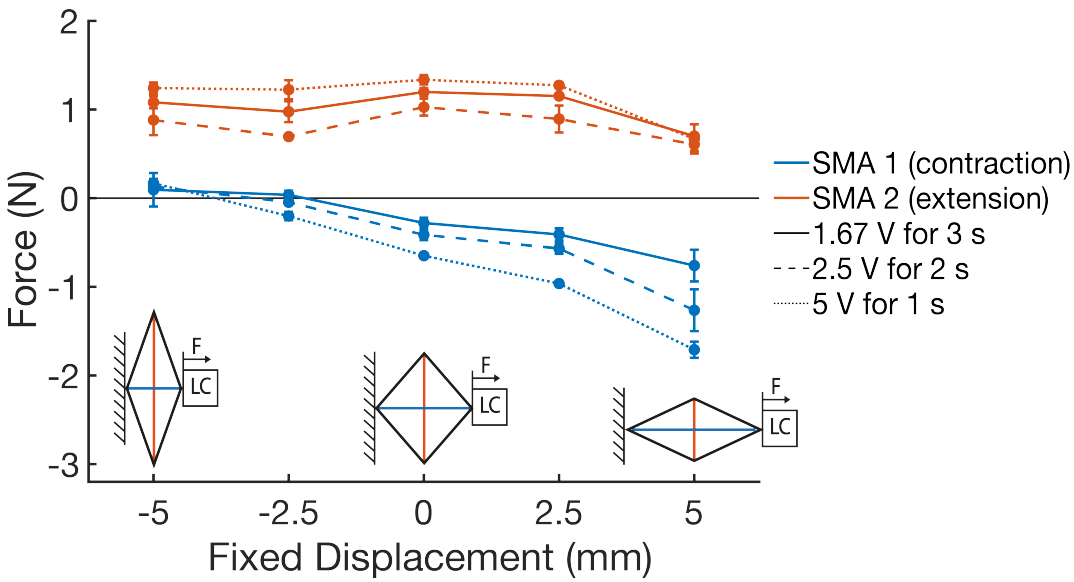

FIGURE 4.5. Peak blocking force for SCWEES device, SMAs individually activated at three voltage levels. Displacement measured from neutral position (-5mm: fully contracted, 5mm: fully extended). Points are averages of three trials and error bars show show standard deviation across trials.

contracted to zero when the device is fully extended, while contractile (negative) force would increase from zero when the device is fully contracted to a maximum when the device is fully extended. Differences in behaviour between the SCWEES device and the idealised system are attributed to buckling of the structure as a result of the slightly offset SMAs.

Contractile force generally matches the idealised system, except for exerting a small positive force when the device is fully contracted: in this case, contraction of the SMA results in the device buckling out of plane, extending slightly and inducing a small positive force on the load cell.

Extensive force differs more from the idealised system. The extensive SMA does not exert force directly in the same way as the contractile SMA, rather exerting it by deforming the SCWEES device structure. Buckling of the structure allows it to exert force by bending out of plane, even when fully extended.

4.1.3 Experiment Design

To evaluate the effectiveness of the SCWEES device we undertook a series of psychophysical experiments. Ten volunteers (8 males, 2 females, with an age range of 20 to 40 years old) were recruited internally to participate in the study and received confectionery as compensation. The device was attached to the inner forearm of the participant's non-dominant arm during the experiment. The duration of the experiment was approximately 30 minutes, comprising of three separate sections outlined below.

4.1.3.1 Experiment Setup

Fig. 4.6 shows the experiment setup used for participants. All three sections of the experiment were controlled through the Arduino Nano via serial communication with MATLAB on a laptop PC. The stimuli were randomly permuted and the order was recorded for each participant.

All electronics were encased to minimise distraction to the participants, and a square tube was fabricated to cover the forearm from view during the experiment, eliminating visual feedback from the device. All other distractions were kept to a minimum by undertaking the experiment in a quiet room with no other people or external disturbances.

4.1.3.2 Section 1: Sensation

In this section, we investigated the affective response of users to the SWEES device. Participants were subjected to six different stimuli; three modes of contraction and three modes of extension. These three modes were defined by their duration of 1, 2, or 3 seconds and voltage of 5, 2.5 and 1.67 V, chosen so that the maximum displacement of the device was consistently reached in each case. We used data from fig. 4.3 to estimate the power delivered to a single SMA: the minimum

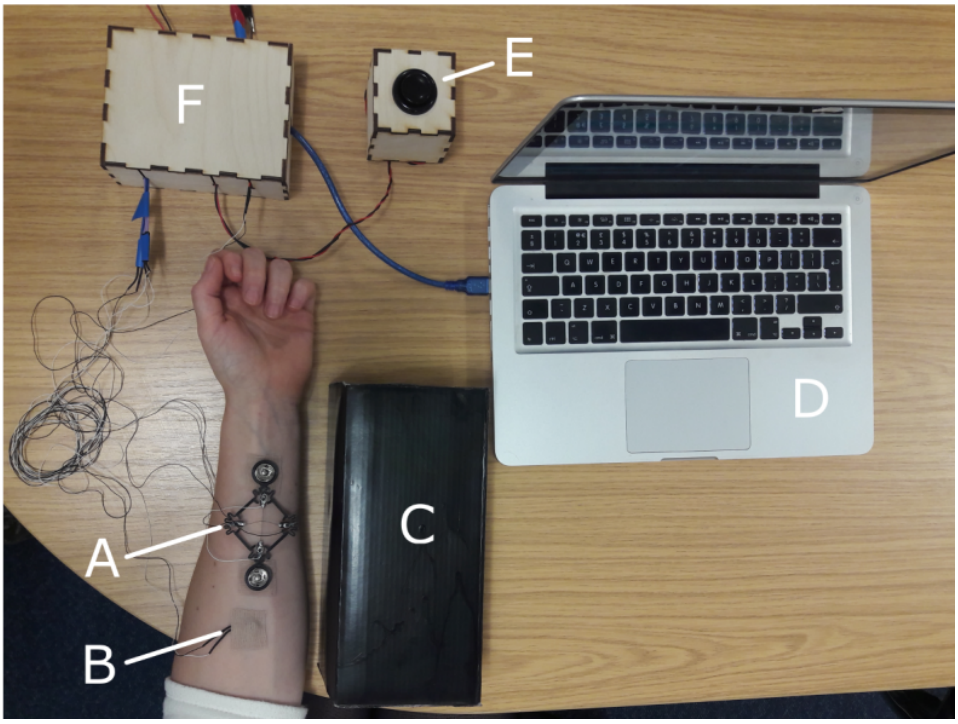

FIGURE 4.6. Experiment setup; A) SCWEES device and B) vibration motor attached to forearm. C) Square tube into which participants place their forearm throughout the experiment. D) Laptop computer as controller. E) Push button for participants to press when detecting stimuli. F) Control box containing Arduino Nano and transistor drivers.

resistance of the SMA coil was 4.34 Ω, implying input powers of 5.77 W, 1.44 W and 0.64 W respectively.

The affective response of participants was recorded by asking them to rate the pleasantness and strength of each sensation experienced. These subjective parameters are defined in the circumplex model of affect [191] commonly used in psychology for measuring affective response. The circumplex model is a means of simplifying the wide range of affective responses into two parameters; valence (pleasantness) and intensity (strength). Both were rated on a 10 point scale, pleasantness from -5 to 5 (very unpleasant to very pleasant, 0 equating to neutral), and strength from 0 to 10 (no sensation to very strong sensation). Each stimulus was repeated 5 times so a total of 30 stimuli were presented in a random order to each participant.

4.1.3.3 Section 2: Mimicking Movement

The ability of participants to detect the type of sensation given by the device and physically respond to it was investigated. One application of this tactile stimulation is in body-to-body communication. The movement of one person, such as flexing their wrist, can be relayed to a second person via the SCWEES device as a form of tactile communication. For the experiment the participants were told to flex their wrist when they felt a contraction on the skin and to extend their wrist when they felt an extension. Ten repetitions of each stimulus - contraction and extension - were given in randomised order and the response of participants was recorded by the experimenter. The SMAs were activated using a 1 s, 5 V step input.

4.1.3.4 Section 3: Distraction

In this section, we investigated the capability of participants to detect sensations from the SCWEES device when performing other tasks. This enabled a comparison of the device with current vibrotactile alerts such as the vibration of a smart watch indicating an incoming message. The vibration motor was run at 3.3 V for 200 milliseconds (selected to mimic the vibration notification of a low-cost ID130Plus smart watch). The SCWEES device was actuated at 3.3 V for 600 milliseconds to provide sufficient time for each SMA to heat and contract. Participants were asked to press a button whenever they felt a sensation from either the vibration motor or the SCWEES device while performing three different tasks: 1. No task - sitting stationary; 2. Reading a book (Harry Potter and the Half-Blood Prince; J. K. Rowling); 3. Playing a continuous arcade-style game (Run 3; Autosaur Games).

Each task lasted 5 minutes, during which 20 repetitions of contraction and 10 repetitions of the vibration stimuli were presented to participants at randomised times. If the button was not

pressed it was assumed that the participant had not noticed the stimulus. A buffer of 6 seconds was included for each stimulus to ensure that they were presented separately and the participant had time to press the button before the next stimulus.

4.1.4 Experimental Results

4.1.4.1 Section 1: Sensation

Fig. 4.7 shows participant responses in the circumplex plane with mean pleasantness of 1.30 (σ 1.70) and mean strength of 4.49 (σ 1.34). Conducting a one-sided t-test across all pleasantness responses at 1% significance level accepted the alternative hypothesis H_1 of mean pleasantness > 0. This indicates that the device was generally found to be pleasant. For individual participants, one-sided t-test results at 1% significance level indicate that 5 participants found the device pleasant (H_1: mean > 0), 4 participants were neutral (H_0 accepted) and 1 participant found it unpleasant (H_2: mean < 0, mean pleasantness rating in this case was -0.3). No participants recorded a pleasantness response less than -3.

Across all participants, the duration of the stimuli made a negligible difference to the perceived pleasantness of the sensation (linear correlation coefficient of -0.036 with p-value of 0.54 at the 1% significance level) as demonstrated in fig. 4.8. However, the perceived strength of sensation had a negative correlation with the stimulus duration (linear correlation coefficient of -0.20 with p-value of 0.00045 at the 1% significance level), indicating that the shorter, faster stimuli felt stronger to participants.

4.1.4.2 Section 2: Mimicking Movement

For the hand flexion test, the mean percentage correct across all participants was 90% (σ 13.3%), split between 89% (σ 14.5%) for contraction (wrist flexion) and 91% (σ 19.1%) for extension (wrist

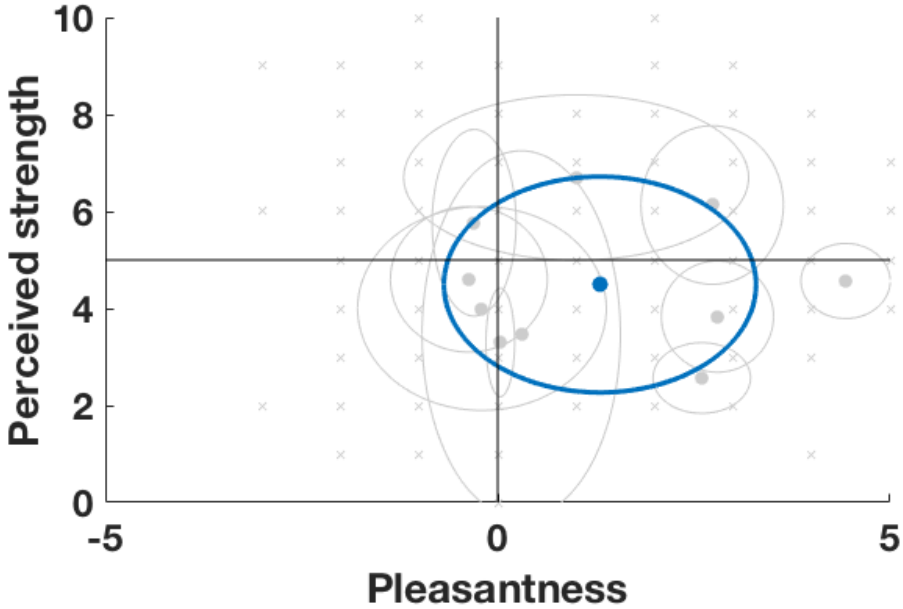

FIGURE 4.7. Mean and standard deviation of responses to all stimuli for all participants in the circumplex plane (blue). Raw data (x's) and individual participant means and standard deviations (solid) shown in grey.

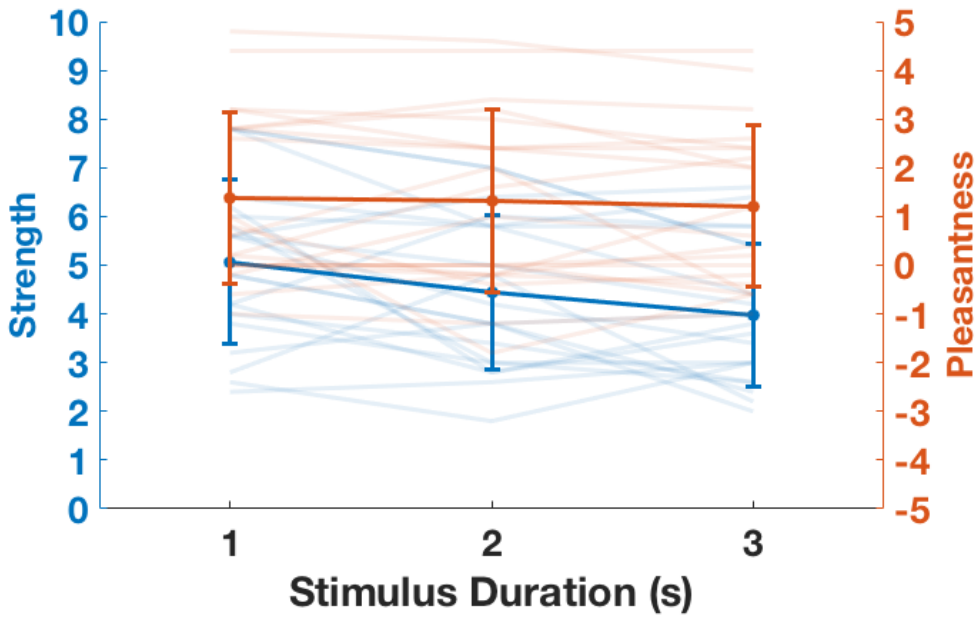

FIGURE 4.8. Mean and standard deviation of perceived strength and pleasantness results across participants for the three durations of stimuli in section 1.

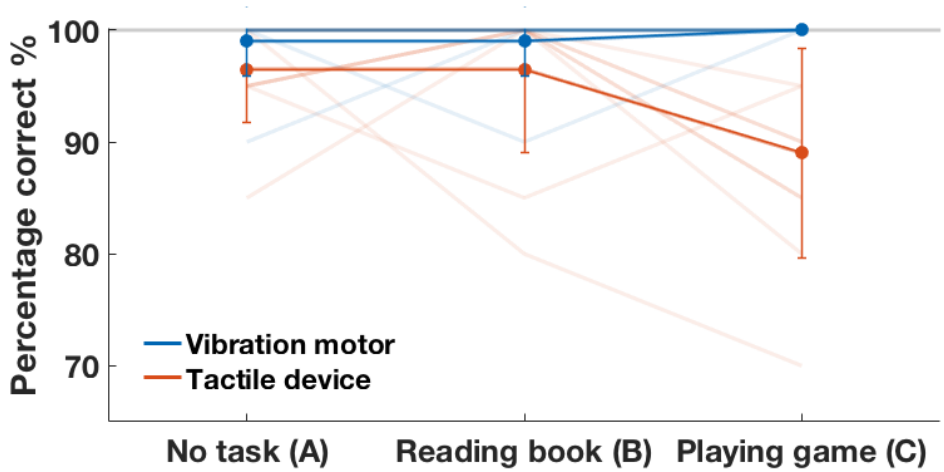

FIGURE 4.9. Mean percentage of correct button presses across all participants for vibration and SCWEES device stimuli during each task; A) no task, B) reading the book and C) playing the game.

extension). At least half of the participants had a success rate greater than 95% demonstrating that the device was very successful at communicating two separate stimuli to the user. A Welch's t-test on the contraction and extension success rates accepts the null hypothesis of equal mean with 1% significance level, suggesting no difference between success at detecting flexion and extension.

4.1.4.3 Section 3: Distraction

Fig. 4.9 shows the success rate across participants in section 3. The mean success rate for the vibration stimuli was 99% during tasks 1 and 2 and 100% during task 3, demonstrating that the vibration stimuli were consistently noticed by participants. This is as expected, given that the vibration alerts on smart watches or phones are designed to be noticed even when the user's focus is elsewhere.

For the SCWEES device stimuli, when participants had no task or were reading a book they noticed the device with a 96.5% average success rate. When distracted by the game there was a

decrease in SCWEES recognition to 89% and many participants commented that the sensation was particularly difficult to notice during this section (see responses in table 4.1). Conducting Welch's t-test at the 1% significance level suggests that the noticeability of the SCWEES device was equal to the vibration for no task (A) and reading (B) but not while playing the game (C), for which SCWEES was less disruptive to the user. Conducting a Welch's t-test between the SCWEES results for playing a game versus no game (C vs A or B) also rejected the null hypothesis. This indicates a significant decrease in noticeability of the device while participants were playing the game.

4.1.4.4 User Comments

After the three sections of the experiment were completed, participants were asked to write down any comments or thoughts they had about the experience of wearing the SCWEES device and the sensations it created. Table 4.1 shows user comments from the different participants, providing further evidence of the overall positive reaction of participants to the device. It was generally stated that the sensations felt natural and pleasant, particularly in comparison to the vibrotactile sensations. A common comment was that the sensation felt like a person touching or squeezing their arm which would make it beneficial for use in mediated social touch scenarios. A number of participants mentioned that the device was more difficult to notice when playing the game and that if they had not been asked to detect the sensations they would easily have ignored it.

4.1.5 Discussion on SCWEES

The SCWEES device was successful in generating natural and pleasant tactile sensations, supported by the results from section 1 for which the mean pleasantness rating was positive, verified by a one-sided t-test.

TABLE 4.1. Comments stated by participants at the end of the experiment (duplicates removed).

Participants' Comments
"The device feels like real fingers squeezing on your arm", "It doesn't feel unpleasant compared with the vibration motor", "Very easy to forget about", "Not as intrusive as other devices", "If I move or shake my hand I will miss the sensation from the device", "Playing a game, I can still [feel the device] but with a slower response", "Simple system that is easy to detect", "So cool!", "The vibration is much easier to notice than the other sensations [from the device]", "It was really nice", "I found it hard to distinguish between the stretching and contracting", "Feels good! Like kind of massage", "I like the feeling of contraction more than that of elongation", "The contraction is not that obvious to tell when reading or playing", "I couldn't really tell the difference between the sensations very well", "I don't think it felt nice or not nice - very neutral. I think expanding was slightly nicer though", "Great", "Very clear sensations, though hard to tell when playing the game", "Very nice experience", "The vibration motor was stronger than the skin stretcher, I really liked that it was continuous in contrast to the binary vibration motor", "Clear sensations", "Mild sensations were unpleasant, larger ones were better", "Extending was easier to detect and felt pleasant", "Did not like the vibrations".

The perceived strength of sensations had a negative correlation of -0.20 to the duration of stimuli, as shown in fig. 4.8, indicating that slower and lower voltage excitations were interpreted as weaker than faster and higher voltage stimuli. Being able to control perceived intensity by changing stimulus duration allows for communication of not only direction (contraction or extension) but also magnitude. Pleasantness was not correlated to stimulus duration overall, rather the affective response was particular to the individual. For example, one participant said that the slower stimuli felt like something crawling on their skin and so were less pleasant, whereas the faster stimuli felt like a person touching or squeezing their arm which they perceived as pleasant.

The SCWEES device can impose either skin compression (contraction) or skin stretching (extension). Overall, the mean discrimination rate across both modalities was 90%, matching previous devices [192], and the difference in how well participants could detect the two stimuli was negligible. This shows the capability of the device to convey information or guide the user's movement via tactile stimulation. Further investigation is required to fully map the affective response landscape and explore increased modalities.

One hypothesis for the SCWEES device was that it could enable non-intrusive notifications. This was verified in section 3; participants were able to easily detect sensations when sitting stationary or reading a book, but found these more difficult to detect while playing an arcade-style game (fig. 4.9).

This indicates that the SCWEES device is less intrusive than vibrotactile stimulation when the user is distracted, an important feature that could enable its use during high-risk activities such as performing surgery or driving a car. In these cases the wearer should not be distracted and these subtle notifications could reduce risk (studies have shown that even handsfree mobile phone use markedly increased mental workload when driving [193]).

Our results confirm that we have met some of the device design requirements set out in section 4.1.1. The device was able to convey non-intrusive notifications when the user was distracted, which was not the case with the more commonly used vibrotactile stimulations. This shows that the device has low auditory disturbance to the user (requirement 1), however during the experiment the user's arm was placed inside a tube to obstruct the user's view of the device and eliminate visual feedback. Therefore, we cannot confirm if our device has low visual disturbance to the user (requirement 1). The device was capable of conveying simple and quantifiable tactile sensations which could be distinguished by the users, and confirms requirement 2. Lastly, the device was lightweight (2.5 g) and easily attached to the user's arm (requirement 3). The majority of wearable tactile devices are much heavier, for example [194] developed a haptic device using servo motors and vibration motors as their modes of stimulation which weighed 220g. The importance of wearable technology weight and distribution on the body has been recognised [195] and more recently more lightweight wearable tactile devices are being developed. For example, [196] use DEAs to create a fingertip tactile device weighing at a comparable weight to our device at 2.6g. However, the electronics for our device were separate to the device which would impact

on the practicality of wearing this device for everyday use.

There was almost universal agreement that the SCWEES device generated pleasant touch and all participants favoured it over vibrotactile stimulation. This is especially noteworthy given the ubiquity of vibration-based stimuli in today's electronic devices. Tactile devices such as SCWEES have the potential to replace vibrotactile stimulation and enable a new type of affective communication channel for mediated social touch and human-robot interactions. This could be delivered via unobtrusive wearable devices worn on the body or embedded into clothing or objects we interact with.

In the future, we plan to improve the SCWEES device by adding more degrees of freedom and minimising the size of the power supply and control unit so that they can be worn unobtrusively and wirelessly on the body.

4.2 Pinch Device

This section presents the Pinch device: a wearable device based on the previous skin-stretching device SCWEES. The device extends the simple squeezing effect explored in SCWEES and is designed to simulate the more complex sensation of pinching as illustrated in fig. 4.1 (bottom left). Its triangular configuration provides more degrees of freedom with subsequent different alignments of skin stretching on the forearm compared with SCWEES. We investigate the emotive responses of wearers to the sensations generated by this device on their forearm.

4.2.1 Device Design

The Pinch device (fig. 4.10) consists of two structural 3D printed parts (Wanhao Duplicator i3). The red part is printed with a flexible filament (TPU) and has six equal legs. At the end of three

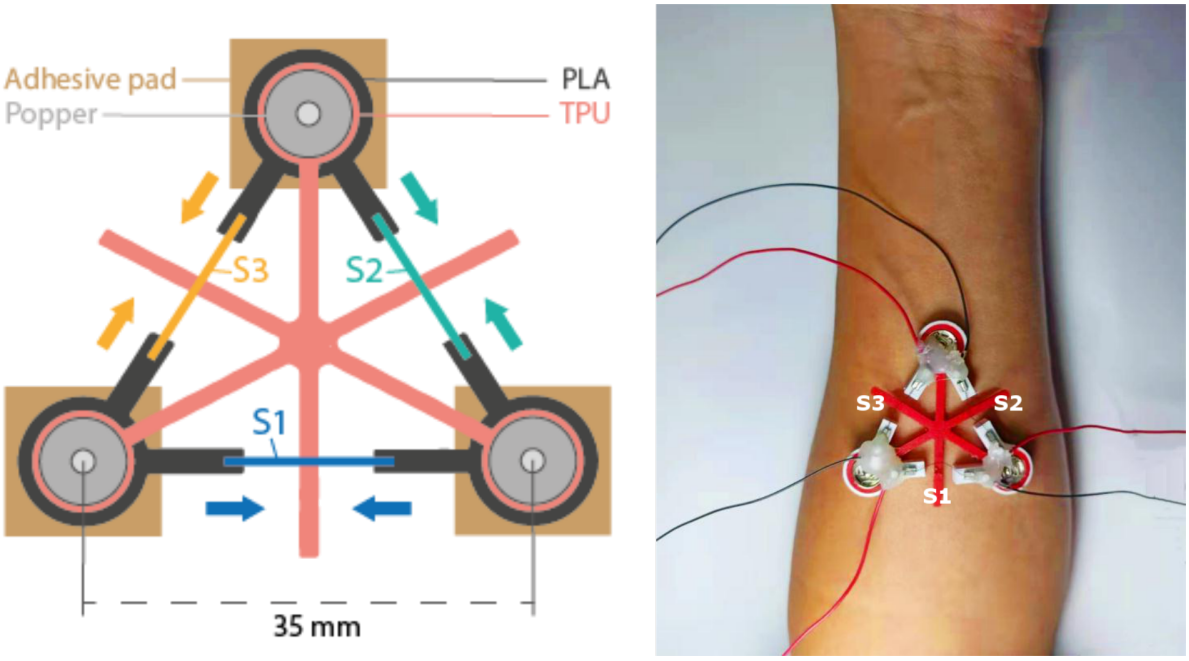

FIGURE 4.10. (Left) Pinch device structure. Arrows indicate the respective contraction of SMA coils S1, S2 and S3. (Right) Orientation of the Pinch device on a user's forearm.

of those legs are circular rings within which poppers were attached and under which adhesive pads attached the device to the skin. Rigid reinforcement elements were 3D printed from PLA to strengthen the rings (shown in black in fig. 4.10, left). The three shape memory alloy (SMA) coiled wires (BioMetal Helix, BMX series 15000) were attached to the ends of these rigid elements to create a triangular shaped device.

4.2.2 User Study

10 volunteers (7 males, 3 females) were asked to wear the device on the inside of their forearm orientated as shown in fig. 4.10 (right). Each SMA on the device was separately activated at three voltages (1.67 V, 2.5 V and 5 V), as described in [96], and participants were asked to rate the strength and pleasantness of the sensation on a scale of 1-10, consistent with the Circumplex

model of affect [191]. For comparison with existing devices, participants were asked to wear the Pinch device, the previous version (SCWEES) [96] and a smart watch which provided vibration stimuli. Participants were asked which sensation(s) they preferred out of these devices.

To determine whether the device could be used to convey information, the three different SMAs were actuated and participants were asked to choose which SMA they thought had been activated. To investigate how subtle the device is, participants were asked to record each time they noticed a sensation from the device while they were doing nothing, reading a book or playing a game. The percentage of correctly noticed activations was recorded.

4.2.3 Results

As shown in fig. 4.11, participants consistently found the Pinch device pleasant with little variation between participants. All participants reported that they preferred the sensations generated by the Pinch device and the SCWEES device in comparison to vibration.

There was no significant difference (Welch's t-test at 1% significance) between the SMA positions for both perceived strength and pleasantness (fig. 4.12, left), but there is a positive Pearson correlation coefficient (r-val=0.866; p-val=0.000) between perceived strength and the voltage of activation (fig. 4.12, right). Pleasantness is slightly increased by increased voltage (r-val=0.314; p-val=0.003).

Participants were able to correctly determine which SMA was activated with 90% mean accuracy. From the confusion matrix (fig. 4.13) it can be seen that all incorrect responses for SMA wires S1 and S2 stimulation were recorded as S3 stimulation (i.e. S3 had the most false positive responses). S3 also generated the fewest incorrect responses.

When participants were distracted by tasks that took more concentration they were significantly less accurate at noticing pinch sensations (supported by Welch's t-test at 1% significance

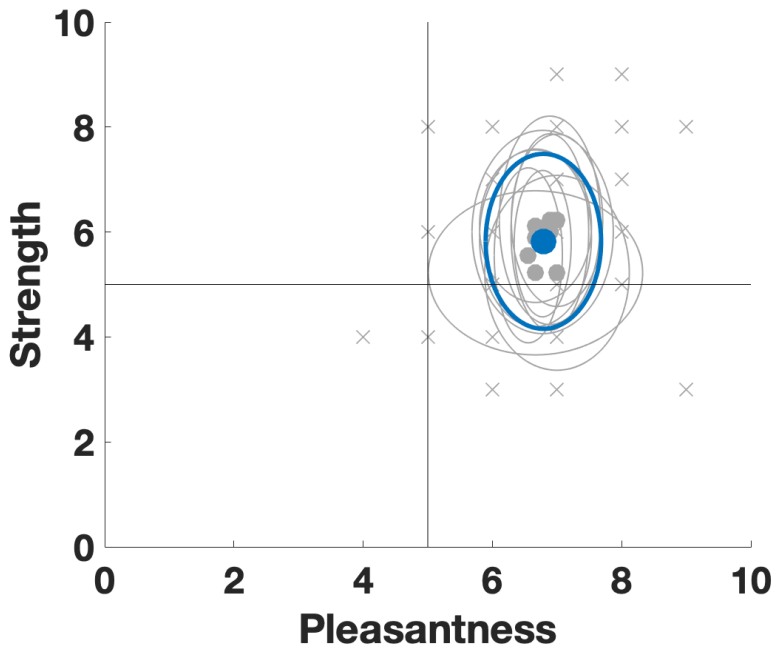

FIGURE 4.11. Perceived strength vs pleasantness of the Pinch device across all participants and voltage levels. Mean and standard deviation of all responses shown in blue (bold); individual participant responses, means and standard deviations in grey.

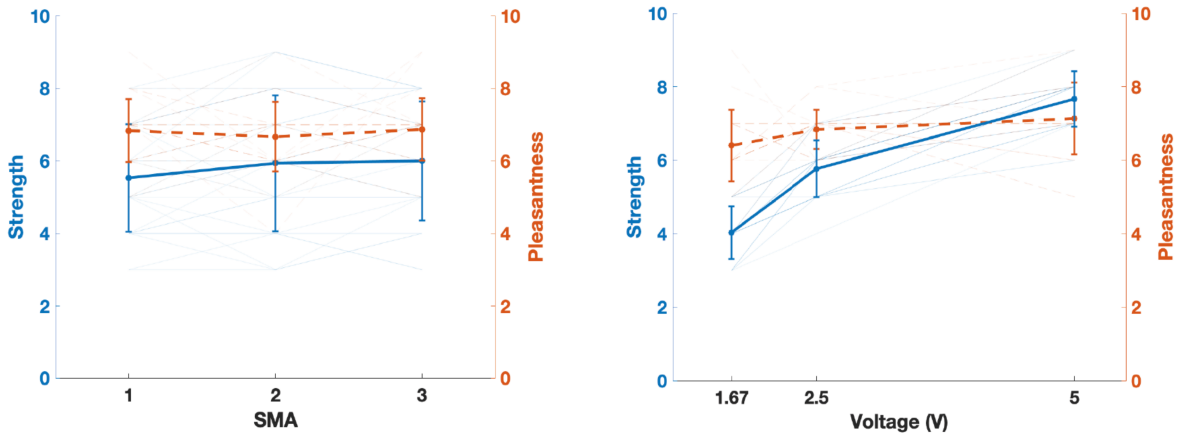

FIGURE 4.12. Perceived strength (blue solid) and pleasantness (orange dashed) across all participants for each SMA S1, S2 and S3 at all voltages (left) and against activation voltage (middle). Bold lines represent mean responses, error bars represent 1 standard deviation.

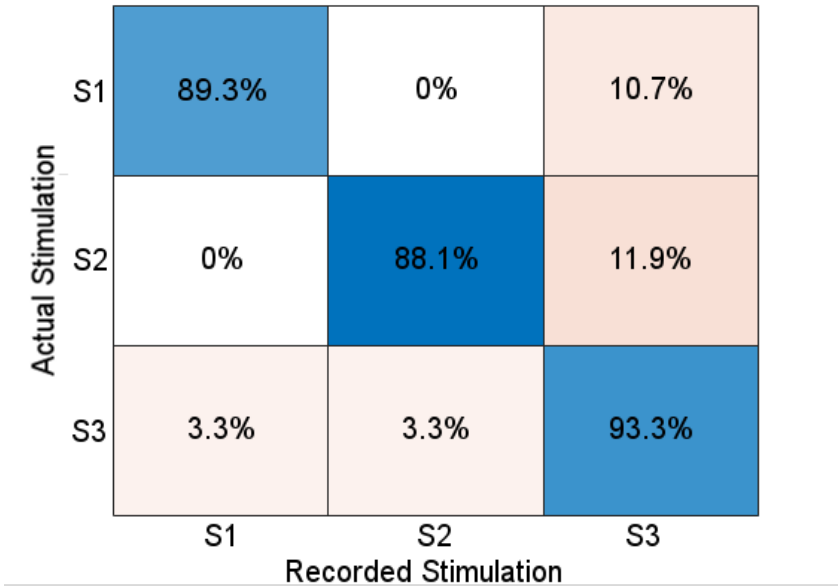

FIGURE 4.13. Confusion matrix of the activated SMA S1, S2 or S3 and the perceived location of stimulation.

showing statistical independence); their % correctly noticed sensations was 99% for no task (std 3.2%), 90% when reading (std 8.2%) and 61% when playing a game (std 15%), as shown in fig. 4.14.

Participants' comments were generally positive with people stating that the Pinch device felt "like a real human hand" and "like someone is touching me". They also commented on the fact that the Pinch device "is really quiet and doesn't affect me and distract my attention" and "it's lightweight and doesn't put an extra burden on my arm". There were, however, some users who felt that the device had too many wires for it to be practical and that "the tactile feeling it brings does not appeal to me".

4.2.4 Discussion on Pinch

Pleasant sensations were generated by the Pinch device (fig. 4.11) which was preferred to vibrotactile sensations. The location of actuation (S1, S2 or S3) did not correlate to pleasantness.

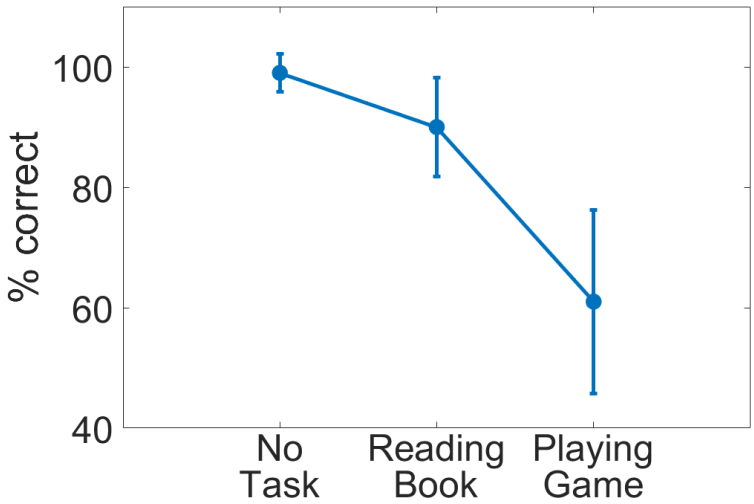

FIGURE 4.14. Accuracy of detecting Pinch device stimulation whilst undertaking three different tasks; no task, reading a book, and playing a game. As concentration levels increase, the detection levels decrease.

However, fig. 4.13 suggests that the area of the forearm at S3 is most sensitive as participants had the least incorrect responses to this stimulation and all incorrect responses for S1 and S2 were recorded as S3. The Pinch device was able to provide information of different strengths as participants recorded an increase in perceived strength as voltage increased from 1.67V to 5V (fig. 4.12, right). This gives the Pinch device the potential to use different levels of voltages on the skin to simulate different sensations or to symbolise emotive meaning.

As concentration on a task increased, participants were less accurate at detecting sensations generated by the Pinch device; comparing no task, reading and playing a game (fig. 4.14). In the previous study [96] it was found that vibration stimuli were consistently noticed (mean 99%) during all tasks. This suggests that the Pinch device is able to convey subtle alerts where the user is less likely to be disturbed when involved in a task that requires more concentration, but when they are not focusing on a task they notice the sensations.

Further development will focus on the practicalities of wearing the Pinch device in real life

settings. As the Pinch device, as well as the SCWEES device, are adhered to the skin, this may cause impractical issues of wearability. To overcome this, other methods of attachment will need to be investigated and in the next section we explore a wristband which fits to the arm without adhesion.

4.3 Squeeze and Twist Wristbands

This section presents the Squeeze and the Twist wristbands. These are both wearable devices designed to simulate squeezing and twisting respectively in an easy-to-wear form (Fig. 4.1, top right and bottom right respectively). They are designed as wristbands to be worn around the wrist rather than adhered to the skin as with the SCWEES and Pinch devices. We investigate the emotive responses of wearers to the sensations generated by these device on their forearm.

4.3.1 Device Design

Both wristbands are based on auxetic structures. The Squeeze wristband (fig. 4.15, top) is made of seven re-entrant hexagons placed end-to-end. It is 3D printed (Wanhao duplicator i3) from flexible filament (TPU). The coiled SMAs are attached along the centre of each auxetic unit. To avoid buckling of the wristband, PLA printed rods were glued to the structure between each unit (shown in black in fig. 4.15, top). Actuation of the SMAs causes the structure to shorten and to squeeze the wrist. The Twist wristband (fig. 4.15, bottom) is made up of a connection of crosses. Four crosses combine to make one auxetic unit. The wristband consists of five auxetic units connected side-by-side. Actuation of the SMAs causes each cross to rotate and to twist the skin. Both wristbands have adjustable velcro straps to ensure a secure fastening on the wrist and direct skin contact.

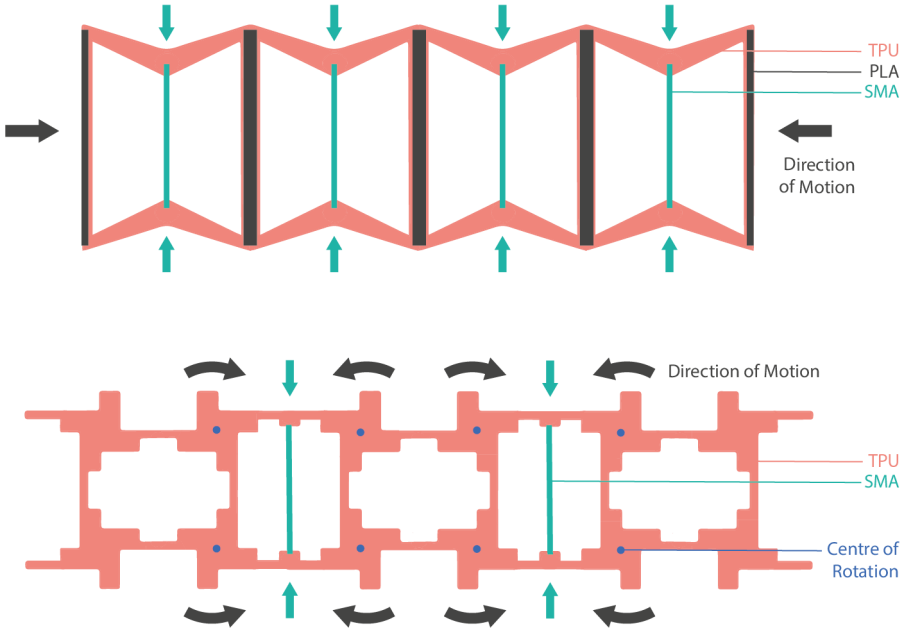

FIGURE 4.15. Structural diagrams of the Squeeze (top) and Twist (bottom) wristbands, illustrating subsections of the whole devices.

4.3.2 User Study

10 volunteers (8 males, 2 females) participated in this study. The wristbands were worn on the user's wrist and participants were asked to rate on a scale of 1-10 the strength of the device and how natural the generated sensations felt. The participants were then asked to compare these sensations to that of a vibration device such as those found in a mobile phone for alerts. To test the devices as a means of long-distance interactions, a second participant activated the device remotely and the wearer was asked to rate out of 10 how effective they felt the interaction was in the context of using the device for mediated social interactions. At the end of the experiment participants were asked for feedback on the device.

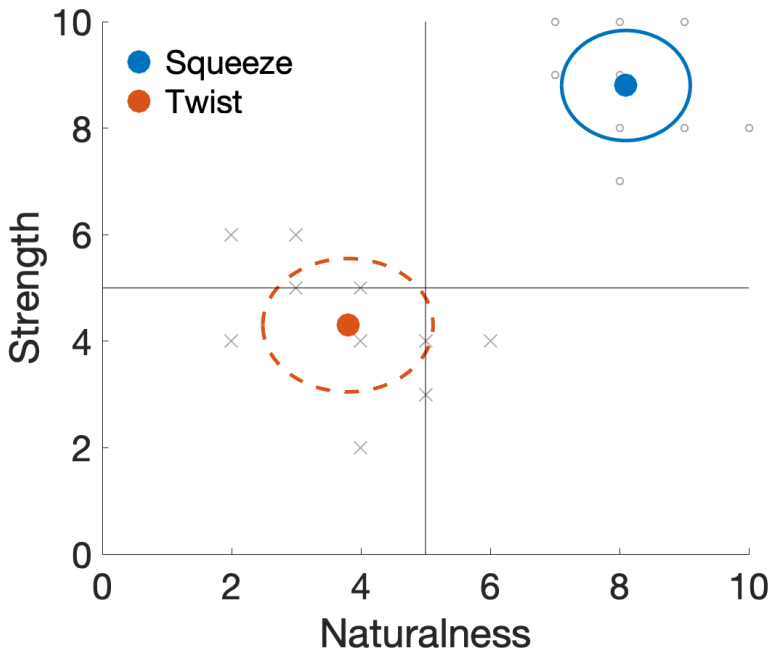

FIGURE 4.16. Perceived strength and naturalness for the Squeeze and Twist wristbands across all participants. Mean and standard deviation shown in bold for Squeeze (blue solid, o markers) and Twist (orange dashed, x markers).

4.3.3 Results

The results show that the Squeeze wristband felt stronger and more natural than the Twist wristband (fig. 4.16). When asked to compare the wristbands to vibration, participants found the Squeeze and Twist devices more natural with a mean rating of 9.3 (std 0.8) and 6.8 (std 1.0) respectively. Participants found the Squeeze wristband more effective than the Twist wristband when used as a remote device and activated by another person, with a mean effectiveness rating of 7.2 (std 1.0) for the Squeeze wristband and 4.2 (std 1.0) for the Twist wristband (fig. 4.17).

Participants' comments indicated that the wires were impractical and suggested making the wristbands remote controlled. Future iterations of the devices can address this. Some participants commented that the rotation wristband did not generate strong enough sensations for them to really feel or appreciate the twisting motion. We will undertake further design iterations to gen-

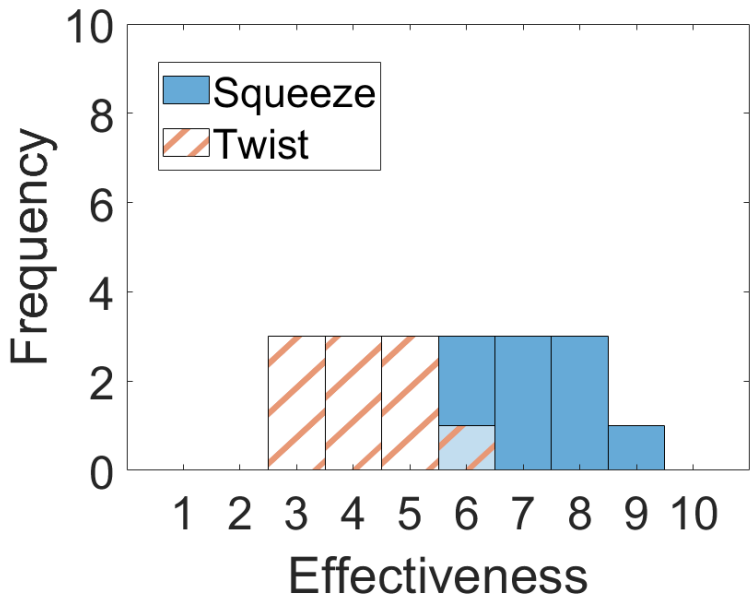

FIGURE 4.17. Histogram of the users' responses (where frequency indicates number of responses) on the effectiveness of the Squeeze (orange stripes) and Twist (blue solid) wristbands as an interaction device when activated by another person.

erate more effective twisting sensations. Aside from these suggested improvements, participants commented that they liked the wristband devices as they were not bulky or noisy.

4.3.4 Discussion on Squeeze and Twist

The Squeeze wristband was able to provide natural sensations (fig. 4.16). An advantage of it over the Pinch and SCWEES device is that it is worn as a wristband rather than adhered to the skin and is therefore more practical as a wearable device. The Squeeze wristband was more effective at generating natural sensations compared to the Twist wristband (fig. 4.16). When used as a communication device between two people, the Squeeze wristband was more effective at providing stimulations compared to the Twist wristband (fig. 4.17).

4.4 Conclusion

We have demonstrated that affective touch can be achieved with skin-manipulating devices that are preferred over devices using vibrotactile sensations, completing objective 2 (section 1.5). We have shown that SMA-driven devices are capable of generating pinching and squeezing sensations on the skin that are pleasant and natural. Although the twisting sensation was less effective, this could potentially be enhanced by adding points of contact to improve skin coupling.

Further development of these devices will predominantly focus on making them untethered and remote controlled so that they can be truly wearable. This will allow us to test their effectiveness in real social interactions, outside of a laboratory environment.

More considerations for developments of these devices is discussed in chapter 7. With these further developments, the devices could be discreetly worn in daily life, giving people a means of both sending and receiving affective touch.

The next chapter considers the use of these affective devices for prosthetic applications and how they can be used to convey other information to the user.

CHAPTER 5

SENSORY FEEDBACK IN PROSTHETIC DEVICES

Chapter 3 looked at smart structures that could potentially be used to overcome the problems associated with pressure experienced at the body-device interface. Unfortunately, pressure is only one of the many aspects to consider for prostheses design, among which are perspiration, weight, functionality and sensory feedback [36, 45].

The tactile feedback devices described in chapter 4 were presented as a means for affective communication. One such communication could be between a device and the body, in particular, to convey sensory information from a prosthesis to the amputee's skin. This chapter addresses objective 3 (section 1.5) and presents the B:Ionic glove, a sensory feedback device capable of relaying pressure experienced at the fingertips of the prosthetic device to the user's residual limb. This work is based on the following publication:

> **Simons, M. F.**, Digumarti, K. M., Le, N. H., Chen, H. Y., Carreira, S. C., Zaghloul, N. S. S., Diteesawat, R. S., Garrad, M., Conn, A. T., Kent, C., Rossiter, J. (2021). B:Ionic Glove: A Soft Smart Wearable Sensory Feedback Device for Upper Limb Robotic Prostheses. *IEEE Robotics and Automation Letters*, vol. 6. no. 2, pp. 3311-3316.

Contribution statement: Simons MF led the research. All authors were involved in device design and fabrication, experimental procedures, data analysis, and manuscript writing.

5.1 B:Ionic Glove

In this chapter we present the B:Ionic glove (fig. 5.1 and 5.2), a prosthetic sensor system capable of providing mechanotactile stimulation on the user's arm relative to the pressure experienced at the fingertips of their upper limb prosthetic device. The glove is worn over a robotic hand and contains sensing, computation and actuation on board. It consists of pressure pads containing conducting fluid located at the fingertips of the glove which can be easily attached to a prosthetic device. When pressure is applied, this fluid travels through a network of silicone channels, connecting pairs of electrodes and closing electrical circuits. These electrical circuits initiate contraction of corresponding SMA actuators integrated into an armband placed on the user's residual limb that gently squeezes their arm.

This chapter presents the following:

- Introducing the B:Ionic glove concept
- Individual characterisation of the three components that form the sensory feedback device
- Proof-of-concept demonstration showing how a user may use the system to grasp an object without visual feedback

5.2 System Design

The B:Ionic glove (fig. 5.1) consists of three components:

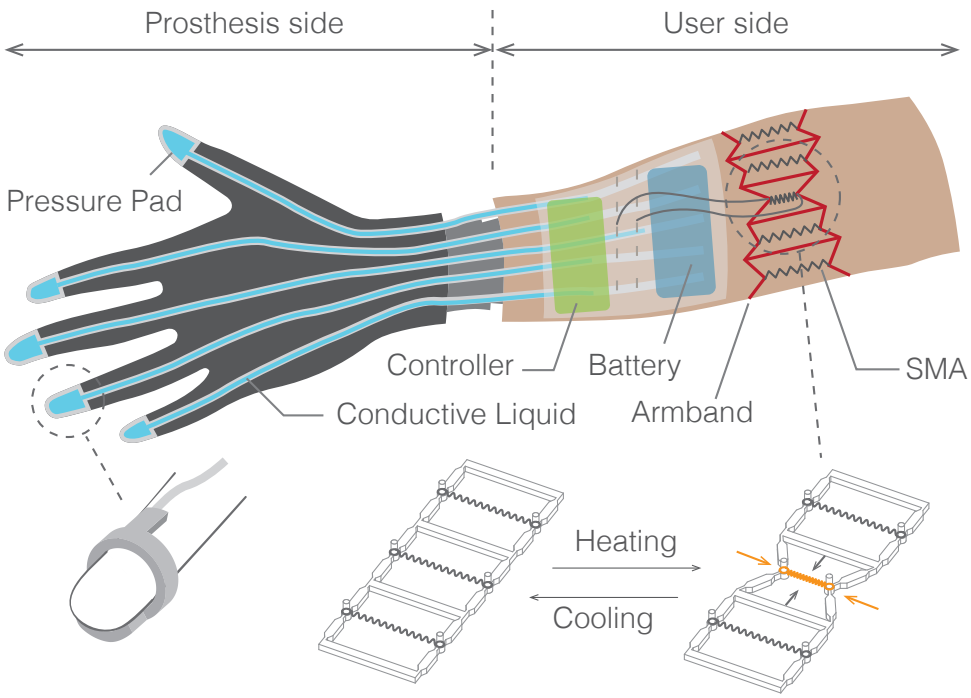

FIGURE 5.1. Illustration of the B:Ionic glove, consisting of pressure pads containing conductive fluid wrapped around the fingertip of a prosthesis, an electro-fluidic control unit including the battery, and an armband actuated by shape memory alloys (SMAs) by way of heating and cooling, generating axial, radial and circumferential forces on the user's arm.

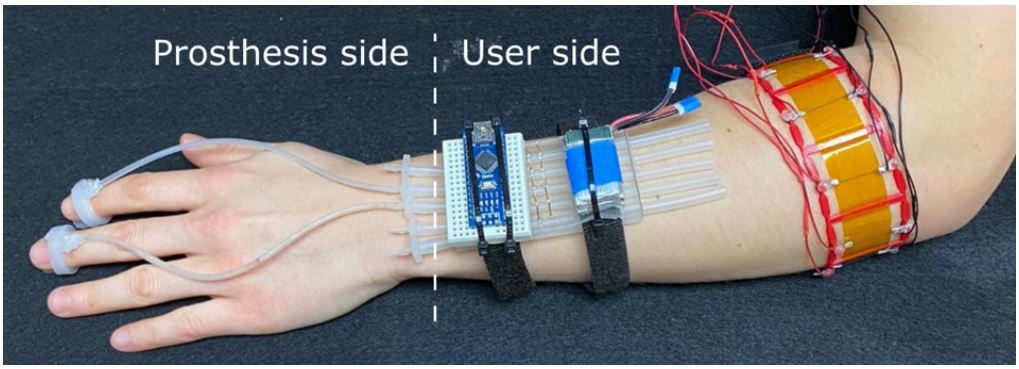

FIGURE 5.2. The B:Ionic glove prototype as demonstrated on a non-amputee, where the components on the left hand side are to be mounted on the upper limb prosthetic device and the components on the right hand side are to be worn on the residual limb of the user.

1. a glove worn on the prosthetic hand with a soft sensor pad underneath each fingertip connected to silicone channels and containing a conductive liquid (section 5.2.1)

2. an electro-fluidic controller (Soft Matter Computer) (section 5.2.2)

3. a tactile armband capable of providing corresponding magnitude and location of feedback (section 5.2.3)

When the fingertip pad is pressed, the volume change forces the conductive liquid through a network of silicone channels. This fluid then bridges the gap between pairs of electrodes along the channel, closing the electrical circuit. In its simplest form, each pad is connected to one coiled SMA actuator on the armband. Once the circuit has been closed, the corresponding SMA on the armband contracts as the current drawn from the battery heats the SMA actuator, generating skin-stretching and squeezing sensations on the skin.

5.2.1 Pressure Pad Tactile Sensors

The pads are fabricated using silicone elastomer (Dragonskin 10, Smooth-On). They are cast in two parts using 3D printed moulds. After curing, the two silicone parts are joined using Sil-Poxy adhesive (Smooth-On) to form an enclosed cavity as illustrated in fig. 5.3. A closeup of the pressure pads is shown in fig. 5.4. The pads have an outlet channel that wraps around the finger to create a fingertip collar, secured with Sil-Poxy adhesive. This also ensures that the silicone tube inserted into this channel runs along the dorsal side of the hand to reduce possible interference. This tube acts as the physical connection between the pads and the Soft Matter Computer (SMC) and carries the fluid that is used for communicating touch.

To characterise the relation between the force applied to the fluidic pad and the displacement of fluid in the channels, an experiment was set up as shown in fig. 5.5. A single pad with an

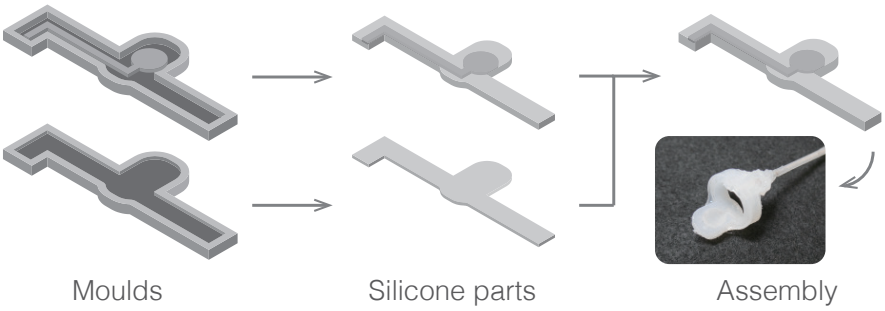

FIGURE 5.3. Three-step fabrication process of the pressure pads. The top and bottom parts of the pads are cast separately from silicone in 3D printed moulds. They are then joined together to form an enclosed cavity. The pad is then rolled up to create a fingertip collar.

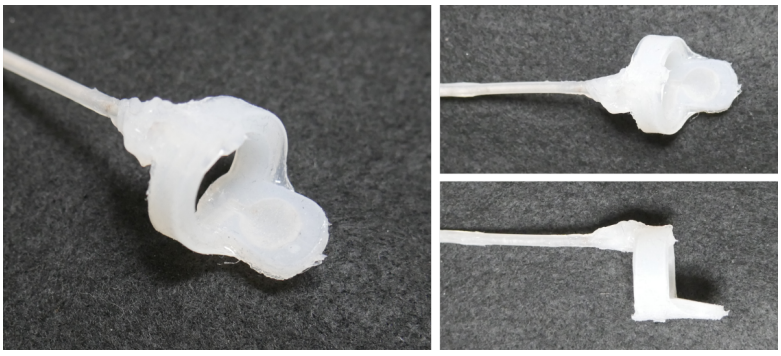

FIGURE 5.4. Closeup of the pressure pads used as a sensor, showing the top view (top right) and side view (bottom right).

outlet channel was affixed to a linear stage. The pad was filled with a coloured fluid for easier visualisation and the initial position of the meniscus in the channel was marked. As the linear stage moved up, a probe pressed down onto the pad. The force applied on the pad was detected by a force transducer placed underneath it. Simultaneously, the displacement of the fluid meniscus in the channel was recorded on camera. Pads with three different cross sections and the same internal volume were tested: rectangle, square and circle. Dimensions of the cross-section of each pressure pad are shown in fig. 5.6. The area of the cross-section is equal across all three geometries (at 64mm^2), with the same depth of 1mm resulting in an overall internal volume of 64mm^3 each.

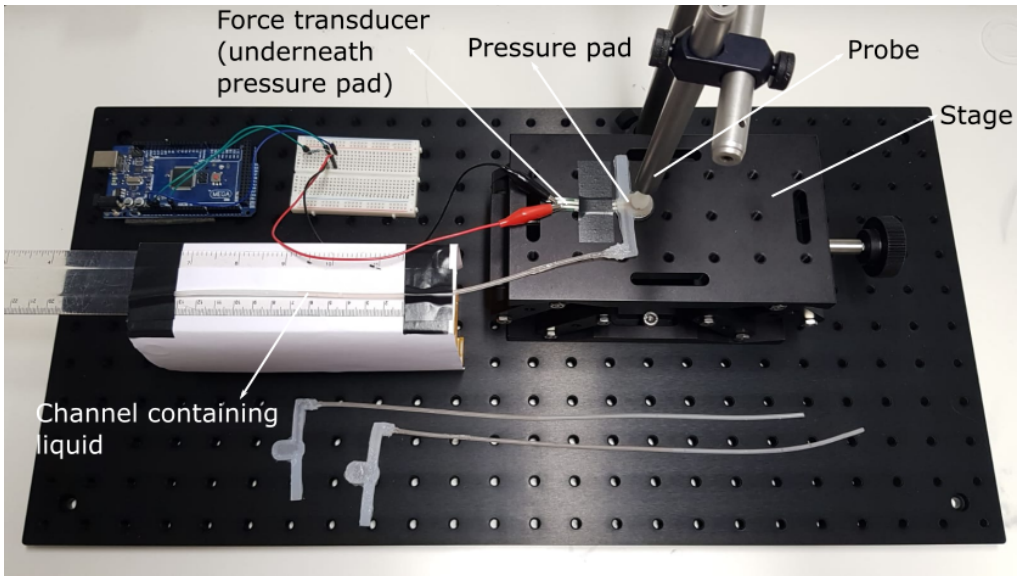

FIGURE 5.5. Experimental setup of the pressure pad sensitivity characterisation. The force transducer measured the pressure exerted on the pressure pad, whilst simultaneously the fluid displacement in the channel was recorded on camera.

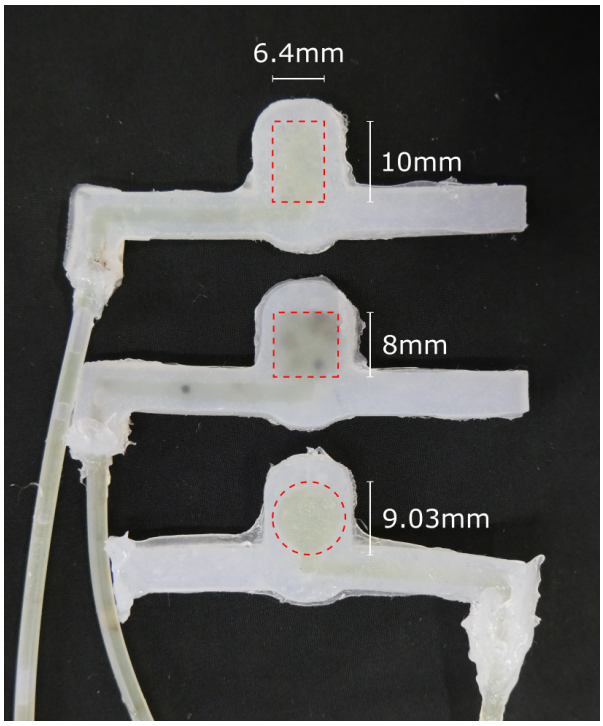

FIGURE 5.6. Dimensions of the internal cavities of the three pressure pads characterised: rectangle, square, and circle (top to bottom). Outline of geometries shown with dashed red line. The cross-sectional area and depth are equal for each geometry (64mm^2 and 1mm respectively) resulting in an internal volume of 64mm^3 each.

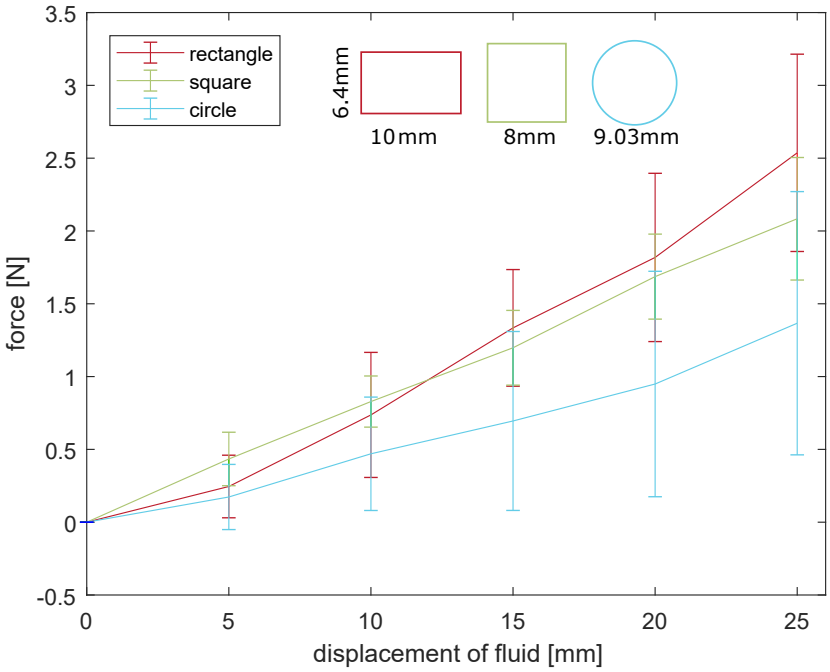

FIGURE 5.7. Characterisation of the sensitivity of pressure pads with three different cavity shapes (rectangle, square and circle). The plot shows the displacement of conductive liquid along a connecting channel under different forces exerting on the pressure pads.

A graph of the relationship between force and displacement of the fluid is shown in fig. 5.7 with the mean and standard deviation of three trials for each shape. The pressure pad with a circular cross-section proved most sensitive, showing the least amount of force for the same fluid displacement. This may be due to the corners of the square and rectangular designs increasing the tension across the surface of the pad as it is pushed, making it harder to displace the liquid compared with the circular design. A displacement of 25mm required a force of 2.5N (σ=0.7N), 2.1N (σ=0.4N), and 1.4N (σ=0.9N) for the rectangle, square and circle geometries respectively. Positional deviation of the probe across trials and complex local interactions at the fluid-wall interface might influence the variance. The circular pad design was found to have the highest sensitivity and was chosen for the following experiments and in the glove prototype.

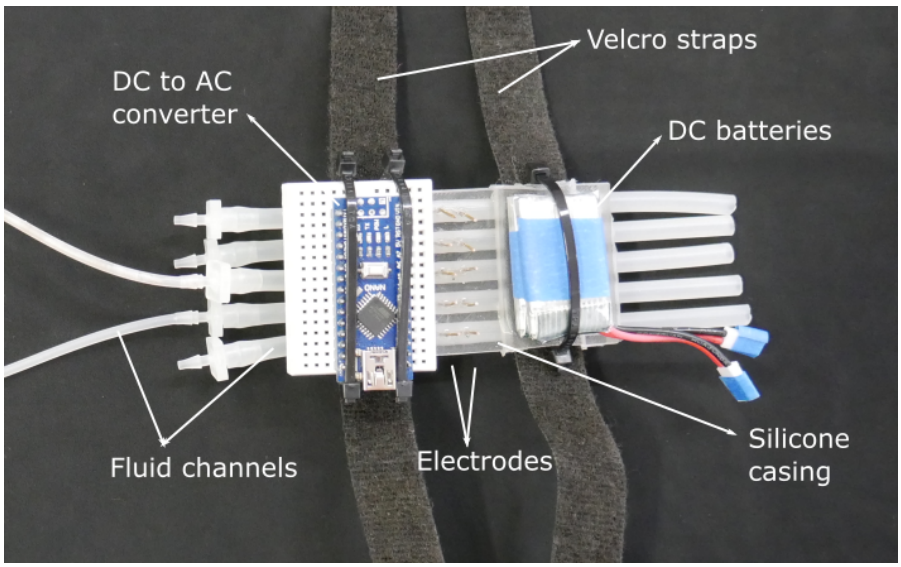

FIGURE 5.8. Picture of the control unit with components labelled.

5.2.2 Electro-Fluidic Control

The control unit (fig. 5.8) is based on the Soft Matter Computer (SMC) developed by Garrad *et al.* [197]. For this device, the SMC was made out of silicone (PDMS, Sylgard 184, Dow Corning) cast into a 3D printed mould. The SMC contains five channels for silicone tubes to slot in to. Each channel has two holes separated by 10mm into which gold plated copper electrodes can be inserted and then sealed with silicone adhesive (Sil-Poxy). Fig. 5.9 shows how a connection is made between two electrodes in a channel. Wires are soldered to each electrode and connected to a DC battery which is turned into an AC current via an H-bridge circuit. Salt water was used as the ionic-conductive liquid due to the ease of handling, accessibility, low-cost and non-toxicity in case of leakage. One disadvantage we encountered was electrolysis that took place at the electrodes (see equation 5.1). To overcome this we used an AC current at frequencies over 1000Hz to prevent the formation of hydrogen and chloride bubbles which would affect conductivity and connectivity.

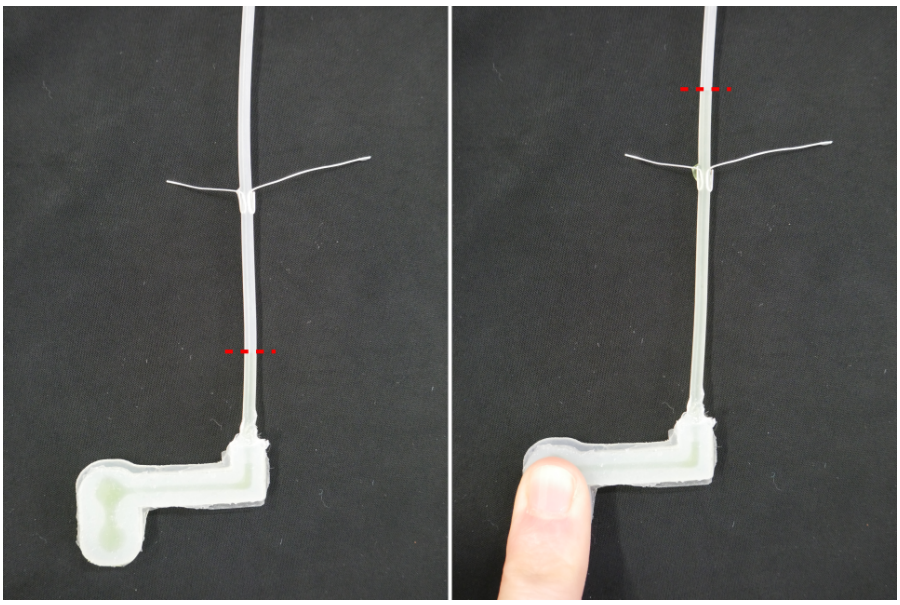

FIGURE 5.9. Closeup of pressure pad with the fluid level marked by the red dashed line. At rest (left), the fluid level does not reach the two electrodes. With pressure (right), the fluid travels through the channel and across the two electrodes which closes the circuit.

$$2NaCl(aq) + 2H_2O(l) \rightarrow 2NaOH(aq) + H_2(g) + Cl_2(g) \tag{5.1}$$

Instead of using saturated saltwater, Galinstan, a liquid metal which is composed of 68.5% gallium, 21.5% indium and 10% tin, could also be used. It possesses several promising features including non-toxicity, high thermal and electrical conductivity, low viscosity and low vapor pressure [198]. Because it does not electrolyse, DC power can be used, greatly simplifying the circuit. However, due to the high surface tension, Galinstan residue would collect and remain on the ends of the electrodes even after releasing the pressure, leading to a constant connection of the circuit (fig. 5.10, left). One solution to this may be to put the electrodes on opposite sides of the channel (fig. 5.10, right).

To demonstrate the potential SMC control of the device, we developed a system that would allow for more complex tactile information processing and feedback (fig. 5.11). Two pressure pads,

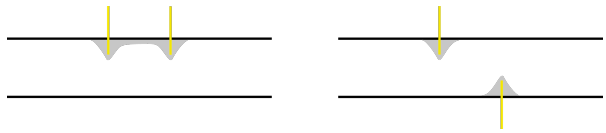

FIGURE 5.10. (Left) Galinstan residue collection at electrodes resulting in a false positive connection. (Right) One solution could be moving one of the electrodes of the pair to the other side of the channel.

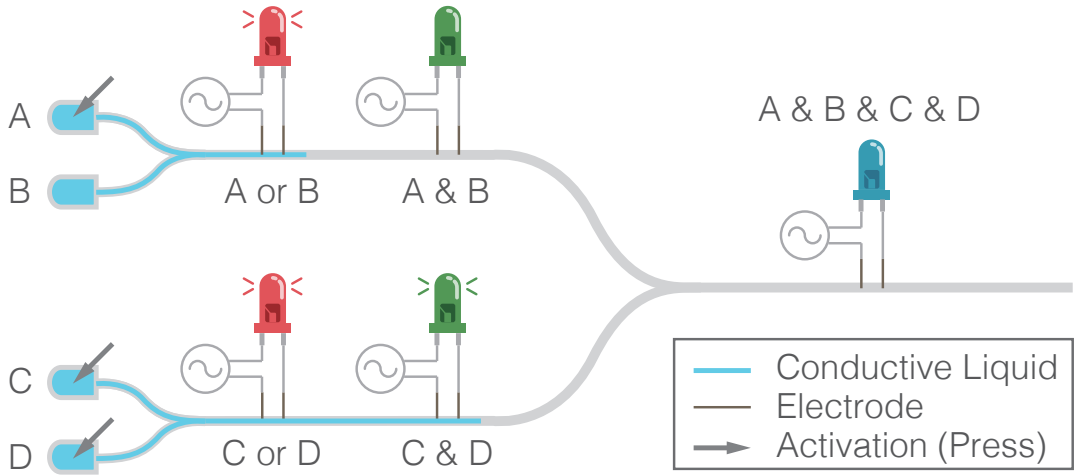

FIGURE 5.11. Model of control setup, including OR and AND gates so that the user may be able to determine when two of the fingers are in contact with an object. The LEDs replace the SMA actuators of the armband for this test setup to visualise connectivity. This model allows for further optimisation of control.

A and B (representing two fingers), were set up with an OR gate followed by an AND gate along the tubing. The channels were filled with saturated salt water (40g NaCl per 100ml water) to the level such that pressing either of the pads activates the OR gate, and pressing both pads activates the AND gate. The SMA actuators were substituted for LEDs to visualise the moment the fluid made an electrical connection, which was recorded on a camera. A gap of 30mm between the OR and AND gates ensured a clear separation between the two different signals.

We also investigated whether there was any significant signal delay in the system as this could affect user's ability to associate tactile sensations with the correlating pressure on the

prosthetic device [199]. We placed a force sensor underneath a pressure pad to record the moment the pad was pressed. The experiment was recorded on camera from which we could derive when an electrical connection was made with the use of the LEDs. We recorded an average delay of 22ms (σ=3ms) for the OR gate when either pad was pressed, and an average delay of 116ms (σ=75ms) for the AND gate when both pads were pressed, across five trials.

5.2.3 Tactile Armband

To provide mechanotactile stimulation to the user's upper limb, we designed a wearable haptic interface (fig. 5.12). The design of the tactile armband was based on the Squeeze armband presented in [200], but further developed and optimised for this study. The armband consists of five re-entrant hexagon auxetic units arranged end-to-end, with the addition of hinges along the beams allowing for strong contraction of each unit. It was 3D printed (Wanhao Duplicator i3) with flexible filament (TPU, RigidInk). Coiled SMA wires (BioMetal Helix, BMX series 150) were connected across the centre of the units and secured with glue. When in its relaxed state, the auxetic units are open and in a square shape. When the SMAs are activated, they contract, squeezing the skin in an axial direction. As the SMA actuators are longer compared to those in the previous Squeeze device (section 4.3), thereby increasing the risk of heat transferring from the activated SMA actuators to the wearer's skin, a Kapton® heat resistant layer was added between the SMA wires and the skin. Small PLA printed circles were adhered to the underside of the armband to increase the sensations felt at contact points on the skin. The SMA actuators have a maximum displacement of approximately 9mm and have a linear relationship between voltage and current within the operating range as shown in fig. 5.13.

Due to the auxetic nature of the armband, contracting one auxetic unit will also result in a shortening or contraction of the armband, generating additional circumferential and radial forces

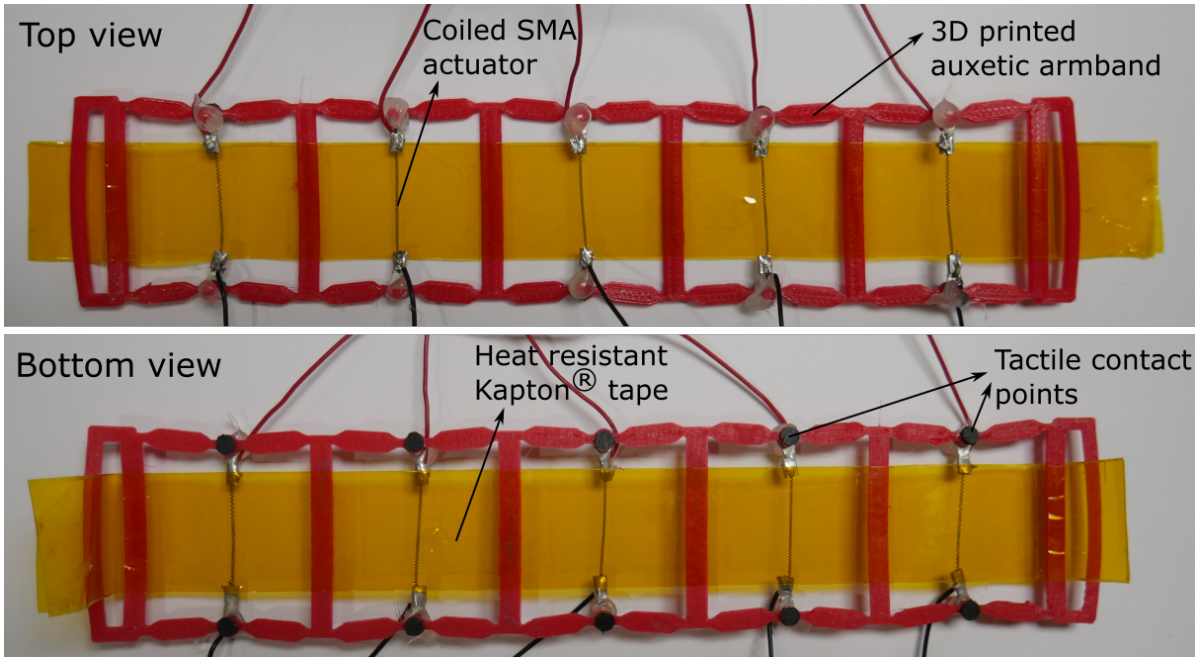

FIGURE 5.12. 3D printed tactile armband consisting of five re-entrant hexagon units. Coiled SMA wires provide contraction of the device, while the Kapton® tape provides a heat resistant layer between these wires and the skin. The tactile points on the bottom of the armband aims to increase the sensations felt on the skin at these points of movement.

on the user's arm (fig. 5.1). The three forces exerted on the arm by the armband are shown in fig. 5.14, and includes an axial force generated by the SMA, a circumferential force generated by the auxetic structure, and a radial force generated by the armband.

5.3 User Study

We investigated subjective responses to the sensations generated by the armband on 20 healthy and non-amputee volunteers (8 female; 12 male; age range 20-50yrs). The volunteers were recruited internally and received confectionery as compensation. The armband was tested in isolation to ensure that the responses provided by the participant were directly related to the armband only. The armband was placed on the participant's arm and activated by an external

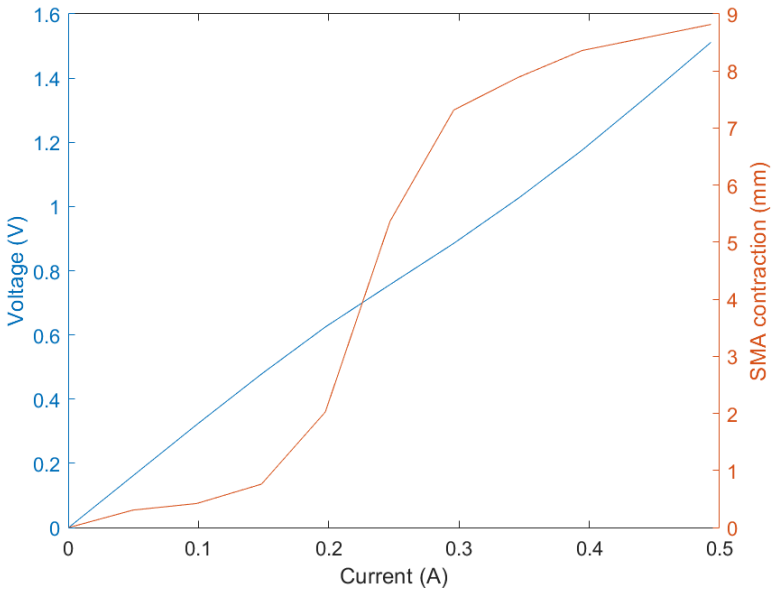

FIGURE 5.13. Current against voltage (left) and contraction (right) graph for a single SMA of the wristband.

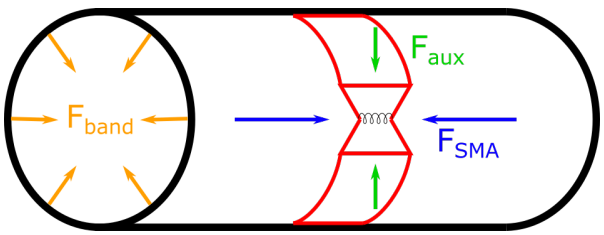

FIGURE 5.14. Forces of the armband on the arm. The arrows indicate the forces exerted on the arm by the: (blue) SMA contraction in the axial direction, (green) auxetic structure in the circumferential direction, (orange) armband in the radial direction.

power supply, with a minimum of 5s between each stimulation to allow the SMA actuators to return to their initial state. They were visually isolated to prevent them from seeing any actuation which may interfere with their responses. The complete setup is shown in fig. 5.15. The user study comprised two parts: determining sensitivity threshold and identifying pressure and position.

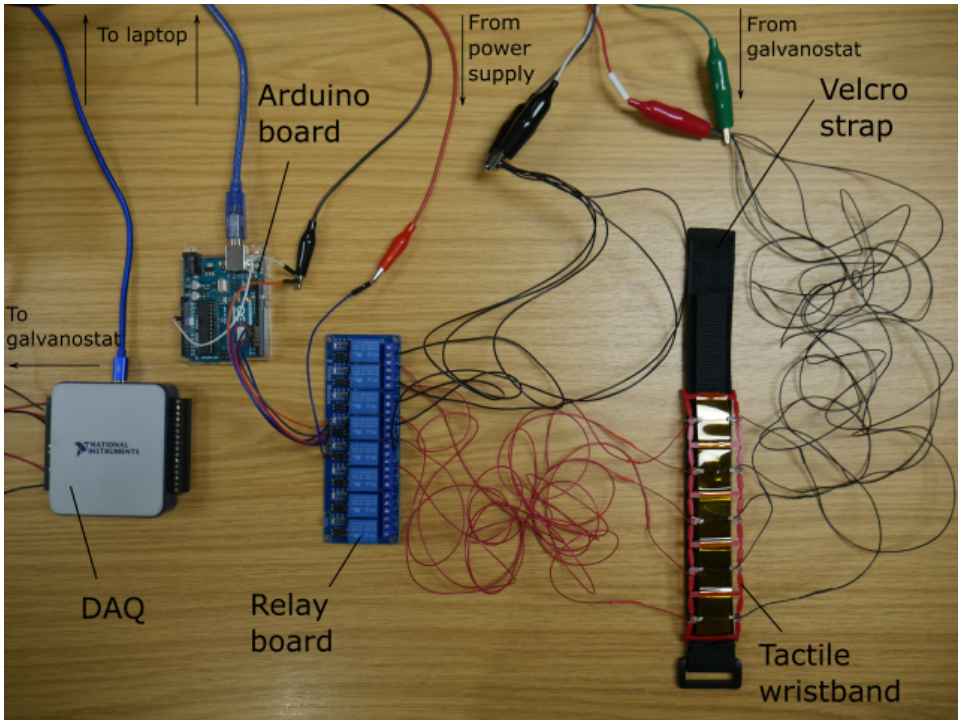

FIGURE 5.15. User study setup.

5.3.1 Sensitivity Threshold

The first part of the user study aimed to determine the sensitivity threshold of the participants' skin; the lowest value of power supplied to the SMA actuator that creates a noticeable sensation on the participant's skin. Two sites for the armband were used: the lower-part of the upper arm and the upper-part of the lower arm, approximately 3cm from the elbow joint either side (fig. 5.16). We used Psychophysics Toolbox Version 3 (PTB-3) on Matlab (2019b) to run the QUEST adaptive algorithm as described by [201]. One SMA of the armband was stimulated (central location) with an initial random estimated threshold of μ=0.1386W (σ=0.03465W), correlating to 200±100mA through 3.465Ω. Depending on the response of the participants, the algorithm would provide a greater or lesser current for each subsequent stimulation, converging on the user's sensitivity threshold (fig. 5.17). Fig. 5.18 shows the sensitivity threshold for all participants for

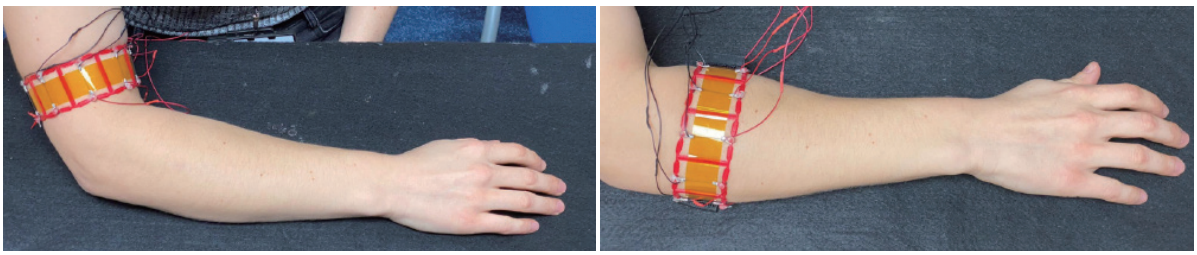

FIGURE 5.16. Location of armband placement on upper arm (left) and lower arm (right) for the user study.

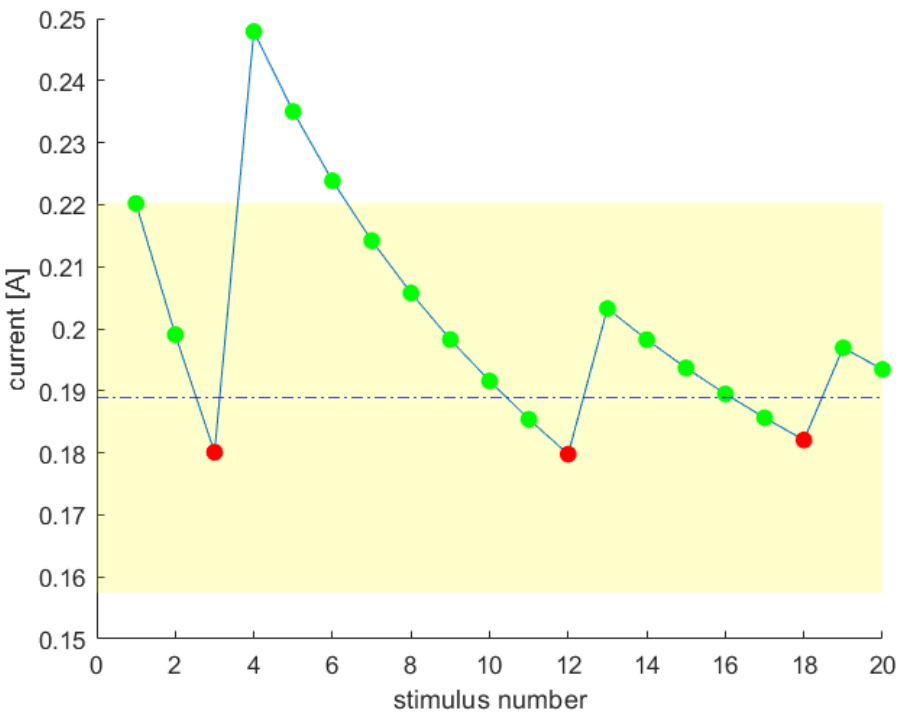

FIGURE 5.17. Example plot of Quest algorithm for one participant. The green data points depict when the participant felt the sensation; red data points depict where sensations were not felt. Calculated sensitivity threshold in blue with yellow standard deviation.

the upper and lower arm. The sensitivity threshold of the two sites are similar, with a mean of 0.149W (σ=0.046) for the lower arm and 0.165W (σ=0.045) of the upper arm. A paired-samples t-test confirmed that there was no reliable difference between the lower and upper arm in terms of sensitivity, $t(19)$=1.39, p=0.182, d=0.31.

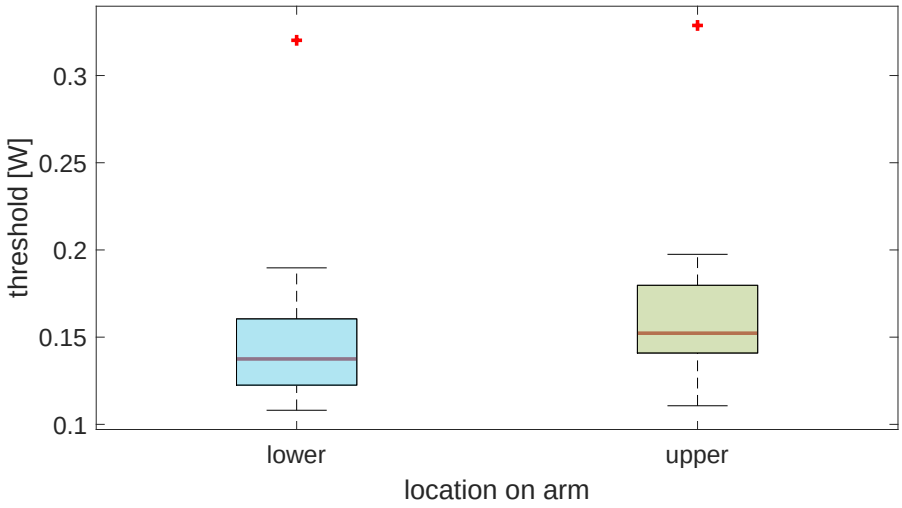

FIGURE 5.18. Skin sensitivity threshold of participants presented as power of SMA contraction, comparing the lower with the upper arm. Median values expressed by the red lines; 50% of the values lie within the box; the whiskers account for 25% either side; outliers depicted by red '+'.

5.3.2 Strength and Location Mapping

The second part of the user study aimed to determine the ability of the participants to distinguish between different strengths and different locations of activation. First, one SMA (central location) was activated randomly at three different powers relative to the participant's threshold value: 1.1, 1.5, and 1.9 times the threshold value. As $P = I^2R$ (P=Power; I=Current; R=Resistance), where R is assumed to be constant, this correlates to 1.05, 1.22 and 1.38 times the current at threshold. The participants were asked to rate the strength of the sensations on a scale of 0-3 (0 = did not feel, 3 = strongest). Secondly, all SMAs were activated individually in a random order at 1.5 times the power of the participant's threshold value. The participants were asked which SMA was activated.

Participants found it difficult to distinguish between different powers of actuation of the armband (fig. 5.19), with only 66% correct responses.

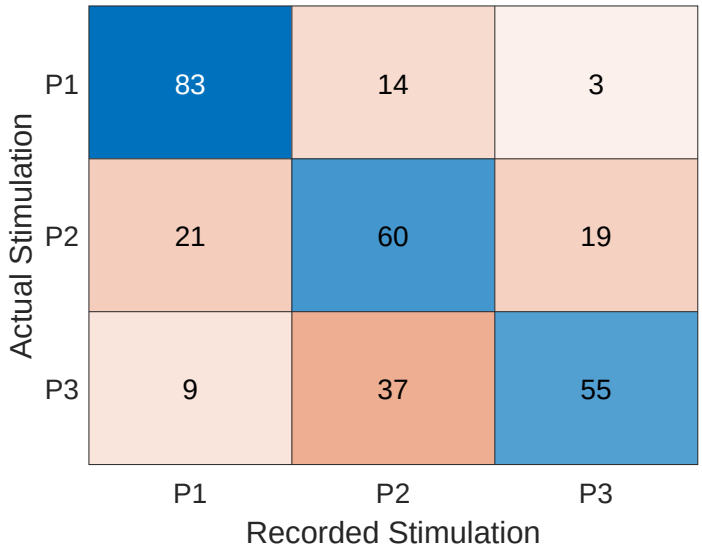

FIGURE 5.19. Confusion matrix in percentages of the three different powers where P1 = 1.1, P2 = 1.5, and P3 = 1.9 times the threshold power.

In comparison, participants found it easier to detect the different locations of tactile stimulation with 81% correct responses. However, where users incorrectly guessed a position, they almost exclusively selected the position next to the correct one (fig. 5.20 and 5.21) with the majority of participants at a mean absolute difference of between 0-0.2 (fig. 5.22).

5.4 Proof-of-Concept

To demonstrate how the device could be used in a real-world scenario, we set up a two fingered robotic gripper controlled by a participant wearing the armband (fig. 5.23). A fluidic sensor pad was attached to each finger of the gripper and connected using the OR/AND gate logic as described above (fig. 5.11). A screen was placed between the participant and the robotic gripper to hinder visual cues and force the participant to rely solely on the tactile feedback provided by the B:Ionic glove. The objective of the task was to grip a Rubik's cube placed between the fingers of the grippers with sufficient force to allow it to be picked up. This test highlights how

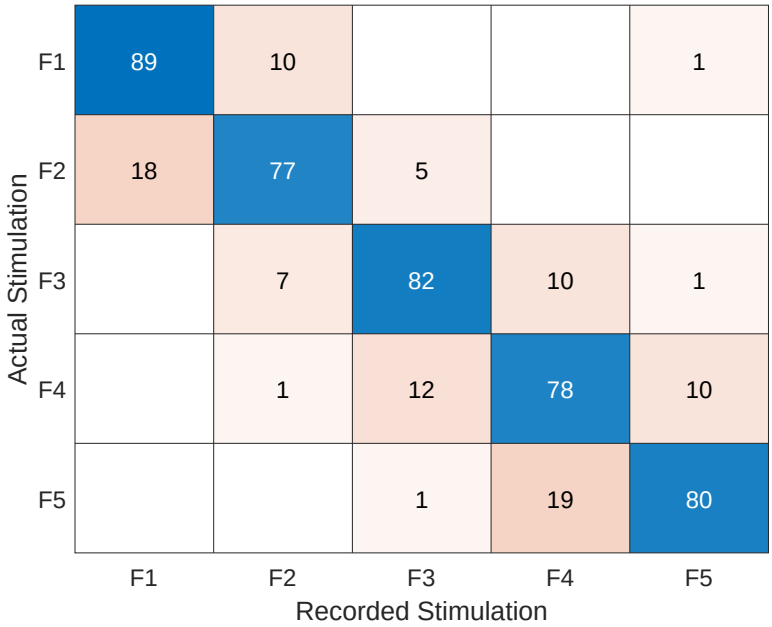

FIGURE 5.20. Confusion matrix in percentages of the five different locations; F1 = thumb, F2 = index, F3 = middle, F4 = ring, and F5 = little finger.

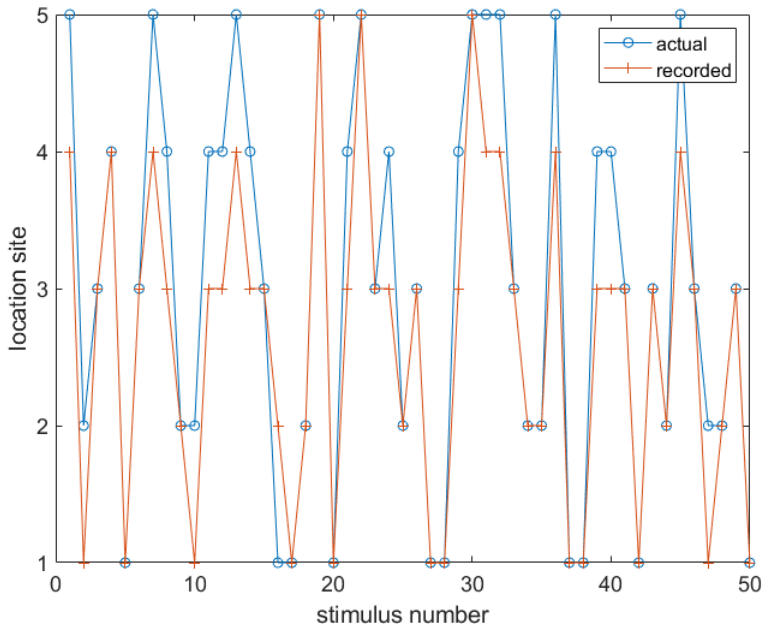

FIGURE 5.21. Example of participant data for detecting location with actual site in blue and recorded site in orange. The graph illustrates that even though participants may not have recorded the correct absolute location, they were able to detect most locations relative to their previous answers.

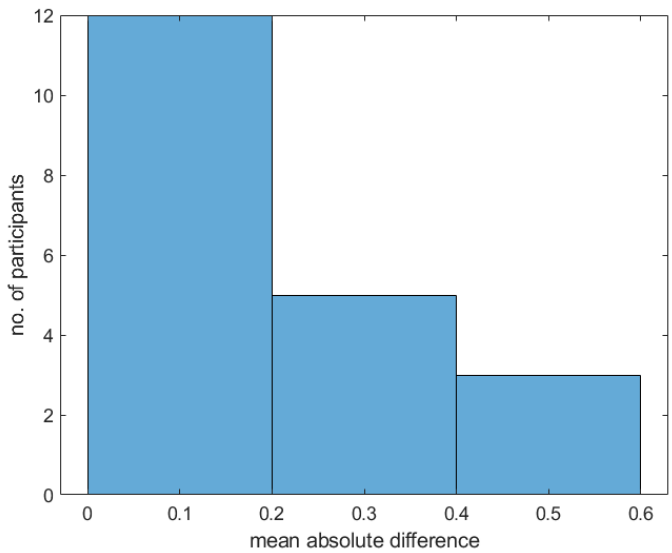

FIGURE 5.22. Mean difference between responses and stimuli for all participants. The graph illustrates that even though participants may not have recorded the correct absolute location, they were able to detect the location relative to their previous answer.

the glove could offer a sense of touch for upper-limb amputees who currently can only rely on their vision to grasp objects [104]. In addition, the glove could assist them in better handling of delicate objects. Both gripper fingers were controlled independently by separate servo motors connected to switches with 3 modes: closing, stop, and opening. The participant attempted to close the gripper until both pressure pads were in contact with the object. If only one of the pads is in touch with the object, only the SMA connected to the OR gate contracts. When both pads contact the object with sufficient force, the SMA connected to the AND gate also contracts, allowing the user to identify when the object is safely gripped. The OR/AND gate logic operates as a discretised version of pressure sensing.

We have successfully demonstrated grasping of a Rubik's cube using the B:Ionic glove sensor system using only tactile feedback from contraction of the SMA actuators. We also showcase how a possible control architecture could be achieved with simple OR/AND gate logic. Although

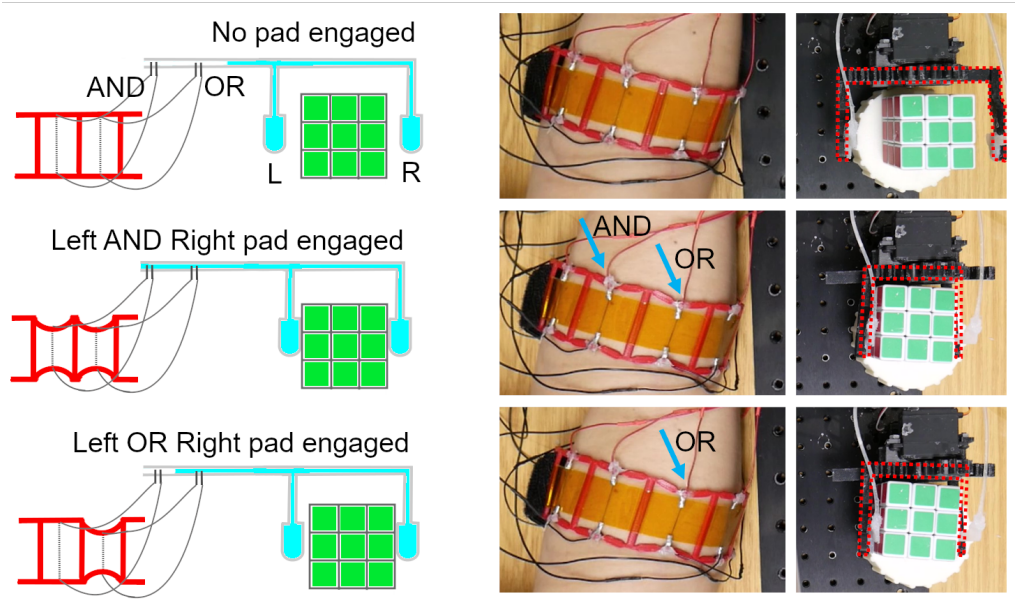

FIGURE 5.23. Illustration and video frames of the proof-of-concept demonstration. The experimenter wears the armband and controls a two fingered gripper (outlined with a red dashed line) bearing pressure pads to grasp a Rubik's cube using the sensory feedback encoded by the control unit (AND/OR gates).

only one participant partook in this proof-of-concept study and only grasping of a Rubik's cube was tested, we aim to expand this to a full-scale user study in future work to investigate the effectiveness of the glove and the tactile response of the system on various objects. The successful demonstration of working OR/AND gate logic, though simple in this first demonstration, opens up the possibility to perform complex computations in more elaborate tasks [197].

5.5 Discussion on B:Ionic Glove

This chapter presents the B:Ionic glove, a wearable tactile feedback device for use with upper limb prosthetic devices. Experiments were conducted to test the ability of the device to bridge the sensory gap between a prosthesis and the skin. The various components were characterised separately and a prototype of the whole device is shown in fig. 5.2.

The pressure pads (section 5.2.1), control unit (section 5.2.2), and tactile armband (section 5.2.3) all showed potential as a sensory feedback device for upper limb prostheses.

The device in its current design can be tailored and altered to the specific wearer. Control is not only affected by the geometry of the pressure pad (fig. 5.7), but can also be fine-tuned by other factors including the volume and viscosity of the conductive fluid in the channels, diameter of the channels, space between the gates, and space between pairs of electrodes. The SMC controller has scope for further control and computation, such as integral memory. For example, fluid could move from one sensor channel (e.g. fig. 5.11A) to another (e.g. fig. 5.11B) after a grasp, self-adjusting sensitivity ready for the next grasp.

Even though there was no significant different between the average sensitivity threshold for the lower and upper arm of participants, it is interesting to note that in 75% of the participants, the sensitivity threshold of the individual's upper arm was higher than their lower arm (fig. 5.24). This corresponds to the data presented in [202] which shows that the two-point discrimination distance is greater on the upper arm than the lower arm. This suggests that there are more sensory nerve endings present on the forearm and therefore we would expect the sensory threshold for the forearm to be lower.

The three levels of power used for differentiation were chosen to ensure a range within the capabilities of the SMA wires (150-400mA) which was tailored to their skin sensitivity. A lower power would result in the SMA contracting more slowly and with a lower contraction than a higher power. Higher powers also require a longer period for cooling and participants noted that it was sometimes the relaxation that they felt as opposed to the initial squeezing. In general, people with a lower skin threshold found it easier to differentiate the lowest strength from the highest two, whereas people with a higher threshold found it easiest to distinguish the highest strength from the lowest two. This may be because when the sensitivity is high, the highest

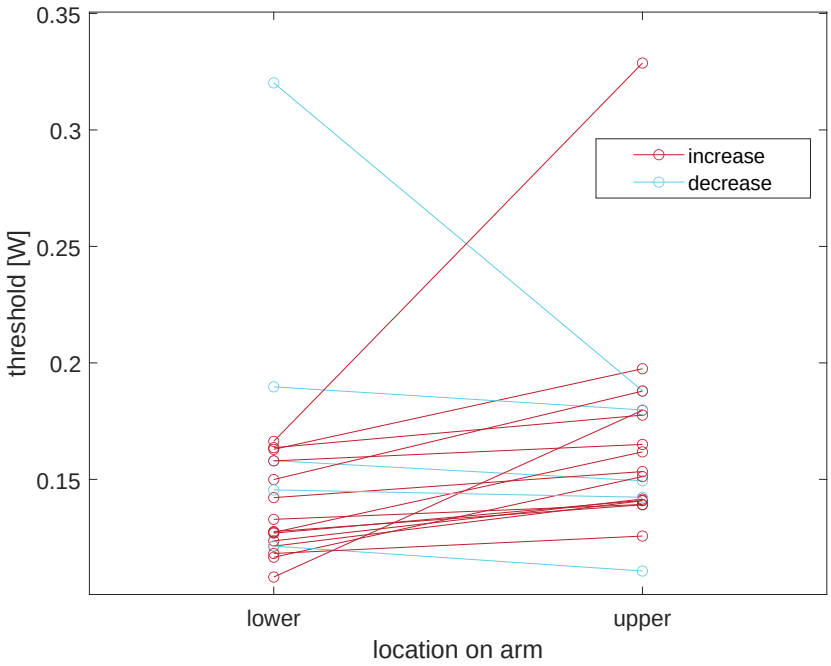

FIGURE 5.24. Skin sensitivity threshold of participants presented as power of SMA contraction, comparing the lower arm with the upper arm. The plot highlights participants with an increase (red) and decrease (blue) in threshold values from their lower to upper arm.

strength is close to the maximum capability of the SMA and some people recorded they could feel a slight heat from the SMA wires.

The participants found the location differentiation test to be intuitive. The normal pressure distributed across the arm generated by the auxetic nature of the armband did not interfere with the participants' ability to distinguish between actuation sites. Some participants found the outer two locations of the armband (i.e. correlating to the thumb and little finger) the hardest to distinguish. This may be due to the thicker velcro strap at the end of the armbands making it stiffer. Most participants could distinguish between three particular regions of stimulations: region containing location 1 and 2, region containing location 3, and region containing location 4 and 5. As location 3 was used throughout the previous part of the user study, participants may

have become familiarised with the location of this stimulation. The two-point discrimination threshold as stated by [202] for the forearm is approximately 38mm. The distance between the SMA actuators on the B:Ionic armband is 32mm, so increasing this distance may also improve user's ability to distinguish between different sites of stimulation. This would need to be explored in future work.

Efforts were made to ensure all SMA actuators were of the same length but variation in resistance from 3.31-3.70Ω was found. Lower resistance instilled a stronger SMA response. We allowed enough time between stimulations for the SMAs to return to their relaxed state. However, repeated stimulation of the same area of skin could lead to saturation of the mechanoreceptors and therefore a lower sensitivity. Further work would need to characterise this.

In general, people tended to find the device pleasant and stated the sensations as "tingling", "twitching", "something crawling", or "muscle activity".

To continue the development of the B:Ionic glove, further user evaluations will need to be completed. While the evaluation in this paper focused on assessing the performance of the individual glove components, these further experiments will need to measure the performance of the entire system on a range of every day tasks including grasping a range of commonly used objects. Experiments will also need to be carried out involving users of prosthetic limbs to test the B:Ionic glove in a realistic scenario, while gathering qualitative feedback about ease of use and device comfort.

For the B:Ionic glove to operate in the real world, it must be capable of operating untethered, with power consumption low enough to enable long-term use. The SMA actuators used in the wristband require an operating voltage of 1.5-3V, meaning they can be powered by a small lithium polymer battery.

By using an electro-fluidic control scheme, we eliminate the need to power pressure sensors

or a micro-controller. While the electro-fluidic control scheme currently requires additional electronics to generate an AC signal, we can use alternative conductive fluids (such as liquid metal) to overcome this limitation.

5.6 Conclusion

This chapter presents the proof-of-concept of the B:Ionic glove which has the potential to be used as a sensory feedback device with upper limb robotic prostheses (objective 3, section 1.5). The device is completely soft and wearable with on-board computation. We have shown that the device can be used to relay different strengths and locations of pressure from prosthetic fingertips to the user's skin, with scope for more complex computation. In future work, we will test the device on upper limb amputees to assess the device in real applications. With this device, they may be able to grasp objects more naturally and intuitively without relying solely on visual feedback. This could reduce phantom limb pain and increase embodiment, consequently increasing acceptance of the prosthetic device and reducing the current high rejection rates.

The tactile feedback devices described in chapter 4 and this chapter are currently worn on the skin where care needs to be taken that external objects, such as clothing, do not interfere with it. To be able to make these devices more wearable and useful in everyday life, it would be beneficial if they could be integrated into fabric so they may be worn as part of clothing. This will be investigated in the next chapter, through the outline development of auxetic textiles.

CHAPTER 6

AUXETIC TEXTILES

Chapters 4 and 5 looked at using auxetics as a means of conveying information to the skin. This chapter investigates various fabrication techniques for generating auxetic textiles that have the potential to make haptic feedback devices more discreet and comfortable to wear, addressing objective 4 (section 1.5).

The majority of current fabrication methods for generating auxetic textiles do so by incorporating the auxetic structure in the weave of the fabric, either on the macro- or micro-scale [149], as described in section 2.7. In contrast, here we generate auxetic textiles by 3D printing the auxetic structure and combining it with a fabric.

This chapter aims to establish a simple fabrication method for generating auxetic textiles and determine the use of auxetic geometries in wearable clothing. Specifically, determining the potential advantage of using auxetic fabrics to adapt to anatomical protrusions, such as joints and bony structures. It is well known that there are people, for example elderly, that can find it difficult to don socks. Additionally, amputees struggle daily with the fluctuating volume of their residual limb, and the prosthetic sockets that do not accommodate it. As we have seen in chapter 2, the properties of auxetics make them a promising option to explore for use in wearables. This

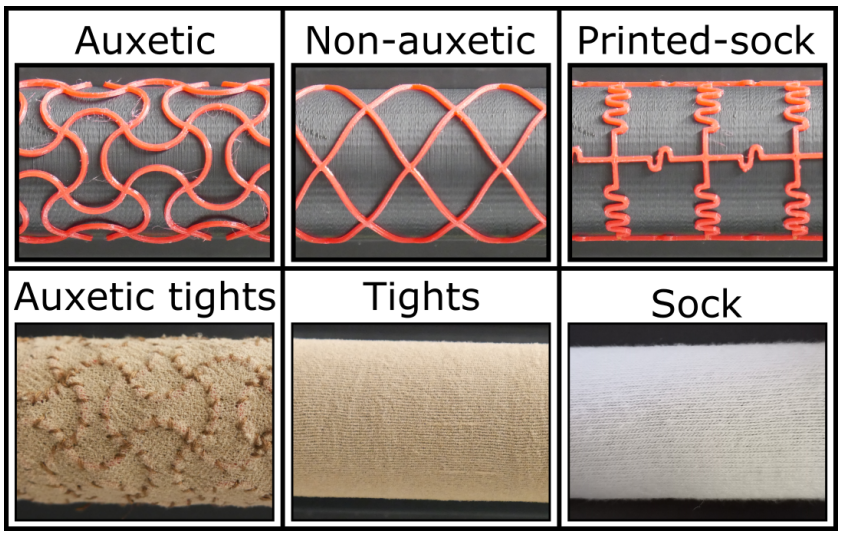

FIGURE 6.1. Reference for the specific sample terminology cited throughout this chapter.

is not only due to their auxetic effect that could accommodate changes in anatomical features (e.g. joints, or fluid retention), but also due to their synclastic nature where out-of-plane bending results in both axes bending in the same direction creating a dome shape (section 2.6.3.2), allowing them to shape more easily around curved surfaces such as joints.

First, we compare the behaviour of three 3D printed sleeves when pulled over a protrusion; an auxetic geometry, a non-auxetic geometry, and a structure that represents the fabric of a sock. We then incorporated the auxetic 3D printed sleeve with a fabric as a first prototype of smart auxetic clothing. We explore various fabrication techniques, aiming to establish a simple method for creating auxetic textiles. Fig. 6.1 acts as a reference for the specific sample terminology cited throughout this chapter.

6.1 3D Printed Sleeves

The following 3D printed cylindrical structures were created for comparison; auxetic, non-auxetic, and printed-sock. The auxetic cylinder is a re-entrant sinusoid Tiled Auxetic Cylinder (TAC)

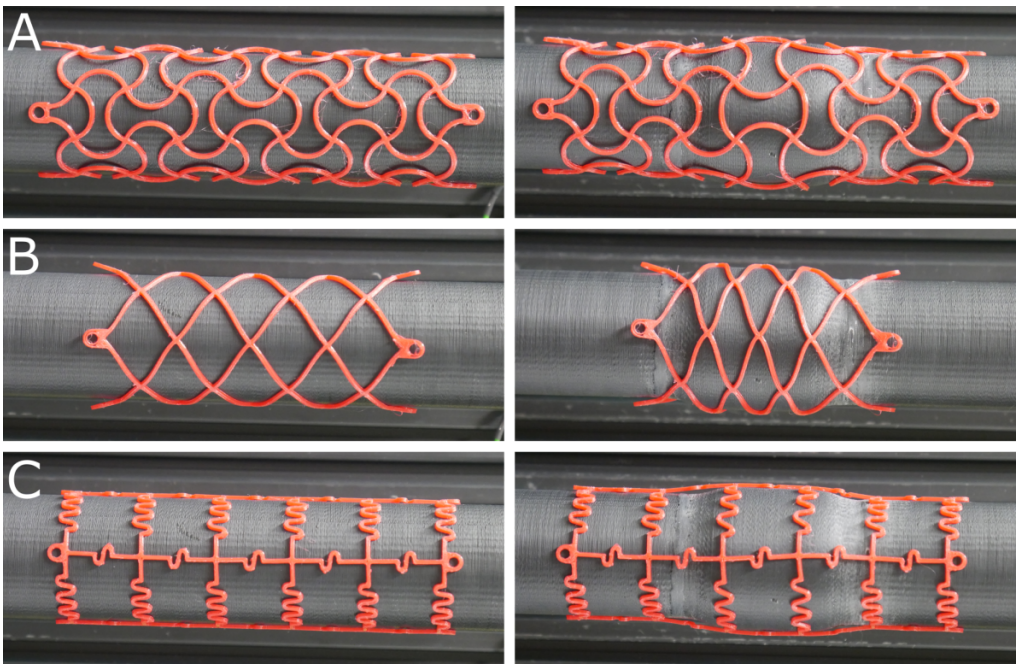

FIGURE 6.2. The three 3D printed cylindrical sleeves studied as shown at rest (left) and when stretched over a protrusion (right); (A) auxetic, (B) non-auxetic, (C) printed-sock.

as seen in chapter 3. The non-auxetic cylinder is made up of a simple diamond pattern. The printed-sock was designed to resemble the characteristics of sock fabric, i.e. less elastic in the longitudinal direction than to the perpendicular. A picture of the different structures can be seen in fig. 6.2, both at rest (left) and when stretched over a protrusion (right). As can be seen in fig. 6.2, the auxetic (A) and sock (C) structures expand radially over the protrusion. In contrast, the non-auxetic diamond structure (B) shortens in length to allow this radial expansion over the protrusion.

6.1.1 Fabrication

The structures were 3D printed (Wanhao Duplicator i3) using flexible filament (rigid-ink TPU) in a flat configuration, after which they were rolled into a cylinder and glued (Loctite superglue). All structures measured 100mm by 100mm when flat.

6.1.2 Force Comparison

Firstly we measured the force required to pull the structures across a protrusion which represented a joint, such as the ankle. The experimental set-up for this is shown in fig. 6.3 with the dimensions illustrated in fig. 6.4. A simple representation of a limb with a protruding joint was 3D printed with the same printer but with PLA (rigid-ink), with a minimum and maximum diameter of 35mm and 40mm respectively. This corresponds to a circumference of 110mm and 125mm respectively. The cylindrical structure was initially placed around the limb below the joint protuberance. Non-extendable metal wires were attached to the ends of the structure. These wires connected to a platform on the linear actuator at the top of the test setup. The actuator pulled the sample along the limb and over the joint at a rate of 10mm/s.

A load cell (DBCR-100N-002-000, Applied Measurements Ltd., max. load 100N, calibrated with 0, 100g, 200g, 500g, and 1000g weights) was attached to the bottom end of the limb to measure the force required to pull it over the joint. A displacement laser (LK-G152, KEYENCE) measured the position of the linear actuator platform as a representation of the distance that the sample travelled. Both sensors were connected to a DAQ National Instrument (USB-6001) that fed into a laptop. MATLAB (R2019a) was used to run the experiment and record the data.

The comparison between the forces recorded as the structure was pulled along the limb are shown in fig. 6.5 as an average of three trials. The first arrow (solid line) indicates the point at which the samples were starting to be pulled. The second arrow (dashed line) indicates the point at which the samples reached the protrusion.

It is clear that the non-auxetic structure greatly increases the force required to pull the structure across the limb, especially when it crosses the protrusion; reaching almost 50N. This can be seen in fig. 6.2B (right) where it is clear that the structure is shortening in length to a

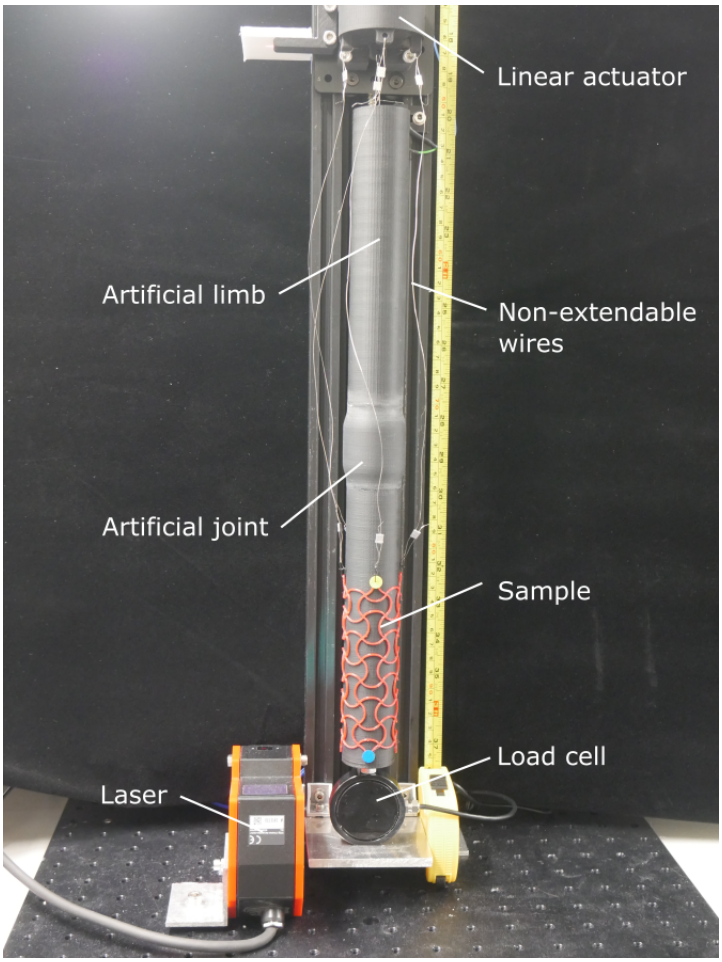

FIGURE 6.3. Experimental set-up for determining the force required to pull the structure over the replicate limb and joint.

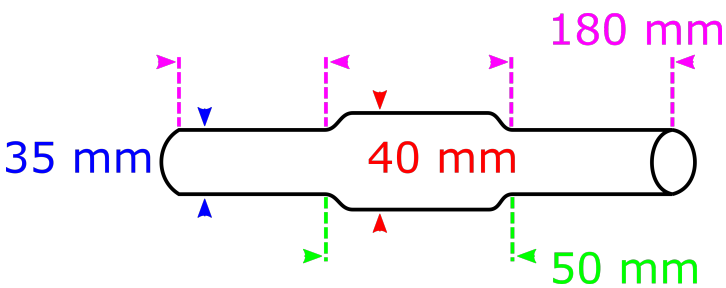

FIGURE 6.4. Dimensions of the limb and joint over which the structures are pulled.

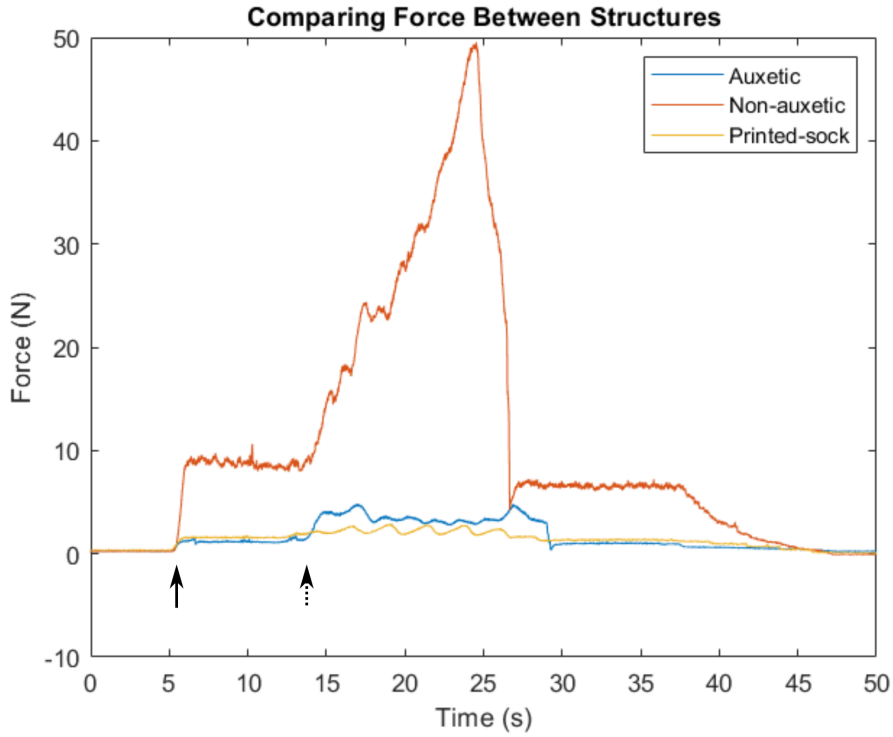

FIGURE 6.5. Force comparison between the three 3D printed structures: auxetic, non-auxetic and printed-sock. The solid lined arrow indicates point of sample being pulled; the dashed lined arrow indicates point of sample reaching joint.

significant degree in an attempt to accommodate the increase in diameter of the protrusion. The auxetic structure requires significantly less force, at approximately 1.20N to 3.20N from limb to joint respectively. Interestingly, the auxetic structure requires some extra force when the first and final circumferential ring reaches the protrusion. This is because once the structure has been pulled onto the joint, the auxetic nature of the sample will open up the cylinder, making it easier for subsequent rings to be pulled on to the protrusion. The printed-sock requires slightly more force compared with the auxetic structure when on the limb, at approximately 1.25N, and the least amount of force out of these three structures when on the joint, fluctuating between approximately 1.50N and 2.50N. This fluctuation in force seen here when it crosses the protrusion is due to the individual circumferential springs in the structure when they reach the start of

the protrusion adding extra constraints. The spiked decreases seen once all the structures reach the end of the protrusion is due to the end of the structures 'jumping' off the protrusion onto the narrower limb.

6.1.3 Relative Poisson's Ratio

To obtain the relative Poisson's ratio of the cylinders, the samples were tested with a similar experimental method as described in [203] (section 3.3, fig. 3.3). The samples were placed in the same set-up as shown in fig. 6.3, with the limb and joint removed. The bottom end of the sample was fixed to the load cell, the top end was attached with the non-extendable metal wires to the carriage on the linear actuator which moved to increase the length of the sample. The elongation was measured using the laser sensor and both the displacement and force was recorded using a data acquisition system at a frequency of 1000Hz. A camera (Panasonic, DMC-G7) recorded each experiment at 50fps with a resolution of 1920x1080 pixels. Each frame was analysed in MATLAB using MATLAB's Image Processing Toolbox add-on to determine the change in length with diameter. The results are shown in fig. 6.6 with the raw data depicted with a solid line and the line of best fit depicted with a dashed line. The relative Poisson's ratio from this line of best fit (taken as the negative of the slope of the graph) are presented in table 6.1. As expected, the non-auxetic sample shows a positive relative Poisson's ratio and the auxetic sample shows a negative relative Poisson's ratio. The printed-sock shows an initial decrease in diameter and then the diameter remains relatively even with increased length. This initial decrease is believed to be due to setup issues where the sample was leaning more towards one side until it became under tension. The diameter was determined in MATLAB by measuring the distance between the furthest most points on each side of the cylinder. Hence if the sample was not completely lined up, this could lead to inaccurate calculations of the diameter.

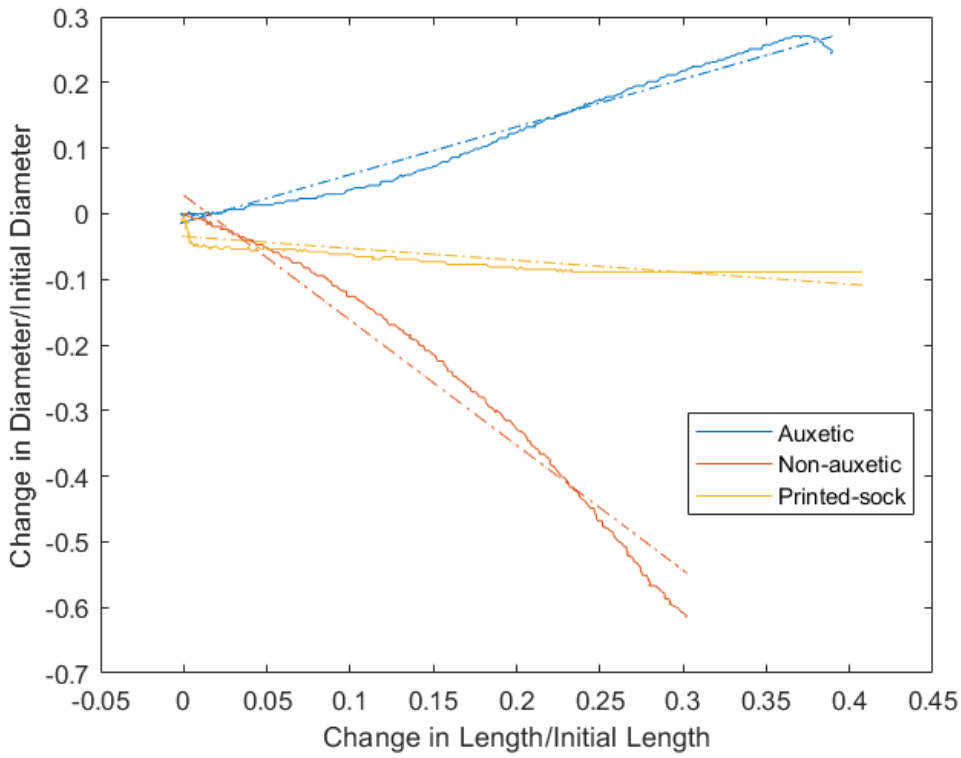

FIGURE 6.6. Normalised strains of the length vs diameter of the three 3D printed samples. Solid line depicts the raw data; dashed line depicts the line of best fit.

Design	Equivalent Poisson's ratio
Auxetic	-0.73
Non-auxetic	1.90
Printed-sock	0.18

TABLE 6.1. Equivalent Poisson's ratio for the three 3D printed samples.

6.2 Auxetic Socks

Next, an auxetic sock was fabricated by incorporating the 3D printed auxetic sleeve characterised above with a piece of fabric. Various fabrication methods were explored generating different prototypes of auxetic socks.

6.2.1 Fabrication

6.2.1.1 Direct Printing

Initially, an auxetic sock was created by stretching a section of tights (94% nylon, 6% elastane LYCRA® fibre, 10 denier, natural) across the 3D printer print-bed before printing the auxetic structure, as characterised above, directly onto it. Although this did not cause any fabrication issues, unfortunately this pre-stretch in the tights constrained the auxetic structure from expanding as it crossed the protrusion (fig. 6.7B). Therefore, the next step was to print on the tights whilst they were not pre-stretched. As this would result in the 3D printer nozzle catching on the loose material, it was first glued to a plastic sheet using PVA (Tiger) (fig. 6.7A). After printing, this glue was washed off to detach the sample from the plastic sheet. However, this method resulted in some detachment of the tights with the printed auxetic structure (fig. 6.7C).

6.2.1.2 Sewing

In order to overcome this bonding issue, stitching was used to sew tights material to both the top and bottom layer of the auxetic structure, effectively encapsulating it (see fig. 6.8). Even though this was an effective bonding technique, the tights material was still constraining the auxetic effect. The cylindrical limb that the samples were pulled across measures 110mm in circumference, so the auxetic structure was scaled up by 10% (i.e. now measuring 110mm by 110mm in a flat configuration) to ensure it was at its complete resting state, allowing maximum expansion of the auxetic effect when crossing the protrusion. However, a fair comparison could not be made between this sample and the 3D printed auxetic sample as the surface friction when pulled across on the limb would be different for the tights and TPU respectively.

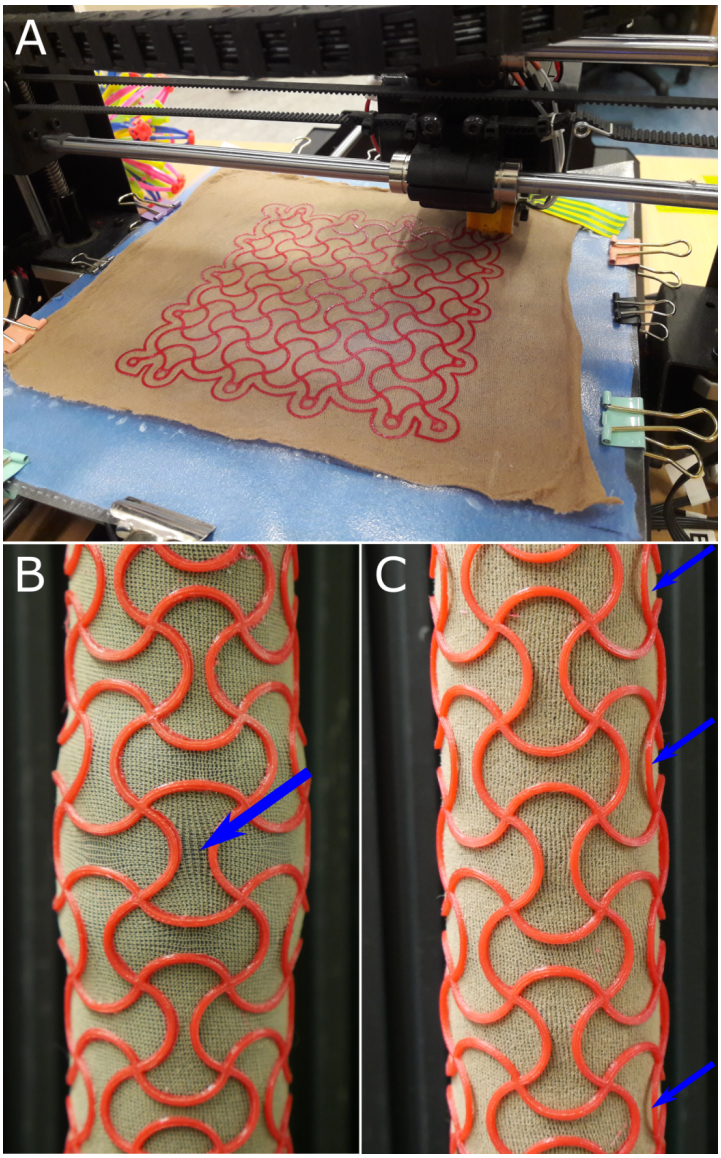

FIGURE 6.7. A) Fabrication method for creating an auxetic sock. The auxetic structure was directly printed onto a section of thin fabric which was either stretched across the print bed to produce the auxetic sock shown in B, or glued onto a plastic sheet (as shown in A) to produce the auxetic sock shown in C. B) First prototype of auxetic sock shown on the protrusion to highlight the tights fabric constraining the auxetic structure from expanding (blue arrow). C) Second prototype of auxetic sock shown on cylinder to highlight the detachment of the auxetic structure from the tights fabric following the washing off of the PVA glue (blue arrows).

FIGURE 6.8. Auxetic tights fabricated by sewing, at rest (left) and when stretched over the protrusion (right).

6.2.1.3 Pre-stretching

Lastly, to overcome the discrepancy in surface friction, we attached fabric to one side of the auxetic structure. In order to prevent any constraining of the auxetic structure by the fabric, the fabric was attached to the 3D printed auxetic whilst the latter was in its expanded state. For this a frame was created, much like an embroidery frame, into which the auxetic structure was mounted. A section of sock material was then laid under the auxetic and sewn on along the beams of the auxetic with a sewing machine (fig. 6.9A). The stitching from the machine was found to be too close together. This constrained the beams of the auxetic from bending sufficiently to return to their relaxed state (fig. 6.9B). Instead, the sock material was sewn onto the auxetic structure by hand, but only at the intersecting points of the beams (fig. 6.9C). Unfortunately, this was a lengthy process and the TPU of the auxetic structure had undergone plastic deformation when mounted on the frame, meaning it did not completely return to its original state. The resulting auxetic fabric sock is shown in fig. 6.9D. Sock material was used instead of tights material as

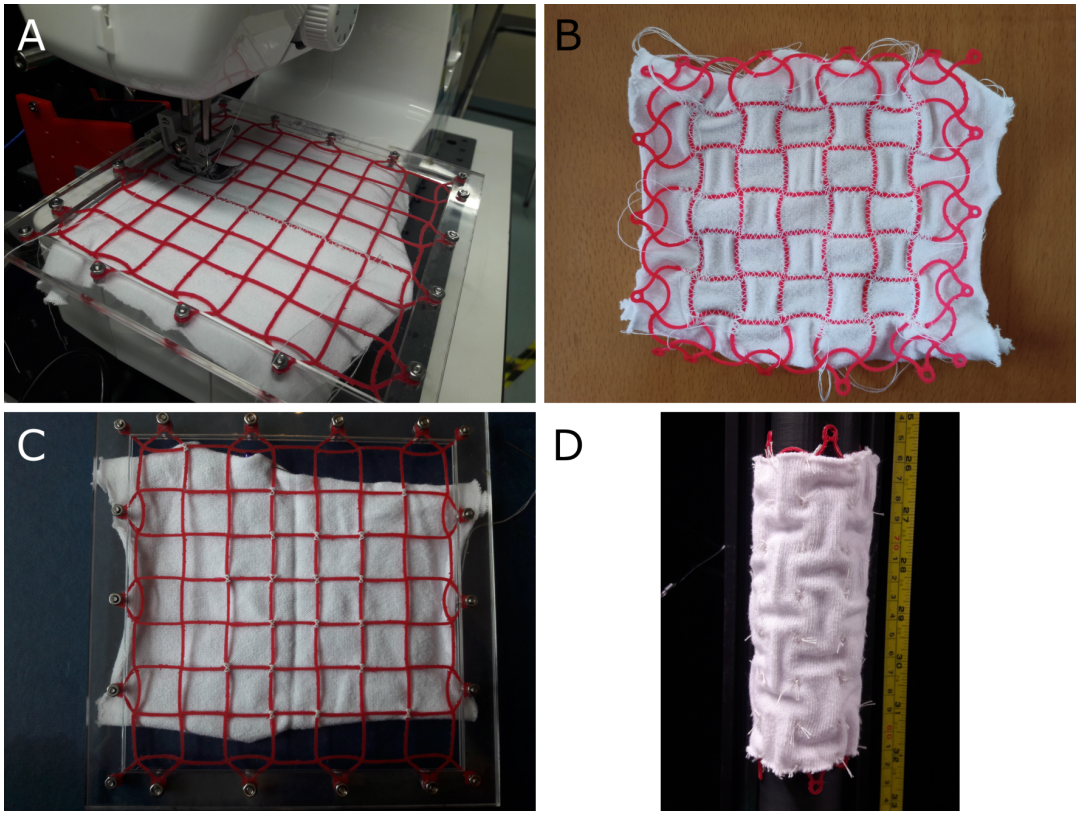

FIGURE 6.9. Auxetic socks fabricated by sewing over pre-stretched auxetic structure; A) method of using sewing machine, B) final structure after using sewing machine illustrating the constraint of the thread on the beams of the auxetic, C) method of sewing by hand at beam intersecting points only, D) final structure after sewing by hand at rest.

this makes a fairer comparison to the 3D printed-sock structure which was created to imitate the characteristics of sock material. Tights fabric was used for direct printing and sewing fabrication methods as this fabric needed to be thin enough for this to be possible.

6.2.2 Force Comparison

The force required to pull an auxetic fabric (auxetic tights, fig. 6.8) across the artificial limb was measured using the same method as outlined in section 6.1.2. Cylindrical samples were also created of sock fabric and tights fabric alone, such that their resting diameter matched that of the auxetic tights (at 35mm) for a fair comparison. A comparison was made between these three

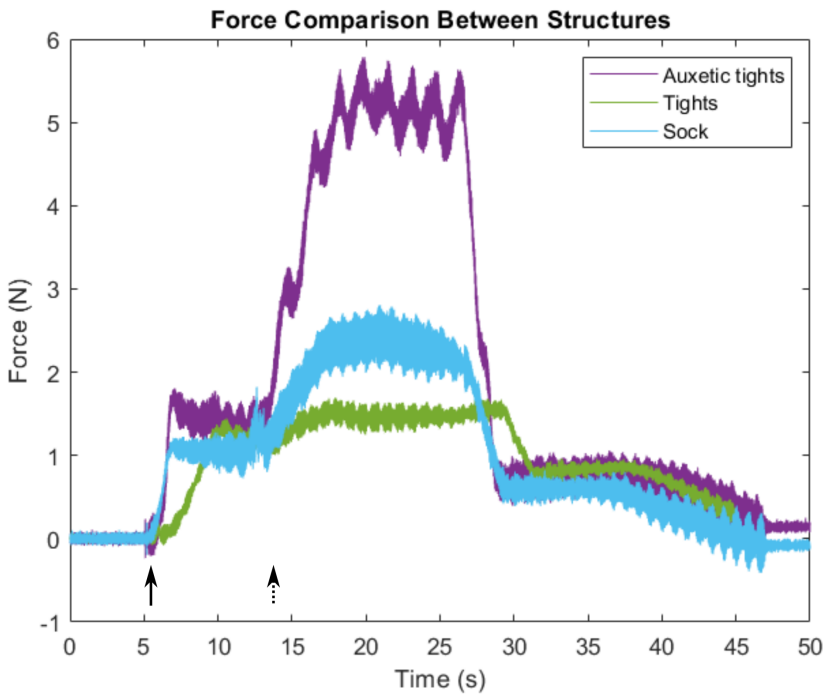

FIGURE 6.10. Force comparison between the three fabric structures: auxetic tights, sock and tights alone. The solid lined arrow indicates point of sample being pulled; the dashed lined arrow indicates point of sample reaching joint.

samples and shown in fig. 6.10. The solid lined arrow denotes the point at which each sample started to be pulled; the dashed lined arrow indicates the point at which each sample reached the protrusion.

The auxetic tights required the greatest amount of force to pull across the cylinder compared to tights fabric alone and sock fabric alone. Despite scaling the auxetic structure within the auxetic tights to have an equal diameter to the limb, there still seemed to be constraints imposed by the interaction of the auxetic structure and the tights fabric.

We also made a comparison of the pulling forces required between the 3D printed structures presented in section 6.1 and the auxetic tights presented in section 6.2. Fig. 6.11 shows the results of the sock fabric compared with the printed-sock and the auxetic structure compared with the auxetic tights. Again, the solid lined arrow denotes the point at which each sample

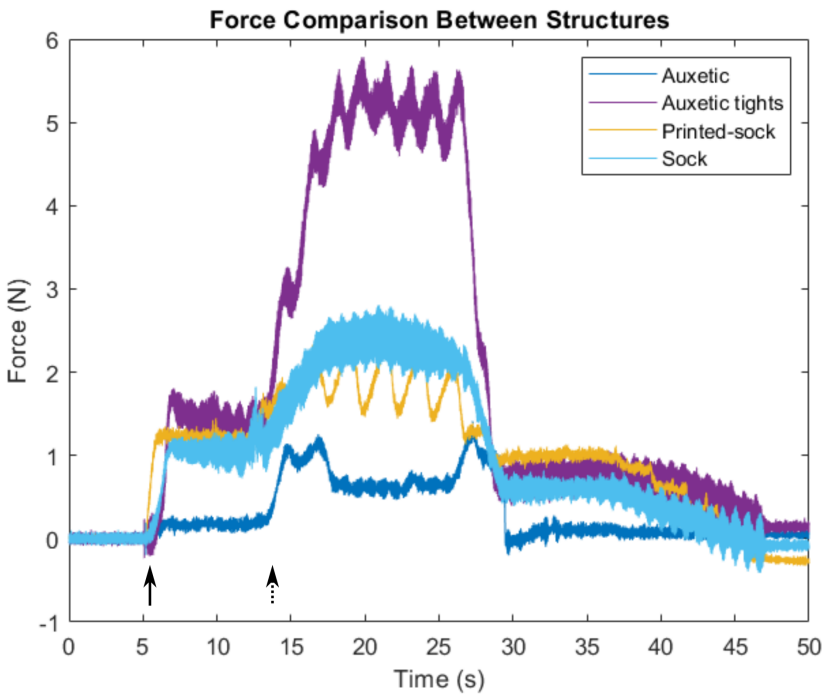

FIGURE 6.11. Force comparison between 3D printed and fabric structures: sock, printed-sock, auxetic and auxetic tights. The solid lined arrow indicates point of sample being pulled; the dashed lined arrow indicates point of sample reaching joint.

started to be pulled; the dashed lined arrow indicates the point at which each sample reached the protrusion. The sock fabric and printed sock samples have comparable forces, although these two samples had different resting circumferences, at 110mm and 100mm respectively. One noticeable difference is that the force required to pull the printed sock fluctuates. This is due to the design of the printed sock where is has circumferential rings along its cylindrical length rather than being a continuous sample as is the case with the sock fabric. The auxetic sample used in this experiment was also at the larger scale (at 110mm circumference) to match that of the auxetic tights and allow maximum expansion of the auxetic geometry when pulled across the protrusion. The auxetic tights require a greater amount of force compared to the 3D printed auxetic sample, again due to the constraints of the tights fabric not allowing the auxetic geometry to expand to its full potential.

In addition to this constraint imposed on the auxetic characteristic by the tights, another aspect which we felt may have an affect on these results is the resting tension of the samples on the limb which may result in different frictional forces.

6.3 Resting Tension

To make a fair comparison between the pulling forces presented above, we need to establish the resting tension of each structure on the artificial limb.

6.3.1 Method

The setup for measuring the resting tension of a sample is shown in 6.12. One circumferential ring of the structure was measured per sample. The structure was orientated perpendicular to the load cell such that the circumferential ring could be attached to it. The other side of the ring was then attached to the linear actuator and extended so that the distance between the two attachment points was equal to half the circumference of the limb (i.e. 55mm). The force to keep the sample in this position was then recorded for 10 seconds and an average taken. The samples measured were the 3D printed auxetic, 3D printed non-auxetic, 3D printed sock, auxetic tights, and tights fabric alone.

6.3.2 Results

As shown in fig. 6.13, the 3D printed non-auxetic has the highest resting circumferential force. This means that it exerts the most force on the limb at rest and may result in higher frictional forces when being pulled along the limb. The tights fabric was the loosest sample on the limb and even shows a slightly negative force. This is attributed to slight inaccuracies in the setup.

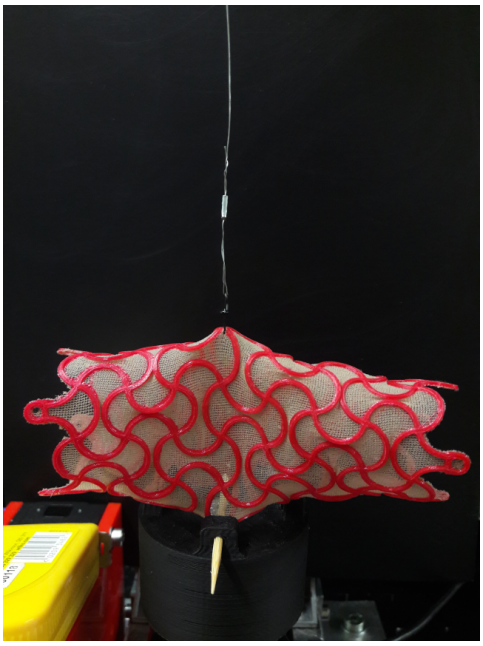

FIGURE 6.12. Resting tension setup as illustrated with one of the printed auxetic tights samples.

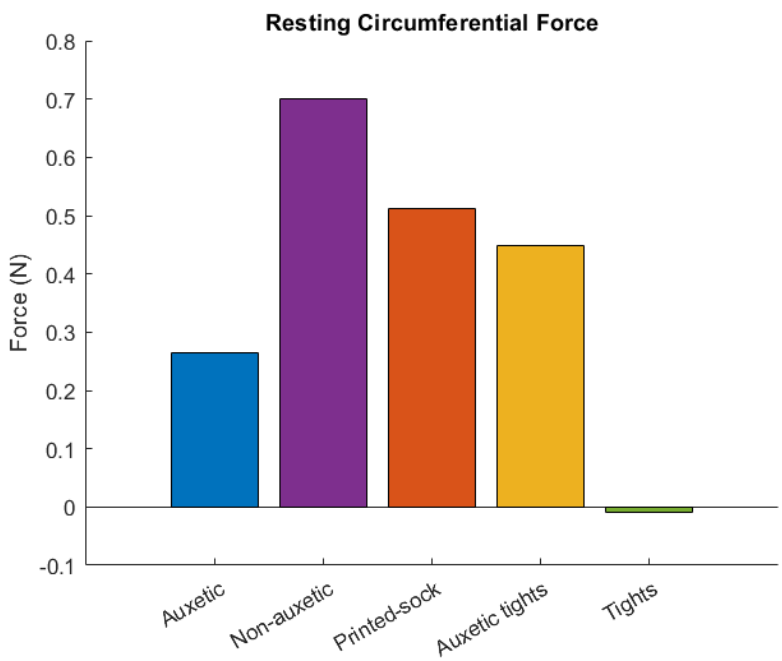

FIGURE 6.13. Resting tension of the structures on the artificial arm.

This was a preliminary experiment and the method of measuring this circumferential force needs to be explored further. Once this has been established, the results could then be used to adjust the pulling forces measured in sections 6.1.2 and 6.2.2 to account for any discrepancies in circumferential resting forces between the samples and make a fair comparison.

6.4 Application

One potential application for the use of smart auxetic fabrics could be to aid the donning of socks. To get an idea of how these geometries and samples relate to this real-world application, the circumference of a lower leg was measured. This was done to determine the change in circumference across various anatomical features, such as the ankle joint. Fig. 6.14a illustrates the circumference measured of a lower leg, from knee to end of foot, at 30mm intervals. The axis of circumference measurement is shown in fig. 6.14b. The re-entrant sinusoid auxetic geometry used throughout this experiment has a strain of 34.4% when at maximum expansion. To get this geometry to stretch over the heel joint (at 308mm circumference), the auxetic structure would need a resting circumference of at least 229mm. The working range of this auxetic geometry is shaded in pink in fig. 6.14. This indicates that the working range of the auxetic is almost sufficient to cover the site variations across the foot and calf. This is just one example of a potential auxetic solution and is open to adjustments where different auxetic geometries will provide different strains on expansion and therefore may be more suitable to this and other wearable applications.

6.5 Discussion on Auxetic Textiles

One of the main difficulties for this experiment was creating the different cylindrical samples in such a way that their pulling force across the artificial limb would be comparable. Two different

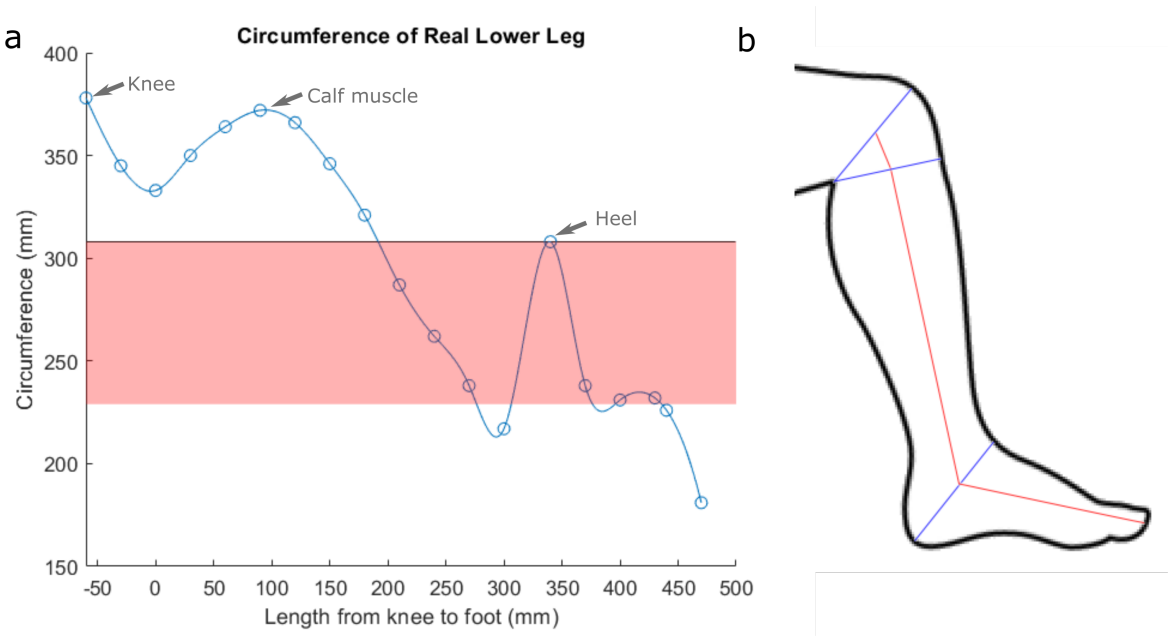

FIGURE 6.14. a) Circumference of real lower leg as measured from knee to end of foot. b) Axis of circumference measurement. The highlighted area is shows the working range of the re-entrant sinusoid auxetic geometry used throughout this experiment when setting the maximum strain of 34.4% to stretch over the heel.

methods of doing this are isometric and isotonic. Isometric samples would be samples of the same dimensions, whereas isotonic samples would be ones with equal tensions. Our initial experiment was conducted using isometric samples, however we found that this was not a fair comparison as the different structures generated different compressive forces on the artificial limb and therefore affected the frictional force. We then measured the circumferential force which could then be used for future experiments to either normalise the results of the pulling forces to take this into account, or scale the samples to make this frictional force equal across the samples.

Most auxetic textiles are generated by incorporating the auxetic structure into the weave of the fabric, either on the micro- or macro-scale, as detailed in chapter 2. These fabrication methods can be challenging and the wearability of these fabrics need to be considered with repeated stretching and contracting [149, 204]. Our aim was to create a simpler fabrication method of

generating auxetic textiles with more structural integrity due to the 3D printed layer, making them more resilient to wear. However, our fabrication technique came with its own challenges.

It was possible to print directly onto tights fabric as this was thin enough, however this required the fabric to be stretched across the print bed to avoid the 3D printer nozzle from catching it. Doing this resulted in the tights being unable to allow further expansion as required for the auxetic effect. Therefore the two layers had to be sewn together whilst the auxetic structure was in its stretched state to ensure there was enough fabric to allow this. Even though this overcame the restrictions of the fabric on the auxetic expansion, other fabrication issues arose including plastic deformation of the TPU whilst the sample was mounted in its expanded state on a frame for sewing.

Other fabrication methods, including knitting and crocheting, are considered for future work and discussed in chapter 7.

6.6 Conclusion

Auxetic textiles is a novel research area to explore, with high potential for developing comfortable and effective solutions to functional wearables and body-device interfaces. This chapter presented an initial investigation into the fabrication of auxetic textiles by a number of different methods (objective 4, section 1.5). One potential application for these is the fabrication of smart socks which are easy to put on and take off for those who may struggle with this daily task (e.g. elderly people). These fabrics would be considered smart in a passive sense, as they passively adapt to the (body) environment. It would also be interesting to explore active auxetic textiles. Active auxetic structures have been discussed in chapters 4 and 5. If active auxetic fabrics could be realised, then the devices characterised in the above chapters could be incorporated into these fabrics,

making them more comfortable and more discreet to wear for everyday use. More considerations for this are discussed in future work (section 7.3).

CHAPTER 7

CONCLUSION AND FUTURE WORK

This thesis has presented novel technology using smart materials and structures that show potential in overcoming some of the challenges at the interface between the human body and medical assistive devices, including prosthetic limbs. This chapter will summarise the main findings to conclude this work, and focus on considerations for the future.

7.1 Thesis Summary

Chapter 1 provided a brief introduction to the thesis that set out the motivation behind the research. Smart materials and structures have recently seen great advances in their development. However, there is still a huge scope for developing these further and finding new applications. The need for assistive devices is rapidly increasing, and this research brings a particular smart textile focus to prosthetic devices as a potential application for the technologies developed. The main challenges identified at the body-device interface include the formation of pressure points and excessive heat and perspiration. In addition to these issues, prosthesis wearers also experience improper fit, weight, and lack of functionality of the devices. These issues are recognised at a huge scale, especially for those in low-income countries. General background information

was presented in chapter 2. We described the skin anatomy to illustrate what makes it both unfavourable as an interface with a device, and how we can utilise its sensory capabilities to our advantage. Some interesting technology is considered for use in this research, such as haptic feedback devices, auxetic structures and textiles. We highlight the main challenges encountered at the body-device interface described in chapter 1 along with some of the latest technology aimed to overcome these.

7.1.1 Fit and Comfort

One of the main challenges with prosthetic limbs is the fit of the prosthetic socket, which is the interface between the residual limb and the prosthetic device. It mechanically couples the two and an improper fit can lead to reduced control of the prosthetic device, in addition to the formation of pressure points and/or rubbing leading to skin degradation. It is therefore crucial that the prosthetic socket fits properly. This is difficult, however, owing to the significant volume fluctuations that amputees experience in their residual limb due to their compromised lymphatic system. Metamaterials are of interest as they can be designed to possess certain characteristics. In chapter 3, we explored the use and characteristics of different auxetic structures in a cylindrical shape as a potential metamaterial to improve the fit of prosthetic sockets, addressing objective 1 (section 1.5). Auxetic structures expand perpendicular to the applied force. They also possess other characteristics which make them favourable for wearable applications. Here we designed and characterised Tiled Auxetic Cylinders (TACs) and presented a simple method of fabrication. These TACs can be tuned through design and geometric parameters, highlighting their potential to improve the fit of prosthetic sockets.

7.1.2 Stimulation

Touch is a predominant sense, not only for perceiving our environment, but also for social interactions. The skin is a great target to act as a communication channel, owing to its great surface area and distribution of a diversity of mechanoreceptors. Most current haptic feedback devices however use vibrations to relay information to the skin which, although effective, is not very natural or localised. We developed three wearable tactile devices able to provide non-intrusive, affective communication to the wearer with the use of Shape Memory Alloys (SMAs), as described in chapter 4 (objective 2, section 1.5). SMAs are smart materials which contract when heated and return to their original state on cooling. They are also lightweight, flexible and actuate silently, beneficial properties for use in an unobtrusive wearable device. These devices were designed to gently mimic the sensation of squeezing and stretching, pinching, and twisting the skin and succeeded in providing natural and pleasant sensations to the user.

7.1.3 Sensing and Computation

Lack of sensory feedback in upper limb prosthetic devices is another area where improvements need to be made. Not only does this result in reduced control of the prosthetic device, but also results in a lack of embodiment and consequently rejection of the device. This led to the design and fabrication of a sensory feedback device, presented in chapter 5 (objective 3, section 1.5). This device relays pressure to the user by a wearable tactile device, such as those seen in chapter 4. It uses simple computation, and we demonstrated its potential use in upper limb prosthetic devices.

7.1.4 Auxetic Textiles

In order to make it more practical to wear these haptic devices presented in the previous chapters, they need to be made more discreet and comfortable to wear. With that in mind, we started by

investigating the fabrication of auxetic textiles into which these haptic devices could potentially be embedded (objective 4, section 1.5). We explored different methods of fabricating these auxetic textiles, by combining TACs (such as those presented in chapter 3) with different textiles, all of which presented their own challenges. This chapter was an initial investigation into smart fabrics and only scratched the surface of this area of research.

7.2 Thesis Contributions

The main contributions of the research presented in this thesis are:

- Presented a simple process for fabricating auxetic cylinders by way of 3D printing a planar auxetic sheet and gluing the ends together (chapter 3)
- Characterised and compared different auxetic cylinders, illustrating the potential to tune these to achieve desired characteristics through altering design and geometric parameters (chapter 3)
- Highlighted the potential for auxetic structures to aid in overcoming fluctuating residual limb volumes and improving the fit of prosthetic sockets (chapter 3)
- Developed skin-manipulating devices, such as those squeezing and stretching the skin, with the use of shape memory alloys (SMAs) that can generate affective touch which is pleasant, natural, and non-intrusive and preferred over vibrotactile devices (chapter 4)
- Designed, fabricated and characterised a sensory feedback device (B:Ionic glove) able to relay pressure information to the user's skin (chapter 5)

- Highlighted the potential use of the B:Ionic glove for use in upper limb prosthetic devices (chapter 5)
- Explored various methods for fabricating auxetic textiles, describing the challenges encountered (chapter 6)
- Highlighted the potential for auxetic sleeves to aid in donning and doffing of clothing (chapter 6)

7.3 Conclusion and Future Considerations

The need for assistive devices is rapidly increasing, however many problems exist at the body-device interface. These problems include the formation of pressure points, lack of breathability of the skin and improper fit of the device with the body. The work presented in this thesis highlights the potential of smart materials and structures to overcome some of these problems experienced at the body-device interface. Conclusions, scope for further work and future considerations are discussed below.

Auxetics is one of the smart metamaterial structures used in this research to develop the innovative devices presented. The unconventional behaviour of auxetics could make them suitable for relieving pressure points on the residual limb of prosthesis wearers, thereby improving the comfort and fit of prosthetic sockets, a major unmet problem [36]. As their residual limb increases in volume due to swelling, the auxetic structure would allow expansion in all directions, thus not constraining or adding pressure to any part. In addition, auxetics could generate interesting sensations on the skin for communicating a range of information. We investigated several auxetic structures in a cylindrical configuration as this most closely represented a wearable sleeve

for use on a limb. We illustrated the scope of tunability of these auxetic structures, either by geometric changes or designing hybrid structures. Although this showed great potential, the best configuration for the application to prosthetic sockets would need to be identified. Therefore, future work should consider the range of strains required to accommodate the full range of limb volume change. One study measured the volume change of the residual limb of trans-tibial amputees after doffing their prosthetic leg. The results ranged between –1.1% to 8.3%, depending on the level of activity prior to doffing the prosthetic leg and between different individuals ([205]). Therefore, the range of strains required may need to be established on an individual basis, where some amputees may experience more substantial changes than others.

To demonstrate a conceptual application of TACs to the design of soft robots and their behaviour in response to an external force, we considered the case of an auxetic cylindrical unit moving through a pipe. The design in this case was similar to that of the modified re-entrant sinusoid presented in chapter 3. However, the design differs from that presented in section 3.2.2 in terms of the configuration at rest. The design presented previously was 3D printed in a contracted configuration (fig. 3.4B, top) whereas the design considered here was printed in an expanded configuration similar to that in the elongated state shown in fig. 3.4B (bottom). This implies that the structure is expanded in its natural resting configuration and is an example of how the zero energy state can be controlled. In this configuration, the elastic biasing force will drive it towards expansion. The initial diameter of this structure was 45mm and it could contract to 35mm.

The structure was made to move through an acrylic pipe, the internal diameter of which was 45mm, sufficiently large to accommodate it in its rest configuration. Motion was achieved through an external longitudinal force. A constriction to motion was provided in the form of a decrease in diameter of the pipe. This was achieved using a 3D printed conical part. At the other end of the

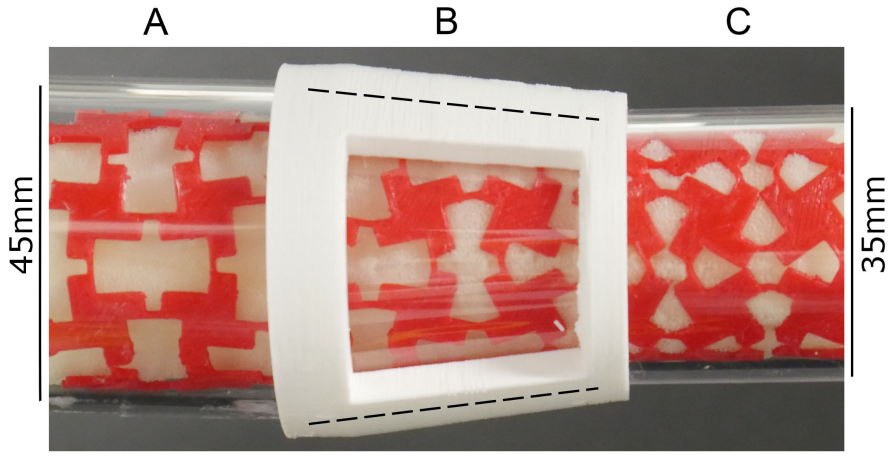

FIGURE 7.1. Demonstration of the change in shape of an auxetic cylinder as it moves through a constricted space. The structure is in its fully expanded configuration in the wider region (A), partially contracted in the constriction (B) and fully contacted in the smaller tubular region (C).

constriction, a second pipe of smaller diameter (35mm) was attached that allowed the structure to pass through only in its contracted configuration but not in its expanded configuration.

As the structure moves through the constriction, reactive forces from the walls of the constriction acting on the structure cause a contraction in length which result in a reduction in diameter, thus allowing the structure to pass through. The change in configuration of the auxetic can be clearly seen in fig. 7.1. In the larger diameter tube, the structure is in a fully expanded configuration (fig. 7.1A). This is followed by a partially contracted configuration in the constriction (fig. 7.1B) and a fully contracted configuration in the smaller pipe (fig. 7.1C).

In this demonstration, the change in shape is not actively controlled but is caused by the structure reacting to a change in the environment in which it is operating. In this sense, the design of the structure is contributing to its control. In other scenarios, where active control of shape is desired, the auxetic structure can still provide this ability. This is an advantage over soft robot designs that purely depend on soft material to passively conform to objects that they interact with.

The internal foam prevents buckling of the structure on compression, however we believe that it does not contribute to the auxetic behaviour. Further study will look at characterising these TACs printed in various states of expansion.

This demonstration illustrates the reactive change in shape of the auxetic structure when moving through a constriction. This property has potential applications in robots designed to move through confined spaces such as in the human body and subterranean exploration where the robot can reconfigure itself relative to its surroundings with minimal complexity of control. We have demonstrated TACs' ability to react to the environment, highlighting their potential to improve the fit of prosthetic sockets.

Studies of cylindrical auxetics seen in the literature, such as cardiovascular stents ([13]), tend to focus on the forces the structures exert on the outside of the cylinder, rather than the inside as would be the case in wearable applications. We explored these forces on the inside of the cylinder as interactions with the skin and utilised them as a form of communicating information. One limitation of the work presented here is that we did not determine the effect that changing the rest configuration of the structure (i.e. whether the structure is 3D printed in its relaxed or expanded state) may have on its properties. The Tiled Auxetic Cylinders (TACs) presented in chapter 3 were 3D printed in a contracted state, whereas the auxetic structures used in the Squeeze and Twist wristbands (chapter 4, section 4.3) and the B:Ionic glove armband (chapter 5) were printed in an expanded state. Different stress-strain curves are therefore expected not only for the different auxetic geometries used to fabricate the TACs, but also the resting shape (i.e. expanded or contracted configuration).

The tiling based approach is amenable to parameterisation. This allows for tuning the design to achieve a desired mechanical response. Following this work, there is scope for more study. Transition between multiple designs within the same structure and the impact of this

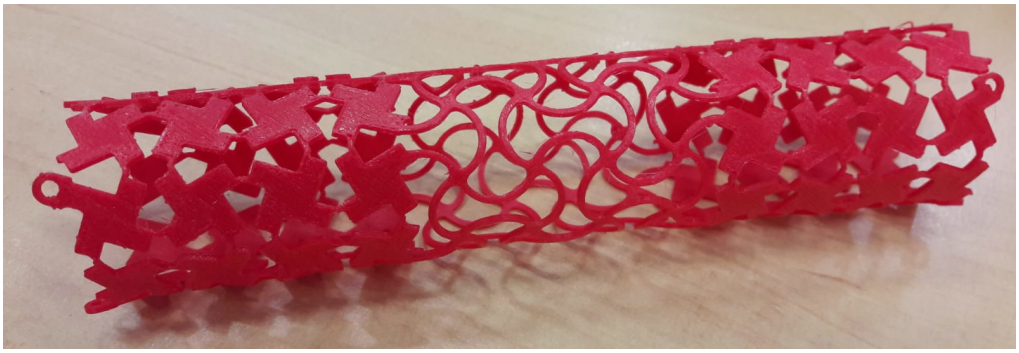

FIGURE 7.2. Prototype of a hybrid TAC soft robot. The TAC design transitions from modified re-entrant sinusoid to re-entrant sinusoid and back to the modified re-entrant sinusoid.

on mechanical properties will also be studied in future work. An example of such a hybrid soft robot is shown in fig. 7.2. Regions with varying stiffness could potentially be created at specific locations on the structure leading to interesting and emergent macroscopic behaviours. This could also alter other properties of auxetic structures such as increasing the indentation resistance [206]. The rest configuration of the 3D printed structure affects its stiffness. The preference for a more contracted or more expanded configuration could be exploited in the design of a robot. This is another topic for investigation.

The devices presented in this work consist of 3D printed components using either polylactic acid (PLA) or thermoplastic polyurethane (TPU), which are both plastics. This material would not allow the skin which is in contact with it to breathe, which could exacerbate the problems of heat and perspiration at the body-device interface. We therefore explored other means of fabrication, such as with the use of textiles (chapter 6). This also has the potential to make these devices fully wearable and practical for everyday use. Currently, all active devices presented require an external power source and control unit to actuate the Shape Memory Alloys (SMAs). The first step would therefore be to make them untethered, with an onboard power source (potentially a small lithium-ion battery) and control unit. The devices are not designed to be robust and the

FIGURE 7.3. Re-entrant sinusoid fabric created by knitting. One re-entrant sinusoid geometry is highlighted in white dashed line.

placement on the skin leaves them exposed and likely to catch on other surrounding objects. Embedding them into more robust materials such as textiles could also overcome this.

Chapter 6 provides an initial investigation into the feasibility of auxetic textiles for assistive devices. Various fabrication methods were presented, each with their own challenges. Alternative fabrication techniques that could be considered for future work include incorporating the auxetic geometry within the weave of a knitted textile. An example of a re-entrant sinusoid fabric is shown in fig. 7.3, which was generated by hand knitting. Re-entrant hexagon and rotating squares auxetic fabrics were created by crocheting (fig. 7.4).

One difficulty with this fabrication technique is the lack of structural support in the resulting textile. With the 3D printed auxetic structures, the material of the TPU beams is stiff enough that the external force is transferred to the beams of the auxetic structure, causing it to expand. In the case of the fabric auxetic structures, the external force is absorbed by slack in the weave

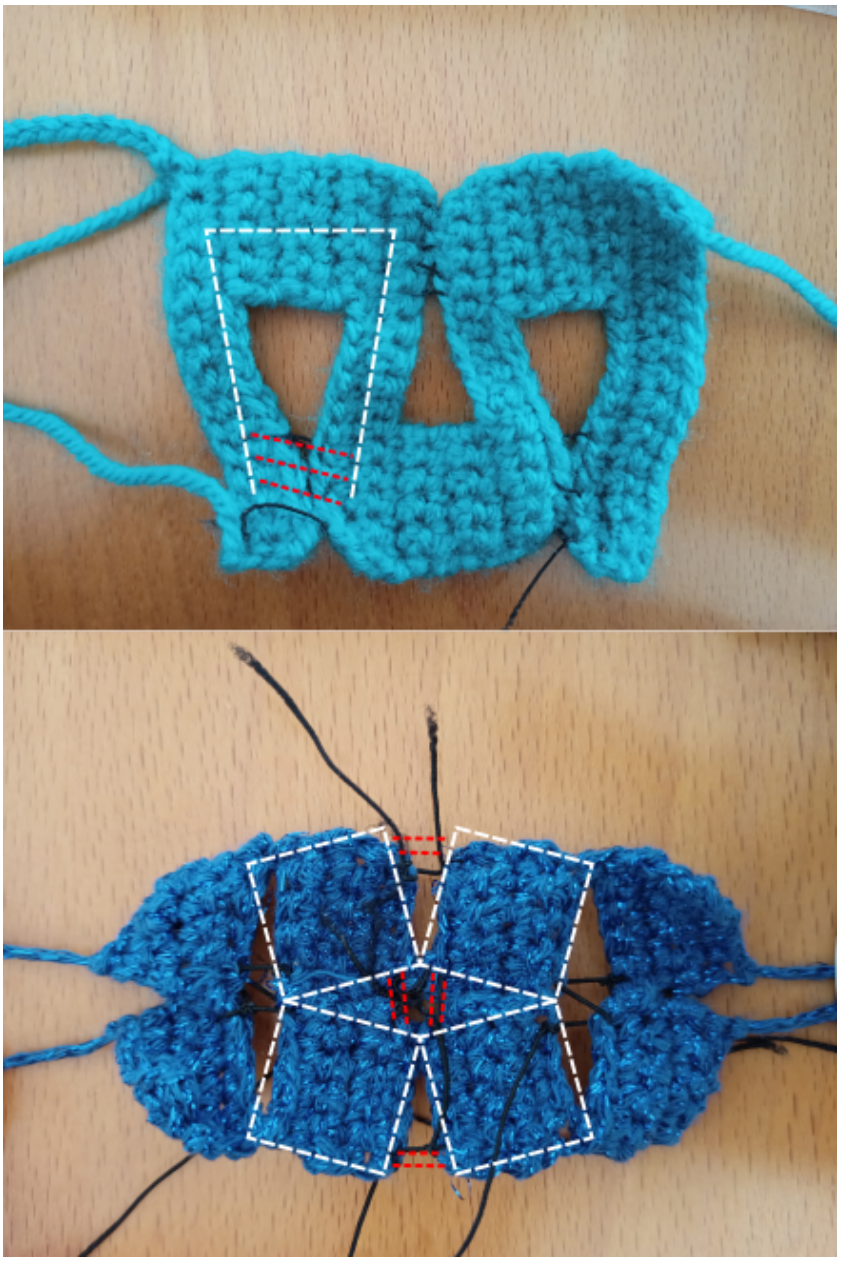

FIGURE 7.4. Re-entrant hexagon (top) and rotating squares (bottom) fabric created by crocheting. Auxetic geometries are highlighted in white dashed line. Red dashed lines represent elasticated yarn used as springs to return geometry to resting (pre-stretched) state.

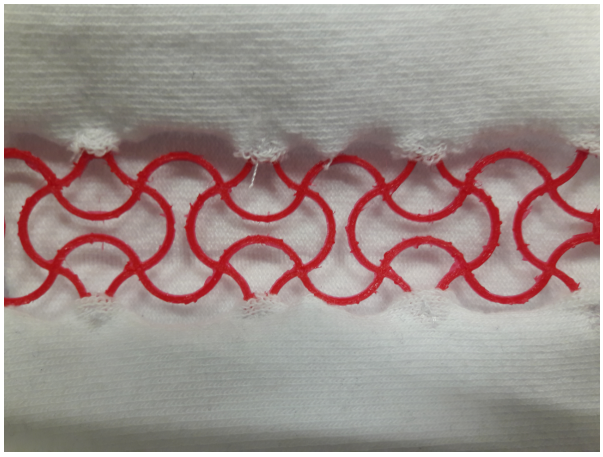

FIGURE 7.5. Hybrid auxetic fabric created by replacing part of the sock material with an auxetic structure.

and extension of the yarn itself. Another idea that could be further explored is the generation of auxetic fabrics by replacing only a section of the sock with an auxetic structure. Fig. 7.5 shows an example. This would allow for the structural component required to generate the auxetic effect whilst maintaining the comfort of the sock material in contact with the skin.

Further work should include characterising the resulting auxetic textiles from the different fabrication techniques to compare the effect this may have on its properties. This could include investigating the differing behaviours of auxetic textiles created with auxetic yarn and those with auxetic geometries.

We have shown that our devices utilising SMA actuators are capable of providing affective communication to the wearer's skin. Most tactile devices utilise vibration as the method of skin stimulation [63, 64], however we have shown that SMAs provide more local and less intrusive alerts. In addition, they are light-weight and small, making them ideal for wearable applications. Creating active auxetic textiles, for example with the use of SMA actuators, could be the next step towards embedded, wearable tactile devices.

The work presented in this thesis does not have a balanced gender and age distribution

in the user studies in chapters 4 and 5. [207] showed that both gender and age affects tactile perception, where tactile perception decreases with age and is higher for women compared to men. In addition, gender can affect the sensitivity of different skin regions on the upper arm, where the medial forearm is the most sensitive region of the arm for women - which is also significantly more sensitive compared to men - and the posterior forearm is the most sensitive region of the arm for men [208]. Therefore, future work should investigate the effects of age, gender and skin region on tactile perception of the devices presented and future user studies should include balanced user groups.

The tactile armband as part of the sensory feedback device for upper limb prostheses (chapter 5 was tested on non-amputees. As we addressed the stimuli from the tactile device separately to the rest of the device, there would not be any interference of the non-amputee's own fingertip sensations. However, amputees may have scar tissue and an altered nervous system around their residual limb which could potentially change their tactile sensations. Future work should include testing the tactile devices on amputees and compare their perceived sensations to the results obtained in non-amputees.

Another area of interest for future work is to combine multiple tactile feedback units together to form a modular network of skin-stretchers. Fig. 7.6 illustrates an example of this with the use of multiple Pinch units. This network can be embedded in fabric and worn discreetly underneath clothing. The modular format could become the haptic equivalent of a prototyping toolkit [209], allowing people to design personalised touch interactions. Having a network of skin-stretchers would greatly increase the information capacity of the tactile communication channel, enabling skin stimulation at different locations and with different strengths and patterns.

We have successfully met our aims and objectives as outlined in section 1.5. Our devices have been developed to highlight their potential in overcoming issues experienced at the interface

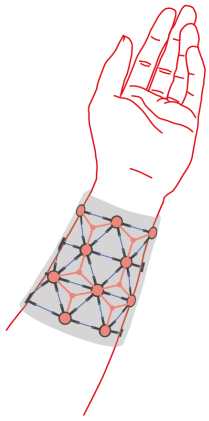

FIGURE 7.6. Illustration of what a future tactile device design could look like; a wearable sleeve containing elements of the Pinch device in an array that is capable of eliciting a range of simulated human touches. Figure reproduced from [200].

between human tissue and machine materials. A specific focus was put on increasing comfort and fit of assistive devices and to act as a communication channel. More specifically we have:

- explored the use and characteristics of different auxetic stuctures in a cylindrical shape as a potential metamaterial to improve the fit of prosthetic sockets
- developed wearable tactile devices able to convey non-intrusive information to the skin with the use of shape memory alloys (SMAs)
- developed a sensory feedback device for the potential use with upper limb prostheses
- explored the fabrication of smart textiles as a step towards making more discreet and comfortable smart wearable interfaces

All the devices presented in this thesis were created with the aim of applying them to prosthetic devices and improving the body-device interface of the residual limb and the prosthetic socket. However this technology may also be tailored to other medical assistive devices which experience similar problems. If this can be realised, countless people could benefit.

BIBLIOGRAPHY

[1] J. Shintake, S. Rosset, B. Schubert, D. Floreano, and H. Shea, "Versatile soft grippers with intrinsic electroadhesion based on multifunctional polymer actuators," *Advanced Materials*, vol. 28, no. 2, pp. 231–238, 2016.

[2] I. Qamar, R. Groh, D. Holman, and A. Roudaut, "Hci meets material science: A literature review of morphing materials for the design of shape-changing interfaces," pp. 1–23, 04 2018.

[3] R. F. Shepherd, F. Ilievski, W. Choi, S. A. Morin, A. A. Stokes, A. D. Mazzeo, X. Chen, M. Wang, and G. M. Whitesides, "Multigait soft robot," *Proc. Natl. Acad. Sci. USA*, vol. 108, pp. 20400–20403, 10/15/11 2011.

1135.

[4] E. Brown, N. Rodenberg, J. Amend, A. Mozeika, E. Steltz, M. R. Zakin, H. Lipson, and H. M. Jaeger, "Universal robotic gripper based on the jamming of granular material," *Proceedings of the National Academy of Sciences*, vol. 107, no. 44, pp. 18809–18814, 2010.

[5] C. S. Haines, M. D. Lima, N. Li, G. M. Spinks, J. Foroughi, J. D. W. Madden, S. H. Kim, S. Fang, M. Jung de Andrade, F. Göktepe, Ö. Göktepe, S. M. Mirvakili, S. Naficy,

X. Lepró, J. Oh, M. E. Kozlov, S. J. Kim, X. Xu, B. J. Swedlove, G. G. Wallace, and R. H. Baughman, "Artificial muscles from fishing line and sewing thread," *Science*, vol. 343, no. 6173, pp. 868–872, 2014.

[6] H. Taniguchi, "Flexible artificial muscle actuator using coiled shape memory alloy wires," *APCBEE Procedia*, vol. 7, pp. 54 – 59, 2013.

[7] A. Rafsanjani, Y. Zhang, B. Liu, S. M. Rubinstein, and K. Bertoldi, "Kirigami skins make a simple soft actuator crawl," *Science Robotics*, vol. 3, no. 15, 2018.

[8] J. M. McCracken, B. R. Donovan, and T. J. White, "Materials as machines," *Advanced Materials*, vol. 32, no. 20, p. 1906564, 2020.

[9] H. Shigemune, S. Sugano, J. Nishitani, M. Yamauchi, N. Hosoya, S. Hashimoto, and S. Maeda, "Dielectric elastomer actuators with carbon nanotube electrodes painted with a soft brush," *Actuators*, vol. 7, no. 3, 2018.

[10] D. Song, D. Han, K. Rhee, D. Kim, and J. Jho, "Fabrication and characterization of an ionic polymer-metal composite bending sensor," *Macromolecular Research*, vol. 25, 10 2017.

[11] N. Novak, M. Vesenjak, and Z. Ren, "Auxetic cellular materials - a review," *Strojniški vestnik - Journal of Mechanical Engineering*, vol. 62, pp. 485–493, 09 2016.

[12] M. Sanami, N. Ravirala, K. Alderson, and A. Alderson, "Auxetic materials for sports applications," *Procedia Engineering*, vol. 72, pp. 453 – 458, 2014.

[13] T. Wei Tan, G. R. Douglas, T. Bond, and A. S. Phani, "Compliance and longitudinal strain of cardiovascular stents: Influence of cell geometry," *Journal of Medical Devices*, vol. 5, pp. 041002–1 – 041002–6, 12 2011.

[14] A. T. Conn and J. Rossiter, "Smart radially folding structures," *IEEE/ASME Transactions on Mechatronics*, vol. 17, pp. 968–975, Oct 2012.

[15] J. Ou, Z. Ma, J. Peters, S. Dai, N. Vlavianos, and H. Ishii, "Kinetix - designing auxetic-inspired deformable material structures," *Computers and Graphics*, vol. 75, pp. 72 – 81, 2018.

[16] E. Mencarini, A. Rapp, L. Tirabeni, and M. Zancanaro, "Designing wearable systems for sports: A review of trends and opportunities in human–computer interaction," *IEEE Transactions on Human-Machine Systems*, vol. 49, no. 4, pp. 314–325, 2019.

[17] M. H. Iqbal, A. Aydin, O. Brunckhorst, P. Dasgupta, and K. Ahmed, "A review of wearable technology in medicine," *Journal of the Royal Society of Medicine*, vol. 109, no. 10, pp. 372–380, 2016.

PMID: 27729595.

[18] A. A. Maimani and A. Roudaut, "Frozen suit: Designing a changeable stiffness suit and its application to haptic games," in *CHI*, 2017.

[19] L. Rasmussen, S. Rodriguez, M. Bowers, D. Smith, G. Martino, L. Rizzo, C. Scheiber, J. D'Almeida, and C. Dillis, "Adjustable liners and sockets for prosthetic devices," *Canadian Prosthetics & Orthotics Journal*, 12 2018.

[20] L. Yao, J. Ou, C.-Y. Cheng, H. Steiner, W. Wang, G. Wang, and H. Ishii, "biologic: Natto cells as nanoactuators for shape changing interfaces," *Proceedings of the 33rd Annual ACM Conference on Human Factors in Computing Systems*, 2015.

[21] "biologic." https://tangible.media.mit.edu/project/biologic/. Accessed: 09.05.2022.

[22] J. A. Simpson, E. S. C. Weiner, and M. Proffitt, *Oxford English Dictionary Additions Series*, vol. 3.
Oxford, UK: Oxford University Press, 1997.

[23] L. J. Davis, ed., *The Disability Studies Reader*.
New York, USA: Routledge, fourth ed., 2013.

[24] "World report on disability," tech. rep., World Health Organization and The World Bank, 2011.

[25] "Demographic yearbook 2004," department of economic and social affairs, United Nations, New York, 2007.

[26] "Guidelines for training personnel in developing countries for prosthetics and orthotics services," tech. rep., World Health Organization, 2004.

[27] G. Shi, A. Palombi, Z. Lim, A. Astolfi, A. Burani, S. Campagnini, F. G. C. Loizzo, M. L. Preti, A. M. Vargas, E. Peperoni, C. M. Oddo, M. Li, J. Hardwicke, M. Venus, S. Homer-Vanniasinkam, and H. A. Wurdemann, "Fluidic haptic interface for mechano-tactile feedback," *IEEE Transactions on Haptics*, vol. 13, no. 1, pp. 204–210, 2020.

[28] A. J. Young and D. P. Ferris, "State of the art and future directions for lower limb robotic exoskeletons," *IEEE Transactions on Neural Systems and Rehabilitation Engineering*, vol. 25, pp. 171–182, Feb 2017.

[29] "What is a limb difference?." https://guides.library.illinois.edu/limbdifference. Accessed: 16.05.2022.

[30] C. S. Harkins, A. McGarry, and A. Buis, "Provision of prosthetic and orthotic services in low-income countries: A review of the literature," *Prosthetics and Orthotics International*, vol. 37, no. 5, pp. 353–361, 2013.

[31] R. Meier and D. H. Melton, "Ideal functional outcomes for amputation levels.," *Physical medicine and rehabilitation clinics of North America*, vol. 25 1, pp. 199–212, 2014.

[32] S. Hussain, S. Shams, and S. Khan, *Impact of Medical Advancement: Prostheses*, ch. 2. IntechOpen, 11 2019.

[33] "Radiofrequency technology improves utility of myoelectric prosthesis." http://www.healio.com/orthotics-prosthetics/prosthetics/news/print/o-and-p-news/%7Bc518aeb7-1a0c-4f6f-8d76-a25ad96c04d0%7D/radiofrequency-technology-improves-utility-of-myoelectric-prosthesis. Accessed: 22.04.2022.

[34] C. W. Heckathorne, "Chapter 16 - upper-limb prosthetics," in *Clinician's Guide to Assistive Technology* (D. A. Olson and F. DeRuyter, eds.), pp. 265–280, Saint Louis: Mosby, 2002.

[35] S. Carey, D. Lura, and M. Highsmith, "Differences in myoelectric and body-powered upper-limb prostheses: Systematic literature review," *Journal of Prosthetics and Orthotics*, vol. 29, pp. P4–P16, 10 2017.

[36] E. Biddiss, D. Beaton, and T. Chau, "Consumer design priorities for upper limb prosthetics," *Disability and rehabilitation. Assistive technology*, vol. 2, pp. 346–57, 12 2007.

[37] E. Ricaurte and N. Mahmoud, "Medical certification strategies in response to technologically advanced prosthetic devices," 06 2018.

[38] "Lower limb prosthetic sockets and suspension systems." https://www.physiopedia.com/Lower_Limb_Prosthetic_Sockets_and_Suspension_Systems. Accessed: 25.04.2022.

[39] "Handbook on the least developed country category: Inclusion, graduation and special support measures," tech. rep., United Nations: Department of Economic and Social Affairs and Committee for Development Policy, 2021.

[40] E. Helander, P. Mendis, G. Nelson, and A. Goerdt, "Training in the community for people with disabilities," tech. rep., World Health Organization, Geneva, 1989.

[41] U. Naidoo and L. Ennion, "Barriers and facilitators to utilisation of rehabilitation services amongst persons with lower-limb amputations in a rural community in south africa," *Prosthetics and Orthotics International*, vol. 43, no. 1, pp. 95–103, 2019.

[42] L. Ennion and S. Manig, "Experiences of lower limb prosthetic users in a rural setting in the mpumalanga province, south africa," *Prosthetics and Orthotics International*, vol. 43, no. 2, pp. 170–179, 2019.

[43] M. S. Cherry, S. Kota, A. Young, and D. P. Ferris, "Running with an elastic lower limb exoskeleton," *Journal of Applied Biomechanics*, vol. 32, no. 3, pp. 269–277, 2016.

[44] J. M. Highsmith, J. T. Highsmith, and J. T. Kahle, "Identifying and managing skin issues with lower-limb prosthetic use," *InMotion - A Publication of the Amputee Coalition*, vol. 21, no. 1, pp. 41–43, 2011.

[45] F. Cordella, A. L. Ciancio, R. Sacchetti, A. Davalli, A. G. Cutti, E. Guglielmelli, and L. Zollo, "Literature review on needs of upper limb prosthesis users," *Frontiers in Neuroscience*, vol. 10, p. 209, 2016.

[46] J. E. Sanders and S. Fatone, "Residual limb volume change: Systematic review of measurement and management," *Journal of Rehabilitation Research and Development*, vol. 48, no. 8, pp. 949–986, 2011.

[47] E. Biddiss and T. T. Chau, "Upper limb prosthesis use and abandonment: A survey of the last 25 years," *Prosthetics and Orthotics International*, vol. 31, pp. 236 – 257, 2007.

[48] W. F. Boron and E. L. Boulpaep, *Medical Physiology*.
Philadelphia, USA: Elsevier Saunders, updated ed., 2005.

[49] A. Zimmerman, L. Bai, and D. D. Ginty, "The gentle touch receptors of mammalian skin," *Science*, vol. 346, no. 6212, pp. 950–954, 2014.

[50] E. McLafferty, C. Hendry, and A. Farley, "The integumentary system: anatomy, physiology and function of skin," *Nursing Standard (through 2013)*, vol. 27, pp. 35–42, Sep 2012.
Copyright - Copyright RCN Publishing Company Sep 19-Sep 25, 2012; Last updated - 2016-04-30; CODEN - NSTAEU.

[51] P. Delmas, J. Hao, and L. Rodat-Despoix, "Molecular mechanisms of mechanotransduction in mammalian sensory neurons," *Nature Reviews Neuroscience*, vol. 12, pp. 139–153, 2011.

[52] V. Z. P. Ariza and M. Santís-Chaves, "Haptic interfaces: Kinesthetic vs. tactile systems," *Revista EIA*, vol. 13, no. 26, pp. 13–29, 2016.

[53] A. M. Okamura, "Haptic feedback in robot-assisted minimally invasive surgery," *Current Opinion in Urology*, vol. 19, pp. 102–107, January 2009.

[54] A. Haans and W. IJsselsteijn, "Mediated social touch: a review of current research and future directions," *Virtual Reality*, vol. 9, no. 2-3, pp. 149–159, 2006.

[55] C. McGregor, B. Bonnis, B. Stanfield, and M. Stanfield, "Design of the araig haptic garment for enhanced resilience assessment and development in tactical training serious games," in *2016 IEEE 6th International Conference on Consumer Electronics - Berlin (ICCE-Berlin)*, pp. 214–217, Sept 2016.

[56] T. Rosenbaum-Chou, W. Daly, R. Austin, P. Chaubey, and D. A. Boone, "Development and real world use of a vibratory haptic feedback system for upper-limb prosthetic users," *American Academy of Orthotists and Prosthetists*, vol. 28, no. 4, pp. 136–144, 2016.

[57] B. Stephens-Fripp, G. Alici, and R. Mutlu, "A review of non-invasive sensory feedback methods for transradial prosthetic hands," *IEEE Access*, vol. PP, pp. 1–1, 01 2018.

[58] L. Li, F. Yu, D. Shi, J. Shi, Z. Tian, J. Yang, X. Wang, and Q. Jiang, "Application of virtual reality technology in clinical medicine," *American Journal of Translational Research*, vol. 9, no. 9, pp. 3867–3880, 2017.

[59] C. Pacchierotti, S. Sinclair, M. Solazzi, A. Frisoli, V. Hayward, and D. Prattichizzo, "Wearable haptic systems for the fingertip and the hand: taxonomy, review, and perspectives," *IEEE Transactions on Haptics*, vol. 10, no. 4, pp. 580–600, 2017.

[60] R. Velázquez and O. Bazán, "Preliminary evaluation of podotactile feedback in sighted and blind users," in *2010 Annual International Conference of the IEEE Engineering in Medicine and Biology*, pp. 2103–2106, Aug 2010.

[61] E. H. Skorina, M. Luo, and C. D. Onal, "A soft robotic wearable wrist device for kinesthetic haptic feedback," *Frontiers in Robotics and AI*, vol. 5, p. 83, 2018.

[62] E. Knoop and J. Rossiter, "A compliant soft-actuator laterotactile display," *Smart Materials and Structures*, vol. 24, no. 4, p. 045034, 2015.

[63] S. Choi and K. J. Kuchenbecker, "Vibrotactile display: Perception, technology, and applications," *Proceedings of the IEEE*, vol. 101, pp. 2093–2104, Sept 2013.

[64] A. U. Alahakone and S. M. N. A. Senanayake, "Vibrotactile feedback systems: Current trends in rehabilitation, sports and information display," in *2009 IEEE/ASME International Conference on Advanced Intelligent Mechatronics*, pp. 1148–1153, July 2009.

[65] Y.-W. Park, C.-Y. Lim, and T.-J. Nam, "Cheektouch: An affective interaction technique while speaking on the mobile phone," in *CHI '10 Extended Abstracts on Human Factors in Computing Systems*, CHI EA '10, (New York, NY, USA), p. 3241–3246, Association for Computing Machinery, 2010.

[66] E. Hoggan, C. Stewart, L. Haverinen, G. Jacucci, and V. Lantz, "Pressages: Augmenting phone calls with non-verbal messages," in *Proceedings of the 25th Annual ACM Symposium on User Interface Software and Technology*, UIST '12, (New York, NY, USA), pp. 555–562, ACM, 2012.

[67] G. Huisman, A. Darriba Frederiks, B. Van Dijk, D. Hevlen, and B. Kröse, "The tasst: Tactile sleeve for social touch," in *2013 World Haptics Conference (WHC)*, (Daejeon, South Korea), pp. 211–216, IEEE, April 2013.

[68] D. Tsetserukou, A. Neviarouskaya, H. Prendinger, N. Kawakami, and S. Tachi, "Affective haptics in emotional communication," in *2009 3rd International Conference on Affective*

Computing and Intelligent Interaction and Workshops, (Amsterdam, Netherlands), pp. 1 – 6, IEEE, 10 2009.

[69] R. Strong and B. Gaver, "Feather, scent, and shaker: Supporting simple intimacy," *Proceedings of CSCW'96*, 1996.

[70] S. Brave and A. Dahley, "intouch: A medium for haptic interpersonal communication," *CHI '97*, 1997.

[71] A. Haans and W. A. IJsselsteijn, "The virtual midas touch: Helping behavior after a mediated social touch," *IEEE Transactions on Haptics*, vol. 2, no. 3, pp. 136–140, 2009.

[72] A. A. Stanley and K. J. Kuchenbecker, "Design of body-grounded tactile actuators for playback of human physical contact," in *2011 IEEE World Haptics Conference*, (Istanbul, Turkey), pp. 563–568, IEEE, IEEE, 2011.

[73] R. Wang, F. Quek, D. Tatar, K. S. Teh, and A. Cheok, "Keep in touch: Channel, expectation and experience," in *Proceedings of the SIGCHI Conference on Human Factors in Computing Systems*, CHI '12, (New York, NY, USA), pp. 139–148, ACM, 2012.

[74] E. Knoop and J. Rossiter, "The tickler: A compliant wearable tactile display for stroking and tickling," in *Proceedings of the 33rd Annual ACM Conference Extended Abstracts on Human Factors in Computing Systems*, CHI EA '15, (New York, NY, USA), p. 1133–1138, Association for Computing Machinery, 2015.

[75] N. A.-h. Hamdan, A. Wagner, S. Voelker, J. Steimle, and J. Borchers, "Springlets: Expressive, flexible and silent on-skin tactile interfaces," in *Proceedings of the 2019 CHI Conference on Human Factors in Computing Systems*, CHI '19, (New York, NY, USA), p. 1–14, Association for Computing Machinery, 2019.

[76] K. Bark, J. W. Wheeler, S. Premakumar, and M. R. Cutkosky, "Comparison of skin stretch and vibrotactile stimulation for feedback of proprioceptive information," in *2008 Symposium on Haptic Interfaces for Virtual Environment and Teleoperator Systems*, pp. 71–78, 2008.

[77] E. P. Gardner, J. H. Martin, *et al.*, "Coding of sensory information," *Principles of neural science*, vol. 4, pp. 411–429, 2000.

[78] H. Olausson, J. Wessberg, I. Morrison, and F. Mcglone, *Affective Touch and the Neurophysiology of CT Afferents*.
New York, USA: Springer-Verlag New York, 01 2016.

[79] R. Velazquez, E. E. Pissaloux, M. Hafez, and J. Szewczyk, "Tactile rendering with shape-memory-alloy pin-matrix," *IEEE Transactions on Instrumentation and Measurement*, vol. 57, no. 5, pp. 1051–1057, 2008.

[80] Y. Mizukami and H. Sawada, "Tactile information transmission by apparent movement phenomenon using shape-memory alloy device," *International Journal on Disability and Human Development*, vol. 5, no. 3, pp. 277–284, 2006.

[81] P. S. Wellman, W. J. Peine, G. Favalora, and R. D. Howe, "Mechanical design and control of a high-bandwidth shape memory alloy tactile display," in *Experimental robotics V*, pp. 56–66, Springer, 1998.

[82] M. Solazzi, W. R. Provancher, A. Frisoli, and M. Bergamasco, "Design of a sma actuated 2-dof tactile device for displaying tangential skin displacement," in *World Haptics Conference (WHC), 2011 IEEE*, pp. 31–36, IEEE, 2011.

[83] M. R. Tucker, J. Olivier, A. Pagel, H. Bleuler, M. Bouri, O. Lambercy, J. del R Millán, R. Riener, H. Vallery, and R. Gassert, "Control strategies for active lower extremity prosthetics and orthotics: a review," *Journal of neuroengineering and rehabilitation*, vol. 12, no. 1, p. 1, 2015.

[84] C. H. Jang, H. S. Yang, H. E. Yang, S. yeong Lee, J. W. Kwon, B. D. Yun, J. Y. Choi, S. N. Kim, and H. W. Jeong, "A survey on activities of daily living and occupations of upper extremity amputees," *Annals of Rehabilitation Medicine*, vol. 35, pp. 907 – 921, 2011.

[85] L. Nikolajsen and T. S. Jensen, "Phantom limb pain," *BJA: British Journal of Anaesthesia*, vol. 87, no. 1, pp. 107–116, 2001.

[86] K. Limakatso, G. J. Bedwell, V. Madden, and R. Parker, "The prevalence of phantom limb pain and associated risk factors in people with amputations: A systematic review protocol," *Systematic Reviews*, vol. 8, 12 2019.

[87] B. Subedi and G. Grossberg, "Phantom limb pain: Mechanisms and treatment approaches," *Pain research and treatment*, vol. 2011, p. 864605, 08 2011.

[88] C. Dietrich, K. Walter-Walsh, S. Preißler, G. O. Hofmann, O. W. Witte, W. H. Miltner, and T. Weiss, "Sensory feedback prosthesis reduces phantom limb pain: Proof of a principle," *Neuroscience Letters*, vol. 507, no. 2, pp. 97 – 100, 2012.

[89] P. D. Marasco, K. Kim, J. E. Colgate, M. A. Peshkin, and T. A. Kuiken, "Robotic touch shifts perception of embodiment to a prosthesis in targeted reinnervation amputees," *Brain*, vol. 134, pp. 747–758, 01 2011.

[90] H. Witteveen, E. Droog, J. Rietman, and P. Veltink, "Vibro- and electrotactile user feedback on hand opening for myoelectric forearm prostheses," *IEEE transactions on bio-medical engineering*, vol. 59, pp. 2219–26, 05 2012.

[91] T. A. Kuiken, P. D. Marasco, B. A. Lock, R. N. Harden, and J. P. A. Dewald, "Redirection of cutaneous sensation from the hand to the chest skin of human amputees with targeted reinnervation," *Proceedings of the National Academy of Sciences*, vol. 104, no. 50, pp. 20061–20066, 2007.

[92] M. R. Motamedi, J. Chossat, J. Roberge, and V. Duchaine, "Haptic feedback for improved robotic arm control during simple grasp, slippage, and contact detection tasks," in *2016 IEEE International Conference on Robotics and Automation (ICRA)*, pp. 4894–4900, 2016.

[93] A. Ajoudani, S. B. Godfrey, M. Bianchi, M. G. Catalano, G. Grioli, N. Tsagarakis, and A. Bicchi, "Exploring teleimpedance and tactile feedback for intuitive control of the pisa/iit softhand," *IEEE Transactions on Haptics*, vol. 7, no. 2, pp. 203–215, 2014.

[94] K. O. Johnson, "The roles and functions of cutaneous mechanoreceptors," *Current Opinion in Neurobiology*, vol. 11, pp. 455–461, 08 2001.

[95] Y. Zheng and J. B. Morrell, "Haptic actuator design parameters that influence affect and attention," in *2012 IEEE Haptics Symposium (HAPTICS)*, pp. 463–470, IEEE, 2012.

[96] A. Haynes, M. F. Simons, T. Helps, Y. Nakamura, and J. Rossiter, "A wearable skin-stretching tactile interface for human–robot and human–human communication," *IEEE Robotics and Automation Letters*, vol. 4, no. 2, pp. 1641–1646, 2019.

[97] C. Antfolk, M. D'Alonzo, M. Controzzi, G. Lundborg, B. Rosen, F. Sebelius, and C. Cipriani, "Artificial redirection of sensation from prosthetic fingers to the phantom hand map on transradial amputees: vibrotactile versus mechanotactile sensory feedback," *IEEE transactions on neural systems and rehabilitation engineering*, vol. 21, no. 1, pp. 112–120, 2012.

[98] C. Antfolk, A. Björkman, S.-O. Frank, F. Sebelius, G. Lundborg, and B. Rosen, "Sensory feedback from a prosthetic hand based on air-mediated pressure from the hand to the forearm skin," *Journal of rehabilitation medicine*, vol. 44, no. 8, pp. 702–707, 2012.

[99] J. J. Huaroto, E. Suarez, H. I. Krebs, P. D. Marasco, and E. A. Vela, "A soft pneumatic actuator as a haptic wearable device for upper limb amputees: Toward a soft robotic liner," *IEEE Robotics and Automation Letters*, vol. 4, no. 1, pp. 17–24, 2019.

[100] S. Muthukumarana, D. S. Elvitigala, J. P. Forero Cortes, D. J. Matthies, and S. Nanayakkara, "Touch me gently: Recreating the perception of touch using a shape-memory alloy matrix," in *Proceedings of the 2020 CHI Conference on Human Factors in Computing Systems*, CHI '20, (New York, NY, USA), p. 1–12, Association for Computing Machinery, 2020.

[101] K. Bark, J. Wheeler, P. Shull, J. Savall, and M. Cutkosky, "Rotational skin stretch feedback: A wearable haptic display for motion," *IEEE Transactions on Haptics*, vol. 3, no. 3, pp. 166–176, 2010.

[102] M. Rossi, M. Bianchi, E. Battaglia, M. Catalano, and A. Bicchi, "Happro: A wearable haptic device for proprioceptive feedback," *IEEE Transactions on Biomedical Engineering*, vol. PP, pp. 1–1, 05 2018.

[103] E. Battaglia, J. P. Clark, M. Bianchi, M. G. Catalano, A. Bicchi, and M. K. O'Malley, "The rice haptic rocker: Skin stretch haptic feedback with the pisa/IIT SoftHand," in *2017 IEEE World Haptics Conference (WHC)*, IEEE, jun 2017.

[104] E. Battaglia, J. P. Clark, M. Bianchi, M. G. Catalano, A. Bicchi, and M. K. O'Malley, "Skin stretch haptic feedback to convey closure information in anthropomorphic, underactuated upper limb soft prostheses," *IEEE Transactions on Haptics*, vol. 12, no. 4, pp. 508–520, 2019.

[105] A. Gupta, A. A. R. Irudayaraj, and R. Balakrishnan, "Hapticclench: Investigating squeeze sensations using memory alloys," in *Proceedings of the 30th Annual ACM Symposium on User Interface Software and Technology*, UIST '17, (New York, NY, USA), p. 109–117, Association for Computing Machinery, 2017.

[106] S. Bhattacharya and R. Mishra, "Pressure ulcers: Current understanding and newer modalities of treatment," *Indian Journal of Plastic Surgery*, vol. 48, no. 1, pp. 4–16, 2015.

[107] M. J. Coggrave and L. S. Rose, "A specialist seating assessment clinic: changing pressure relief practice," *Spinal Cord*, vol. 41, pp. 692–695, 2003.

[108] B. M. Bates-Jensen, H. E. McCreath, and V. Pongquan, "Sub-epidermal moisture is associated with early pressure ulcer damage in nursing home residents with dark skin tones: Pilot findings," *Journal of Wound, Ostomy and Continence Nursing*, vol. 36, no. 3, pp. 277–284, 2009.

[109] J. J. Harrow and H. N. Mayrovitz, "Subepidermal moisture surrounding pressure ulcers in

persons with a spinal cord injury: A pilot study," *The Journal of Spinal Cord Medicine*, vol. 37, no. 6, pp. 719–728, 2014.

[110] J. Kottner, G. Dobos, A. Andruck, C. Trojahn, J. Apelt, H. Wehrmeyer, C. Richter, and U. Blume-Peytavi, "Skin response to sustained loading: A clinical explorative study," *Journal of Tissue Viability*, vol. 24, no. 3, pp. 114 – 122, 2015.

[111] J. Fletcher, "A 160 patient evaluation of dolphin fluid immersion therapy," tech. rep., Medstrom, 2016.

[112] R. Brånemark, Ö. Berlin, K. Hagberg, P. Bergh, B. Gunterberg, and B. Rydevik, "A novel osseointegrated percutaneous prosthetic system for the treatment of patients with transfemoral amputation," *The Bone & Joint Journal*, vol. 96-B, no. 1, pp. 106–113, 2014.

[113] P. T. Pospiech, R. Wendlandt, H.-H. Aschoff, S. Ziegert, and A. P. Schulz, "Quality of life of persons with transfemoral amputation: Comparison of socket prostheses and osseointegrated prostheses," *Prosthetics and Orthotics International*, 2020.

[114] "About osseointegration." https://www.blatchfordclinic.com/services/osseointegration/about-osseointegration/. Accessed: 09.05.2022.

[115] J. Hebert, M. Rehani, and R. Stiegelmar, "Osseointegration for lower-limb amputation: A systematic review of clinical outcomes," *JBJS Reviews*, vol. 5, p. 1, 10 2017.

[116] C. J. Pendegrass, A. E. Goodship, J. S. Price, and G. W. Blunn, "Nature's answer to breaching the skin barrier: an innovative development for amputees," *Journal of Anatomy*, vol. 209, no. 1, pp. 59–67, 2006.

[117] N. Charkoudian, "Skin blood flow in adult human thermoregulation: How it works, when it does not, and why," *Mayo Clinic Proceedings*, vol. 78, no. 5, pp. 603–612, 2003.

[118] K. Ghoseiri and R. Safari, "Prevalence of heat and perspiration discomfort inside prostheses: Literature review," *The Journal of Rehabilitation Research and Development*, vol. 51, p. 855 — 868, 11 2014.

[119] H. D. Thomas, "Affordable, modular, and breathable upper-limb prosthetic sockets for use in underdeveloped areas with hot, humid climates," *Journal of Young Investigators*, vol. 28, 2015.

[120] C. M. Webber and B. L. Davis, "Design of a novel prosthetic socket: Assessment of the thermal performance," *Journal of Biomechanics*, vol. 48, no. 7, pp. 1294–1299, 2015.

[121] "Socket-less socket." https://martinbionics.com/above-knee-socket-less-socket/. Accessed: 05.05.2022.

[122] M. Skobe and M. Detmar, "Structure, function, and molecular control of the skin lymphatic system," *Journal of Investigative Dermatology Symposium Proceedings*, vol. 5, no. 1, pp. 14–19, 2000.

[123] M. A. Swartz, "The physiology of the lymphatic system," *Advanced Drug Delivery Reviews*, vol. 50, no. 1, pp. 3–20, 2001.

Transport and absorption of Drugs Via the Lymphatic System.

[124] L. Paternò, M. Ibrahimi, E. Rosini, G. Menfi, V. Monaco, E. Gruppioni, L. Ricotti, and A. Menciassi, "Residual limb volume fluctuations in transfemoral amputees," *Scientific Reports*, vol. 11, 06 2021.

[125] L. Paternò, M. Ibrahimi, E. Gruppioni, A. Menciassi, and L. Ricotti, "Sockets for limb prostheses: A review of existing technologies and open challenges," *IEEE Transactions on Biomedical Engineering*, vol. 65, no. 9, pp. 1996–2010, 2018.

[126] R. Greenwald, R. Dean, and W. Board, "Volume management: Smart variable geometry socket (svgs) technology for lower-limb prostheses," *JPO: Journal of Prosthetics and Orthotics*, vol. 15, p. 107–112, 07 2003.

[127] B. Wang, C. Zhang, C. Zeng, L. D. Kramer, and G. Arlene. U.S. Patent: Prosthetic Socket Apparatus and Systems. US20130274896A1, 2016.

[128] "Open bionics hero arm." https://openbionics.com/clinicians/. Accessed: 06.05.2022.

[129] "Ossur re-flex shock." https://www.ossur.com/en-gb/prosthetics/feet/re-flex-shock. Accessed: 06.05.2022.

[130] "Carbon fiber vs thermoplastic in prosthetics and orthotics." https://www.infinitetech.org/carbon-fiber-vs-thermoplastic-in-prosthetics-and-orthotics/. Accessed: 06.05.2022.

[131] "Open bionics azdeco covers." https://shop.openbionics.com/product/azdeco-covers/?v=79cba1185463. Accessed: 09.05.2022.

[132] "Klippa: Prosthetic leg for rock climbers." https://www.behance.net/gallery/16820519/KLIPPA-Prosthetic-Leg-for-Rock-Climbers. Accessed: 06.05.2022.

[133] J. Grima, D. Attard, R. Gatt, and R. Cassar, "A novel process for the manufacture of auxetic foams and for their re-conversion to conventional form," *Advanced Engineering Materials*, vol. 11, pp. 533 – 535, 07 2009.

[134] D. Prall and R. Lakes, "Properties of a chiral honeycomb with a poisson's ratio of — 1," *International Journal of Mechanical Sciences*, vol. 39, no. 3, pp. 305 – 314, 1997.

[135] R. S. Lakes, "Negative-poisson's-ratio materials: Auxetic solids," *Annual Review of Materials Research*, vol. 47, no. 1, pp. 63–81, 2017.

[136] K. K. Saxena, R. Das, and E. P. Calius, "Three decades of auxetics research —materials with negative poisson's ratio: A review," *Advanced Engineering Materials*, vol. 18, no. 11, pp. 1847–1870, 2016.

[137] X. Ren, R. Das, P. Tran, T. D. Ngo, and Y. M. Xie, "Auxetic metamaterials and structures: a review," *Smart Materials and Structures*, vol. 27, p. 023001, jan 2018.

[138] I. Masters and K. Evans, "Models for the elastic deformation of honeycombs," *Composite Structures*, vol. 35, no. 4, pp. 403 – 422, 1996.

[139] C. Smith, J. Grima, and K. Evans, "A novel mechanism for generating auxetic behaviour in reticulated foams: missing rib foam model," *Acta Materialia*, vol. 48, no. 17, pp. 4349 – 4356, 2000.

[140] J. N. Grima and K. E. Evans, "Auxetic behavior from rotating squares," *Journal of Materials Science Letters*, vol. 19, pp. 1563–1565, Sep 2000.

[141] Y. Prawoto, "Seeing auxetic materials from the mechanics point of view: A structural review on the negative poisson's ratio," *Computational Materials Science*, vol. 58, p. 140–153, 06 2012.

[142] K. Kuribayashi, K. Tsuchiya, Z. You, D. Tomus, M. Umemoto, T. Ito, and M. Sasaki, "Self-deployable origami stent grafts as a biomedical application of ni-rich tini shape memory alloy foil," *Materials Science and Engineering: A*, vol. 419, no. 1, pp. 131 – 137, 2006.

[143] K. E. Evans and A. Alderson, "Auxetic materials: Functional materials and structures from lateral thinking!," *Advanced Materials*, vol. 12, no. 9, pp. 617–628, 2000.

[144] X. Ren, J. Shen, P. Tran, T. D. Ngo, and Y. M. Xie, "Auxetic nail: Design and experimental study," *Composite Structures*, vol. 184, pp. 288 – 298, 2018.

[145] R. LAKES, "Foam structures with a negative poisson's ratio," *Science*, vol. 235, no. 4792, pp. 1038–1040, 1987.

[146] M. Fortes and M. Teresa Nogueira, "The poison effect in cork," *Materials Science and Engineering: A*, vol. 122, no. 2, pp. 227 – 232, 1989.

[147] A. Alderson, J. Rasburn, S. Ameer-Beg, P. Mullarkey, W. Perrie , and K. Evans, "An auxetic filter: A tuneable filter displaying enhanced size selectivity or defouling properties," *Industrial & Engineering Chemistry Research*, vol. 39, pp. 654–665, 01 2000.

[148] A. Alderson, J. Rasburn, K. Evans, and J. Grima, "Auxetic polymeric filters display enhanced de-fouling and pressure compensation properties," *Membrane Technology*, vol. 2001, no. 137, pp. 6 – 8, 2001.

[149] P. Ma, Y. Chang, A. Boakye, and G. Jiang, "Review on the knitted structures with auxetic effect," *The Journal of The Textile Institute*, vol. 108, no. 6, pp. 947–961, 2016.

[150] M. Mir, M. N. Ali, J. Sami, and U. Ansari, "Review of mechanics and applications of auxetic structures," *Advances in Materials Science and Engineering*, vol. 2014, pp. 1–17, 2014.

[151] T. Li, F. Liu, and L. Wang, "Enhancing indentation and impact resistance in auxetic composite materials," *Composites Part B: Engineering*, vol. 198, p. 108229, 2020.

[152] T. Allen, N. Martinello, D. Zampieri, T. Hewage, T. Senior, L. Foster, and A. Alderson, "Auxetic foams for sport safety applications," *Procedia Engineering*, vol. 112, pp. 104 – 109, 2015.

[153] K. Evans, M. Nkansah, and I. Hutchinson, "Auxetic foams: Modelling negative poisson's ratios," *Acta Metallurgica et Materialia*, vol. 42, no. 4, pp. 1289 – 1294, 1994.

[154] J. Smardzewski, R. Kłos, and B. Fabisiak, "Design of small auxetic springs for furniture," *Materials & Design*, vol. 51, pp. 723 – 728, 2013.

[155] V. Chaithanya Vinay and D. S. Mohan Varma, "Fabrication and testing of auxetic foams for rehabilitation applications," *Journal of the Indian Institute of Science*, vol. 99, pp. 511–518, 10 2019.

[156] O. Duncan, T. Shepherd, C. Moroney, P. Venkatraman, K. Winwood, T. Allen, A. Alderson, and L. Foster, "Review of auxetic materials for sports applications: Expanding options in comfort and protection," *Applied Sciences*, vol. 8, 06 2018.

[157] R. Naboni and L. Mirante, "Metamaterial computation and fabrication of auxetic patterns for architecture.," in *SIGraDi 2015, XIX Congress of the Iberoamerican Society of Digital Graphics*, no. 3 in Blucher Design Proceedings, pp. 129–136, Blucher, Nov. 2015.

[158] G. Fallacara, M. Barberio, and M. Colella, "Learning by designing: Investigating new didactic methods to learn architectural design," *Turkish Online Journal of Educational Technology*, vol. 2017, pp. 455–465, 11 2017.

[159] M. Konaković, K. Crane, B. Deng, S. Bouaziz, D. Piker, and M. Pauly, "Beyond developable: Computational design and fabrication with auxetic materials," *ACM Trans. Graph.*, vol. 35, July 2016.

[160] K. Alderson, R. Webber, U. Mohammed, E. Murphy, and K. Evans, "An experimental study of ultrasonic attenuation in microporous polyethylene," *Applied Acoustics*, vol. 50, no. 1, pp. 23–33, 1997.

[161] F. Scarpa, L. G. Ciffo, and J. R. Yates, "Dynamic properties of high structural integrity auxetic open cell foam," *Smart Materials and Structures*, vol. 13, pp. 49–56, nov 2003.

[162] C. P. Chen and R. S. Lakes, "Micromechanical Analysis of Dynamic Behavior of Conventional and Negative Poisson's Ratio Foams," *Journal of Engineering Materials and Technology*, vol. 118, pp. 285–288, 07 1996.

[163] M. J. Mirzaali, S. Janbaz, M. Strano, L. Vergani, and A. A. Zadpoor, "Shape-matching soft mechanical metamaterials," *Scientific Reports*, vol. 8, pp. 965:1 – 965:7, 2018.

[164] A. G. Mark, S. Palagi, T. Qiu, and P. Fischer, "Auxetic metamaterial simplifies soft robot design," in *2016 IEEE International Conference on Robotics and Automation (ICRA)*, pp. 4951–4956, May 2016.

[165] J. Rossiter, K. Takashima, F. Scarpa, P. Walters, and T. Mukai, "Shape memory polymer hexachiral auxetic structures with tunable stiffness," *Smart Materials and Structures*, vol. 23, no. 4, p. 045007, 2014.

[166] K. Ramachandra, C. J. Cai, S. Lalithkumar, X. Cai, Z. T. Tse, and H. Ren, "Chapter 12 - tunable stiffness using negative poisson's ratio toward load-bearing continuum

tubular mechanisms in medical robotics," in *Control Theory in Biomedical Engineering* (O. Boubaker, ed.), pp. 317–358, Academic Press, 2020.

[167] K. Wang, Y.-H. Chang, Y. Chen, C. Zhang, and B. Wang, "Designable dual-material auxetic metamaterials using three-dimensional printing," *Materials & Design*, vol. 67, pp. 159 – 164, 2015.

[168] A. Lazarus and P. M. Reis, "Soft actuation of structured cylinders through auxetic behavior," *Advanced Engineering Materials*, vol. 17, no. 6, pp. 815–820, 2015.

[169] X. Ren, J. Shen, A. Ghaedizadeh, H. Tian, and Y. M. Xie, "A simple auxetic tubular structure with tuneable mechanical properties," *Smart Materials and Structures*, vol. 25, p. 065012, may 2016.

[170] J. I. Lipton, R. MacCurdy, Z. Manchester, L. Chin, D. Cellucci, and D. Rus, "Handedness in shearing auxetics creates rigid and compliant structures," *Science*, vol. 360, no. 6389, pp. 632–635, 2018.

[171] B. Mosadegh, P. Polygerinos, C. Keplinger, S. Wennstedt, R. F. Shepherd, U. Gupta, J. Shim, K. Bertoldi, C. J. Walsh, and G. M. Whitesides, "Pneumatic networks for soft robotics that actuate rapidly," *Advanced functional materials*, vol. 24, no. 15, pp. 2163–2170, 2014.

[172] A. Sedal, M. Fisher, J. Bishop-Moser, A. Wineman, and S. Kota, "Auxetic sleeves for soft actuators with kinematically varied surfaces," in *2018 IEEE/RSJ International Conference on Intelligent Robots and Systems (IROS)*, pp. 464–471, 2018.

[173] A. Rafsanjani and D. Pasini, "Bistable auxetic mechanical metamaterials inspired by ancient geometric motifs," *Extreme Mechanics Letters*, vol. 9, pp. 291 – 296, 2016.

[174] X. Shang, L. Liu, A. Rafsanjani, and D. Pasini, "Durable bistable auxetics made of rigid solids," *Journal of Materials Research*, vol. 33, no. 3, p. 300–308, 2018.

[175] Z. Wang and H. Hu, "Auxetic materials and their potential applications in textiles," *Textile Research Journal*, vol. 84, no. 15, pp. 1600–1611, 2014.

[176] S. C. Ugbolue, Y. K. Kim, S. B. Warner, Q. Fan, C.-L. Yang, O. Kyzymchuk, and Y. Feng, "The formation and performance of auxetic textiles. part i: theoretical and technical considerations," *The Journal of The Textile Institute*, vol. 101, no. 7, pp. 660–667, 2010.

[177] V. Carneiro, J. Meireles, and H. Puga, "Auxetic materials — a review," *Materials Science-Poland*, vol. 31, pp. 561–571, 10 2013.

[178] C. Borcea and I. Streinu, "Geometric auxetics," *Proc. R. Soc. A*, vol. 471, no. 2184, p. 20150033, 2015.

[179] C. S. Kaplan and D. H. Salesin, "Escherization," in *Proceedings of the 27th Annual Conference on Computer Graphics and Interactive Techniques*, SIGGRAPH '00, (New York, NY, USA), pp. 499–510, ACM Press/Addison-Wesley Publishing Co., 2000.

[180] C. Schumacher, S. Marschner, M. Cross, and B. Thomaszewski, "Mechanical characterization of structured sheet materials," *ACM Trans. Graph.*, vol. 37, pp. 148:1–148:15, July 2018.

[181] J. C. Á. Elipe and A. D. Lantada, "Comparative study of auxetic geometries by means of computer-aided design and engineering," *Smart Materials and Structures*, vol. 21, no. 10, p. 105004, 2012.

[182] F. Scarpa, P. Panayiotou, and G. Tomlinson, "Numerical and experimental uniaxial loading on in-plane auxetic honeycombs," *The Journal of Strain Analysis for Engineering Design*, vol. 35, no. 5, pp. 383–388, 2000.

[183] X. Ren, J. Shen, A. Ghaedizadeh, H. Tian, and Y. M. Xie, "Experiments and parametric studies on 3d metallic auxetic metamaterials with tuneable mechanical properties," *Smart Materials and Structures*, vol. 24, p. 095016, aug 2015.

[184] F. B. Coulter and A. Ianakiev, "4d printing inflatable silicone structures," *3D Printing and Additive Manufacturing*, vol. 2, no. 3, pp. 140–144, 2015.

[185] H. Qi and M. Boyce, "Stress–strain behavior of thermoplastic polyurethanes," *Mechanics of Materials*, vol. 37, no. 8, pp. 817 – 839, 2005.

[186] Y. Liu and H. Hu, "A review on auxetic structures and polymeric materials," *Scientific Research and Essays*, vol. 5, no. 10, pp. 1052–1063, 2010.

[187] H. A. Kolken and A. A. Zadpoor, "Auxetic mechanical metamaterials," *RSC Adv.*, vol. 7, pp. 5111–5129, 2017.

[188] C. S. Kaplan, *Introductory Tiling Theory for Computer Graphics*.
Morgan and Claypool Publishers, 2009.

[189] A. Alomarah, D. Ruan, S. Masood, I. Sbarski, and B. Faisal, "An investigation of in-plane tensile properties of re-entrant chiral auxetic structure," *The International Journal of Advanced Manufacturing Technology*, vol. 96, 05 2018.

[190] K. M. Digumarti, A. T. Conn, and J. Rossiter, "Euglenoid-inspired giant shape change for

highly deformable soft robots," *IEEE Robotics and Automation Letters*, vol. 2, no. 4, pp. 2302–2307, 2017.

[191] J. Posner, J. A. Russell, and B. S. Peterson, "The circumplex model of affect: An integrative approach to affective neuroscience, cognitive development, and psychopathology," *Development and psychopathology*, vol. 17, no. 3, pp. 715–734, 2005.

[192] Y. Kuniyasu, M. Sato, S. Fukushima, and H. Kajimoto, "Transmission of forearm motion by tangential deformation of the skin," in *Proceedings of the 3rd Augmented Human International Conference*, p. 16, ACM, 2012.

[193] J. E. B. Törnros and A. K. Bolling, "Mobile phone use-effects of handheld and handsfree phones on driving performance," *Accident Analysis and Prevention*, vol. 37, no. 5, pp. 902–909, 2005.

[194] M. Aggravi, F. Pausé, P. R. Giordano, and C. Pacchierotti, "Design and evaluation of a wearable haptic device for skin stretch, pressure, and vibrotactile stimuli," *IEEE Robotics and Automation Letters*, vol. 3, no. 3, pp. 2166–2173, 2018.

[195] C. Zeagler, "Where to wear it: functional, technical, and social considerations in on-body location for wearable technology 20 years of designing for wearability," pp. 150–157, 09 2017.

[196] J.-H. Youn, H. Mun, and K.-U. Kyung, "A wearable soft tactile actuator with high output force for fingertip interaction," *IEEE Access*, vol. 9, pp. 30206–30215, 2021.

[197] M. Garrad, G. Soter, A. Conn, H. Hauser, and J. Rossiter, "A soft matter computer for soft robots," *Science Robotics*, vol. 4, no. 33, 2019.

[198] J. Yan, Y. Lu, G. Chen, M. Yang, and Z. Gu, "Advances in liquid metals for biomedical applications," *Chemical Society Reviews*, vol. 47, no. 8, pp. 2518–2533, 2018.

[199] C. Antfolk, M. D'Alonzo, B. Rosén, G. Lundborg, F. Sebelius, and C. Cipriani, "Sensory feedback in upper limb prosthetics," *Expert Review of Medical Devices*, vol. 10, no. 1, pp. 45–54, 2013.

[200] M. F. Simons, A. C. Haynes, Y. Gao, Y. Zhu, and J. Rossiter, "In contact: Pinching, squeezing and twisting for mediated social touch," in *CHI '20: CHI Conference on Human Factors in Computing Systems Extended Abstracts Proceedings*, ACM, 2020.

[201] A. B. Watson and D. G. Pelli, "Quest: A bayesian adaptive psychometric method," *Perception & Psychophysics*, vol. 33, pp. 113–120, 1983.

[202] Y. Visell, "Tactile sensory substitution: Models for enaction in HCI," *Interacting with Computers*, vol. 21, pp. 38–53, 08 2008.

[203] M. F. Simons, K. M. Digumarti, A. T. Conn, and J. Rossiter, "Tiled auxetic cylinders for soft robots," in *2019 2nd IEEE International Conference on Soft Robotics (RoboSoft)*, pp. 62–67, 2019.

[204] A. Zulifqar and H. Hu, "Auxetic textile materials - a review," *Journal of Textile Engineering and Fashion Technology*, vol. 1, pp. 1–20, 09 2016.

[205] J. E. Sanders, D. S. Harrison, J. C. Cagle, T. R. Myers, M. A. Ciol, and K. J. Allyn, "Post-doffing residual limb fluid volume change in people with trans-tibial amputation," *Prosthetics and Orthotics International*, vol. 36, no. 4, pp. 443–449, 2012.

PMID: 22588848.

[206] H. Wang, Z. Lu, Z. Yang, and X. Li, "A novel re-entrant auxetic honeycomb with enhanced in-plane impact resistance," *Composite Structures*, vol. 208, pp. 758–770, 2019.

[207] A. ABDOUNI, R. Vargiolu, and H. Zahouani, "Impact of finger biophysical properties on touch gestures and tactile perception: Aging and gender effects," *Scientific Reports*, 08 2018.

[208] M. F. Nolan, "Two-Point Discrimination Assessment in the Upper Limb in Young Adult Men and Women," *Physical Therapy*, vol. 62, pp. 965–969, 07 1982.

[209] K. Zhu and S. Zhao, "Autogami: a low-cost rapid prototyping toolkit for automated movable paper craft," in *Proceedings of the SIGCHI conference on human factors in computing systems*, pp. 661–670, 2013.